Ca' Foscari
University
of Venice

Master's Degree programme

in Conservation Science and
Technology for Cultural Heritage

Final Thesis

3D Printing Applied to Cultural Heritage.
Analysis of the chemical-mechanical properties and evaluation of the environmental impact of pure PLA, printed by FDM technology coupled with cold plasma source at atmospheric pressure.

Graduand
Federica Biasiolo
Matriculation Number 858166

Supervisor
Ch. Prof. Elisabetta Zendri

Assistant supervisor
Dafne Cimino, PhD
Silvio Cristiano, PhD

Academic Year
2020/2021

INDEX

Index of acronyms **5**
Aim of the thesis **8**
Chapter 1 ..... **10**
1.1 3D PRINTING 12
1.1.1 Subtractive and additive manufacturing 14
1.1.2 Fused Deposition Modelling (FDM): process and materials 19
1.1.3 Limits of 3D printing 25
1.2 USING DIGITAL FABRICATION IN THE FIELD OF CULTURAL HERITAGE 26
1.3 COLD PLASMA AT ATMOSPHERIC PRESSURE 34
1.3.1 Atmospheric plasma sources 36
1.3.2 The different functionalities of atmospheric plasmas 38
1.4 APPLICATION OF PLASMA IN 3D PRINTING 40
1.5 LCA: "LIFE CYCLE ASSESSMENT" 45
1.5.1 Phase 1: Goal and scope definition 47
1.5.2 Phase 2: Life Cycle Inventory (LCI) 47
1.5.3 Phase 3: Life Cycle Impact Assessment (LCIA) 48
1.5.4 Phase 4: Life Cycle Interpretation (LCI) 48
1.5.5 Possible disadvantages in using LCA 49
Chapter 2 ..... **50**
2.1 MATERIALS 51
2.1.1 Filament and specimens 51
2.1.2 Plasma torch 55
2.2 INVESTIGATION METHODS 58
2.2.1 Colourimetric analysis 58
2.2.2 Fourier transform infrared (FT-IR) spectroscopy in attenuated total reflectance (ATR) mode 60
2.2.3 Raman spectroscopy 62
2.2.4 Thermogravimetry (TGA) and Differential Scanning Calorimetry (DSC) 64
2.2.5 Dynamometric tests 67
2.3 ACCELERATED AGING 69
2.4 DURABILITY OF THE FILAMENT 72
2.4.1 Acid attack resistance tests 72
2.5 LIFE CYCLE ASSESSMENT OF A COMPARATIVE ANALYSIS 74
2.5.1 Comparative analysis 74
2.5.2 Definition of the functional unit 74

2.5.3 Definition of boundaries 75
2.5.4 Life Cycle Inventory (LCI) 80
2.5.5 Life Cycle Impact Assessment (LCIA) 87
Chapter 3 90
3.1 RESULTS: FILAMENT AND SAMPLES CHARACTERIZATION 91
3.1.1 Colorimetric analysis 91
3.1.2 Fourier transform infrared spectroscopy (FT-IR) in ATR mode 92
3.1.3 Raman spectroscopy 96
3.1.4 Thermogravimetry (TGA) and Differential Scanning Calorimetry (DSC) 97
3.1.5 Dynamometric tests 102
3.2 RESULTS OF ACCELERATED AGING 105
3.2.1 Colorimetric analysis 105
3.2.2 Fourier transform infrared spectroscopy (FT-IR) in ATR mode 115
3.2.3 Raman spectroscopy 119
3.2.4 Thermogravimetry (TGA) and Differential Scanning Calorimetry (DSC) 122
3.2.5 Dynamometric tests 124
3.3 FILAMENT STRENGTH EVALUATION 130
3.3.1 Acid attack resistance tests 130
3.4 LIFE CYCLE INTERPRETATION 134
3.4.1 ReCiPe 2016 Midpoint (H) 134
3.4.2 IPCC GWP 100a 140
Conclusion 144

Index of acronyms

ABS	Acrylonitrile-Butadiene-Styrene
ADP	Atmospheric Pressure Discharge
AP	Acidification
APP-DB	Atmospheric Pressure Plasma – Dielectric Barrier
APPJ	Atmospheric Pressure Plasma Jet
ASTM	International Association for Testing Materials
ATR	Attenuated Total Reflection
CAD	Computer Aided Design
CAM	Computer Aided Manufacturing
CDT	Corona Discharge Treatment
CIE	International Commission on Illumination
CNC	Computer Numerical Control
DBD	Dielectric Barrier Discharge
DC	Direct Current
DMLS	Direct Metal Laser Sintering
DOD	Drop-on-demand
DSC	Differential Scanning Calorimetry
E	Egalitarian
EBM	Electron Beam Melting
EDM	Electric Discharge Machining
EDP	Environmental Product Declaration
EN from CEN	Comité Européen de Normalisation
EPS	Sintered Expanded Polystyrene
ETP	Ecotoxicity
FDM	Fused Deposition Modelling
FFF	Fused Filament Fabrication
FTIR	Fourier-Transform Infrared spectroscopy
GLO	Global
GWP	Global Warming Potential
H	Hierarchical
HMDSN	Hexamethyldisilazane
HV	High Voltage
I	Individualistic
ICP	Inductive Coupled Plasma

IPCC	Intergovernmental Panel on Climate Change
IS	Information System
ISO	International Organization for Standardization
LBM	Laser Beam Machining
LCA	Life Cycle Assessment
LCI	Life Cycle Inventory
LCIA	Life Cycle Impact Assessment
LOM	Laminated Object Manufacturing
LPD	Low Pressure Discharge
LTE	Local Thermodynamic Equilibrium
LUDT	Linear Variable Differential Transformer
MIP	Microwave Induced Plasma
MIT	Massachusetts Institute of Technology
Non-LTE	Non-Local Thermodynamic Equilibrium
NP	Entrophication
ODP	Ozone Depletion in the Stratosphere
PC	Poly-Carbonate
PET	Polyethylene Terephthalate
PLA	Poly-lactic Acid
PM	Particulate Matter
PS	Polystyrene
RepRap	Replicated Rapid Prototyper
RF	Radio Frequency
RoW	Rest of the World
RP	Rapid Prototyping
S	System
SCE	Specular Component Excluded
SCI	Specular Component Included
SETAC	Society of Environmental Toxicology and Chemistry
SLA	Stereolithography
SLM	Selective Laser Melting
SLS	Selective Laser Sintering
STL	Standard Triangulation Language
STP	STandard for the Exchange of Product model data
TEOS	Tetraethylorthosilicate

TG or TGA	Thermogravimetry
TPE	ThermoPlastic Elastomer
TPU	Thermoplastic Polyurethane

Aim of the thesis

Three-dimensional manufacturing has reached considerable success not only in industry, but also in the medical, aerospace, automotive, food, consumer goods, research, education, architectural and craft sectors, etc., thanks to its versatility, reliability and ease of use.

Originally, 3D printing devices were too expensive for the mass market, for this reason they were mainly used by large companies. Subsequently, the increasing availability of inexpensive devices has seen their use expanded from small and medium-sized businesses to the individual professional and users.

Therefore, the increase in accuracy of current technologies and the reduction in reproduction costs have enabled the spread of digital fabrication into new areas, among which cultural heritage is very important.

3D printing and scanning offer greater flexibility than traditional techniques and can be used to digitally preserve artworks, to monitor shape and colour, to perform ageing and deterioration simulations, to create 3D archives and catalogues, to assist in various restoration operations, to provide multimedia museum exhibitions, and much more.

Recently, in addition to the creation of supports and the temporary replacement of fragile objects, the application of 3D modelling has been proposed to reproduce missing parts of various artefacts, placing the printed pieces as integration on the artwork. Obviously, the substantial increase in prototyping has led to the development of different methodologies and innovative materials, each of them can be chosen and adapted according to the case study considered.

One of the most widely used rapid prototyping methods is the FDM (*Fused Deposition Modelling*) technology, whereas the preferred and most environmentally friendly and biocompatible polymeric material is PLA, which can come in different colours and can be modified with a variety of different inert materials.

This thesis aims, therefore, to study the behaviour of a filament used in 3D printing, based on PLA. In particular, a comparison between specimens treated and untreated with cold plasma at atmospheric pressure, an innovative technology used to increase the adhesiveness and surface wettability of the material, as well as to deposit a protective coating, in order to obtain objects that are particularly resistant in an outdoor environment, i.e. against wear and tear and atmospheric agents is proposed. All specimens were made using the FDM, or FFF (Fused Filament Fabrication) technique.

To this end, a series of preliminary analyses are proposed, such as colorimetric analysis.

Then, the thermal properties are analysed, through the TGA and DSC techniques, and the mechanical characteristics, through the dynamometric test, both before and after the ageing tests, which make it possible to simulate the external conditions in which the created object could be

found. Furthermore, in order to evaluate the actual effectiveness of the plasma treatment, i.e. the increase of adhesiveness between layers, acid resistance tests are carried out

At the end, it is important to emphasise that the material chosen for this research, i.e. PLA is supposed to have a low environmental impact, as it compostable and frequently described as "sustainable".
Therefore, by means of the LCA (Life Cycle Assessment) standardized methodology, an evaluation of the sustainability and environmental impact of PLA treated with atmospheric plasma technology. In particular, a comparison between two generic cases of integrative restoration is proposed, considering first the material under analysis and then a traditional integrative method, based on the use of silicon rubber, for the making of the mould, and gypsum. The methodology therefore aims to establish whether, in terms of environmental sustainability, it is preferable to perform a traditional technique or to follow the path of innovation.

Chapter 1

This chapter provides a brief introduction to 3D printing and the different technologies, in order to better understand their main characteristics and the limitations that may be encountered during their use. In particular, a description of the FDM technique is given, presenting the process and the materials used.

Subsequently, examples are proposed regarding the possible use of 3D modelling in the field of Cultural Heritage.

From 3D printing, a description of cold plasma technology at atmospheric pressure is provided, presenting its main characteristics and the various uses to which it can be put, focusing above all on the possible use of the technology in 3D prototyping.

Finally, a brief description of life cycle assessment is given, presenting the four phases of work that follow:

1. Definition of goal
2. Life cycle inventory (LCI)
3. Life cycle impact assessment (LCIA)
4. Interpretation of results.

1.1 3D PRINTING

3D printing refers to an additive or subtractive manufacturing process in which tangible three-dimensional objects are created starting from an abstract digital 3D model. Thus, by depositing layers of photopolymers, extruded thermoplastics, welded metals or molten powders, or conversely, by removing and processing a block of material, the digital model is transformed into a solid three-dimensional object [1].
In recent years, efforts have been made to standardise the concepts and terminology inherent in 3D printing, through the 2015 ISO/ASTM 52900 standard, which defines the technology as "*the process of joining materials to make parts from 3D model data, usually layer upon layer, as opposed to subtractive manufacturing and formative manufacturing methodologies*" [2].
The concept of '3D printing' began to spread in 1977, thanks to WK Swainson, who obtained an early patent for the use of "*a laser to create covalent cross-linking on the surface of a liquid monomer where the workpiece rested on a tray that was gradually lowered into a tank one step at a time*".
After a series of patents, in 1984 Chuck Hull invented the Stereolithography Apparatus (SLA), which he defined as follows:

"*A system for generating three-dimensional objects based on the creation of a transverse pattern of the object to be formed, on the surface of a fluid medium capable of altering its physical state in response to synergistic stimuli such as incident radiation, particle bombardment or chemical reactions, in adjacent laminae representing successive adjacent cross-sections of the object that integrate with each other, providing for progressive growth by affixing the desired object, whereby an object is created from a substantially planar surface of the fluid medium during the formation process."* [3,4].

Although the invention of the 3D printer is attributed to Chuck, at the end of the 1980s, several technologies were proposed and several companies founded, with the sole aim of being able to develop a technique focused on the use of rapid prototyping (RP). One example is the Japanese Hideo Kodama, of the Nagoya Municipal Research Institute, who in 1981 proposed a patent, later abandoned, for an apparatus capable of producing prototypes and models of various kinds, based on the use of a UV beam capable of polymerising liquid photopolymers [5]. A similar project was presented by French inventors Alain Le Mehaute, Olivier de Witte and Jean Claude Andrè in 1984, and, as before, the idea was soon rejected. Therefore, only a few weeks later, the American Charles 'Chuck' Hull presented his patent, promoting the use of stereolithography and thus starting the production of three-dimensional objects [1].

Since 1986, digital fabrication has evolved and diversified, leading to the development of new printing techniques and a wide range of materials with different mechanical properties that can be printed either individually or in combination, thus enabling its spread from the industrial to the medical and artistic fields [4].

In 1987 Chuck himself invented the .stl file (Standard Triangulation Language or "Stereo Lithography interface format") a file format consisting of a tessellation of triangles describing the surface geometry of the object, from which the three-dimensional prototype is subsequently obtained.

The same year saw also the patent deposited by the American Carl Deckard for the SLS (Selective Laser Sintering) technique, and a couple of years later the patent for FDM.

From the late 1980s to the early 1990s, there was the rapid commercial development in industry, leading to large and expensive prototyping machines, particularly in the automotive, healthcare, aerospace and consumer goods sectors. The main objective of 3D modelling is, in fact, to speed up the creation of industrial products through faster prototyping.

3D printing began to become affordable for small and medium-sized enterprises in the early 2000s, when projects such as RepRap (Replicated Rapid Prototyper) were launched, the aim of which was to produce self-replicating 3D printers [1]. Formlabs and FabLabs (from the English *fabrication laboratory*) were soon set up, accessible and open to the public. These are small laboratories consisting of computerised digital fabrication tools so as to offer services tailored to local needs or individual users [6,7]. In fact, compared to traditional techniques, 3D printers make it possible to assemble, in a fast, flexible and reliable way, parts made of different materials with different physical and mechanical characteristics, offering a product that best reflects the original abstract idea.

Precisely for these reasons, especially in recent years, there has been a considerable development of this technology; survey published in early 2015 revealed that, at the time, there were more than 70 laboratories throughout Italy, and more than 1000 FabLabs distributed in 78 countries, according to the Fab Foundation, an organisation developed by the Center for Bits & Atoms Fab Lab Program at MIT [8].

The thesis provides a brief introduction to the various 3D printing technologies, focusing in particular on the additive technique FDM. With the aim of better understanding its operation and characteristics, it describes the production process and the most commonly used materials, and finally lists the main limitations of digital fabrication.

In the following paragraphs, possible applications of 3D scanning and digital photo-modelling in the field of Cultural Heritage are reported, proposing some case studies. Finally, an innovative treatment is described, based on the use of FDM 3D printing coupled with a plasma torch, with the aim of obtaining a reinforced material, able to resist wear and atmospheric agents.

1.1.1 Subtractive and additive manufacturing

Three-dimensional modelling can be divided into two broad categories, depending on the production technology to be used: on one hand there are the techniques defined as 'traditional' or subtractive, on the other hand the more 'innovative' or additive techniques.
The subtractive production techniques refer to mechanical processes of material removal; therefore, starting from solid blocks, metal or other materials, often defined as "raw", a certain shape is given through removal, drilling, cutting and grinding (Fig.1).

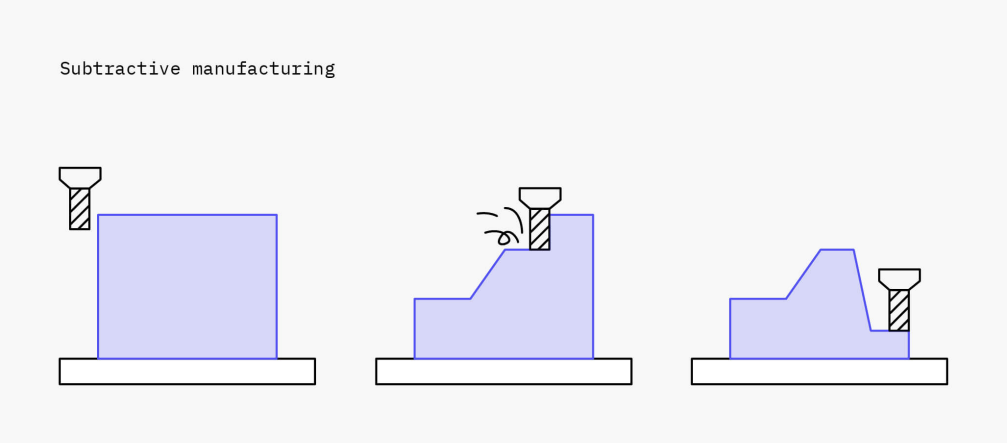

Figure 1. Three main steps of subtractive manufacturing [1].

These processes can be executed through manual work, or, more commonly, through the use of a computer numerical control (CNC). When the user interfaces with the CNC he should, first of all, make a virtual model with *AutoDesk* (CAD) software, thanks to which the necessary commands to guide the tool are generated, thus carrying out cuts, holes and other removal operations; in addition to CAD software, another software is also recommended, choosing from free and open source as well, such as: *Agisoft Metashape*, for photogrammetric mapping, *Meshlab*, for 3D modelling and treatment, *Visual SFM*, for photogrammetric surveying, *iWitness Pro*, for photogrammetric mapping, and *Blender*, again for 3D modelling and treatment.
In this way, fusing the Computer Aided Manufacturing (CAM), each process is constantly controlled, giving the production process excellent accuracy and repeatability.
Generally, the subtractive modelling technique is used when geometries are particularly complex and difficult to achieve through traditional processes. This technique also allows a variety of different materials and process methods to be used. On the other hand, however, one of the limitations of the subtractive methodology is that the cutting tool should be able to reach all surfaces, so that the material can be removed, and this obviously limits the design complexity. During the machining process, therefore, the most complex parts have to be reoriented, leading

to an increase in time and cost; in this respect, modelling is costly, especially because of the large amount of material that have to be removed before the desired geometry is achieved [1,9].
Subtractive modelling processes are:

- CNC production. By means of milling and turning processes, it is possible to obtain prototypes made of plastic, metal or polyurethane or acetal resin [10].
- Electric Discharge Machining (EDM). The technique modifies the material through mechanical processing carried out by electrical discharges, and is mainly used on metals [11].
- Laser cutting. This type of machining, defined according to the acronym LBM (Laser Beam Machining), uses a laser beam, which, when interact with the material, causes it to partially melt or boil, removing it through vaporisation or ablation phenomena [12]. The most commonly used materials are thermoplastics, wood and metals [9].
- Water Jet. The process consists of cutting different types of materials, such as plastics, light and heavy metals, stone, glass and composite materials [9], by means of a water jet with a high pressure (up to 7000 bar) [13].

The *additive manufacturing*, on the contrary, consists in the creation of 3D objects starting from a digital model through a subsequent and progressive accumulation of material on a base layer (Fig.2).

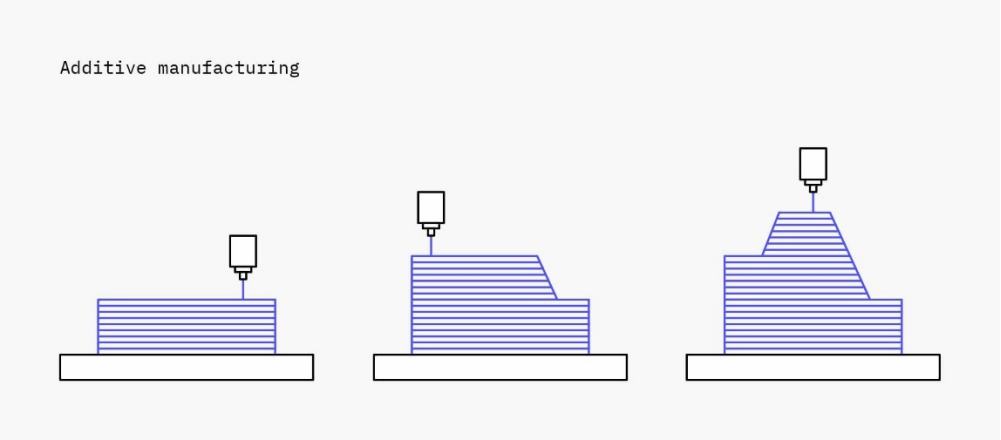

Figure 2. Three main steps of additive manufacturing [1].

As with subtractive modelling, whose techniques involve the use of the CNC system, additive modelling also has a common functionality, namely the use of specific 3D modelling software, such as the CAD program, the 3D scanner or the use of an online repository to download the model of interest. Therefore, thanks to a slicing software, the technique is fast and efficient, and the 3D printer has the ability to selectively deposit and mix different types of materials.

Once printed, the object requires a post-curing process, during which cleaning and finishing takes place, giving the object optimal final properties.

Additive manufacturing is an ideal method for prototyping, as it has a wide range of applications within the engineering and manufacturing fields, and one of the main features of the 3D printer is that it can produce objects with particularly complex geometry.

At the same time, however, the two three-dimensional modelling techniques do not guarantee high levels of precision and repeatability in all cases, since the various prints can vary if there are fluctuations during cooling or polymerisation [1,12].

Additive manufacturing techniques differ depending on how the individual layers are created and, according to the ISO document, can be grouped into seven categories:

1. *Photopolymerisation in a bath* (Stereolithography), where the material, consisting of a liquid photopolymer undergoes polymerisation in the presence of a light beam.
2. *Extrusion of material* (Melt Deposition Modelling), in which the molten material, passing through a high-temperature nozzle, is deposited on the work surface.
3. *Powder Bed Melting* (Selective Lase Sintering), whereby the pulverised material is melted using a high energy source.
4. *Direct Energy Deposition* (Laser Metal Deposition and Laser Engineered Network Modelling), where the metal material is deposited and melted.
5. *Sheet Laminating* (Production of Laminated Objects), in which the various sheets are cut together and laminated.
6. *Material Casting* (Multi-Jet Modelling), whereby the photosensitive material, in its liquid state, is deposited on a surface covered with powder and polymerised.
7. *Binder casting* (3D printing) uses a bed of powders, similar to those used in the SLS, SLM techniques, which are deposited on the print bed and adhered by means of a liquid binder. The binder is released by means of an inkjet head. Once a first layer has been created, the print bed is lowered, and a new layer of powder is released; the process continues until the object has been produced [1,14-16].

Besides to the technique, three types of additive manufacturing processes can be distinguished, according to the material used; the processes are classified as:

I. *Liquid-based processes* in which a liquid resin, or photopolymer, is solidified when exposed to a laser or other light source. 3D printers based on this technology allow to create objects by combining different materials as well.

II. *Powder-based processes*, where the various layers are made up of very fine powder, which are joined together by the application of an adhesive and a heat source, such as a laser, which allows the various layers to fuse and adhere.

III. *Processes based on solids*, where the material, melted or semi-liquid, passes through the printer nozzle and solidifies rapidly to produce the object [17].

Thus, depending on the methodology and the nature of the material, the following additive manufacturing techniques can be distinguished:

- *Stereolithography* (SLA). Patented by Charles Hull in 1986, it is one of the earliest methods of 3D printing, converting liquid plastic into three-dimensional solid materials. Using an STL file, the tool obtains information about the printing of each layer. Once all layers have been printed, the final object is rinsed with a solvent and placed in an ultraviolet oven. Many companies use this technology, as it is moderately low cost and it can be applied to elastic, rigid, flexible, heat-resistant resins, etc [12].
- *Selective Laser Sintering* (SLS). A technique proposed by Carl Deckard and his professor Joe Beaman in the 1980s, it can be applied to a variety of materials, such as nylon, ceramics, glass and metals, including aluminium, steel and silver. Compared to other additive printing processes, it does not require support structures, precisely because the object is continuously surrounded by non-intersintering powder [12].
- *Material Jetting*. This sophisticated type of 3D printer is based on the drop-on-demand (DOD) printing method, which is capable of precisely depositing different materials, avoiding waste. In particular, the printing system is combined with a photopolymerisation system, which promotes polymerisation and thus the curing of the resin on the substrate. Due to its similarity to popular 2D printers, it can be used comfortably in the office [14].
- *Binder Jetting*. Compared to other 3D printing methods, Binder Jetting combines powder and binder, allowing the application of different materials from plaster to metals.
  It is mainly used for medical and architectural prototypes [15].
- *Selective Laser Melting* (SLM), or Direct Metal Laser Sintering (DMLS). The SLM technique is the result of a German research project by a group from the Fraunhofer Institute ILT in 1995. Like the other additive processes, it starts with an STL file that is loaded onto the printer, which then processes the path using a series of values and parameters. Commonly used materials are light and heavy metals, whose powders, coming into direct contact with a laser, are totally melted, thus creating a series of consecutive layers. This type of three-dimensional modelling can be used to create objects with a complex geometry, thin thickness or voids within the structure. For this reason, the employment of the technology is limited to the aerospace and medical fields [12].
- *Electron Beam Melting* (EBM). A process developed by Arcam AB Inc., EBM, like SLM, melts and creates layers of metal powders. The only difference between the two prototyping techniques lies in the type of beam applied: while SLM uses a high-power laser beam, EBM employs an electron beam, with a temperature of around 1000 °C. This

method of additive manufacturing is not very widespread, both because of the limited availability of materials and because it is particularly slow and expensive. The technology is therefore mainly used in the aerospace field and for medical implants [12].

- *Laminated Object Manufacturing* (LOM). Additive prototyping, developed by the company Helisys Inc, which applies heat and pressure, via a roller, to cut layers of paper covered with adhesive, plastic or metal. Once a first layer is finished, a second sheet is applied, which is adhered thanks to the roller; the process continues until the object of interest has been completely produced, and the excess material is cut off and discarded. Although this method is not particularly popular, it is quite convenient and accessible for both large and small companies and for domestic use [12].

The choice of production process will depend above all on the design requirements; the Figure 3 proposes a comparison between subtractive and additive manufacturing, taking into consideration: precision, mechanical resistance, production time, choice of materials and geometric complexity.

Precision derived from the evaluation of the deviations between the digital model, created in CAD, and the three-dimensional model obtained. From this point of view, subtractive prototyping has a higher level of precision, thanks to the use of CNC machines; on the other hand, the materials used in additive manufacturing, often made up of resins, can undergo dimensional variation when exposed to light or when subjected to a change in temperature.

In addition to precision, subtractive manufacturing allows the creation of prototypes with good mechanical resistance, another characteristic of the CNC system.

In contrast, additive technologies offer relatively low times and costs. Compared to the subtractive technique, additive manufacturing has a higher production speed for materials and, in general, does not produce much waste.

As far as materials are concerned, 3D printing is also the best alternative to traditional techniques, as it offers the possibility of creating the various layers using different materials; the CNC technology of subtractive manufacturing, on the other hand, allows the various parts to be created separately and assembled at a later stage. Finally, one of the limitations of subtractive manufacturing lies in the inability to create objects with internal cavities and removable supports; in this respect too, additive prototyping is the most advantageous option [18].

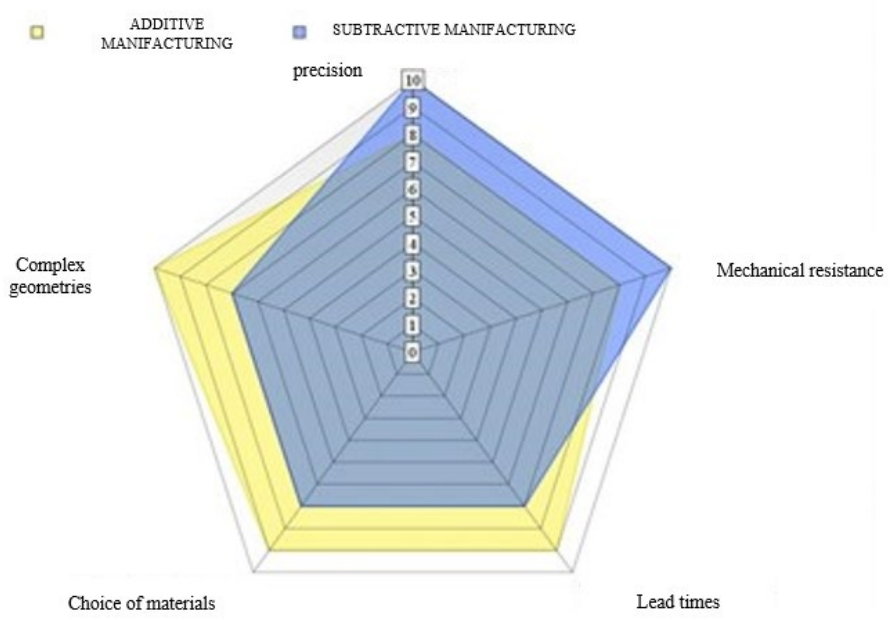

Figure 3. Comparison between additive and subtractive manufacturing in terms of precision, mechanical resistance, production time, choice of materials and geometric complexity [18].

1.1.2 Fused Deposition Modelling (FDM): process and materials

FDM (*Fused Deposition Modelling*) additive prototyping was developed in the late 1980s by S. Scott Crump, the founder of Stratasys Ltd [19], a global leader in 3D printing. Crump, with the aim of building a toy for his daughter, decided to use a hot glue gun, melting the plastic, distributing the material and creating a series of layers; the technique was called Fused Deposition Modelling.

FDM technology is suitable for modelling, prototyping and manufacturing objects made of different materials. Typically, a filament of thermoplastic polymer material is deposited on a work surface, using a nozzle or extruder, and the object of interest is produced by superimposing consecutive layers.

The 3D printer is connected directly to a spool of thermoplastic filament, and once the nozzle has reached the desired temperature, the filament passes through the extrusion head and into the nozzle where it melts; the nozzle is heated to a temperature slightly higher than the melting temperature of the polymer.

For this reason, it is essential to start from a digital model, using a numerically controlled instrument, adjusted and controlled by a specific software. The software allows, in fact, to adjust the different process parameters: temperature of the nozzle and of the working plane, the construction speed, the height of the layer and the speed of the cooling fan.

The first step is then the creation of an .stl file that, thanks to a mathematical algorithm, is able to divide the digital model into different sections, which are called slices, and studies the way in which each layer is built by the extruder, i.e. translates the dimensions of the object according to X, Y and Z coordinates.

Then, as the various layers are deposited, they cool until they solidify as soon as they come into contact with the working surface (for example the foam sheet in Fig.4) or with the previous layer, and the nozzle, thanks to the parameters set previously, is able to take a specific direction and deposit the right amount of material, depending on the size of the layer and the degree of filling chosen. In some cases, the cooling of the material can be accelerated through the use of cooling fans, present on the extrusion head.

Once printing is complete, the object can be removed from the work surface by hand or using a squeegee [20-25].

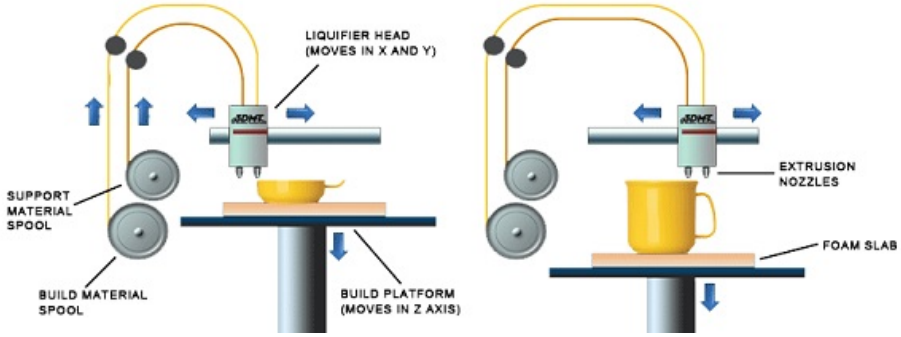

Figure 4. The process of Fused Deposition Modelling (FDM) [21].

A variety of thermoplastic filaments can be used in FDM technology, such as: ABS (Acrylonitrile-Butadiene Styrene) or Cycolac™, PC (polycarbonate), PLA (Poly Lactic Acid), Nylon (polyamide 6.6), PS (polystyrene) and PET (Polyethylene Terephthalate), but it is also possible to combine different materials, such as polymers with wood or with carbon, if added together or if there are two extruders. Recently, in fact, elastomeric thermoplastic (TPE) filaments have been produced that allow two different plastics to be combined; the combination of a rigid thermoplastic material and an elastomeric one gives the possibility of creating multifunctional products.

Of the above materials, the most widely used in FDM are ABS and PLA. ABS is a petroleum derivative, has good strength but is not environmentally friendly, because it's a non-biodegradable plastic. This thermoplastic copolymer is derived from polymerised styrene, which reacts with acrylonitrile in the presence of polybutadiene; its chemical formula is: $(C_8H_8{*}C_4H_6{*}C_3H_3N)_n$. Each monomer, therefore, provides particular properties to the material: styrene gives good processability, butadiene makes the material resilient and tough, whereas acrylonitrile confers

rigidity and thermal chemical resistance. ABS has also little resistance to UV radiation, has an amorphous structure and, for this reason, does not have a specific melting point [26,27].

The extrusion temperature is approximately 240-260°C, which is why it is preferable to heat the work surface on which the object is deposited, to slow down the solidification process and promote a good substrate-base adhesion. After printing, the copolymer can be processed using dimethyl ketone as a solvent.

Therefore, it is preferable to use PLA because it has antimicrobial and antioxidant properties and, being of plant origin, it is biodegradable, compostable and renewable, and is composed of 100% renewable raw materials [28]; in fact, the thermoplastic polymer is derived from a fermentation process of corn or wheat.

Polylactic acid is, therefore, a rigid thermoplastic polymer, the geometry of which varies from semi-crystalline to amorphous depending on the optical purity of the polymer structure. It is, moreover, composed of two optically active forms, namely L-lactic acid, which is the natural form, or D-lactic acid, which is produced by microorganisms or racemization.

Therefore, since PLA is produced by the polymerization of lactic acid, which can be derived from two methods, chemical method or fermentation method, two compounds can be obtained that differ in optical purity.

The chemical method, which uses petrochemical resources, using HCN and an acid-specific catalyst, produces a racemic mixture of D (-) and L (+) lactic acid. The chemical method, on the other hand, which relies on the use of renewable resources such as carbohydrates (monosaccharides, disaccharides), produces only an optically pure form of lactic acid D (-) or L (+).

The following is a brief description of the two methods of producing lactic acid.

- *Chemical method*. Acetaldehyde is reacted with hydrocyanic acid in the presence of a catalyst to produce lactonitrile. Lactonitrile is then purified and hydrolyzed to produce lactic acid. a description of the method is shown in the Figure 5.

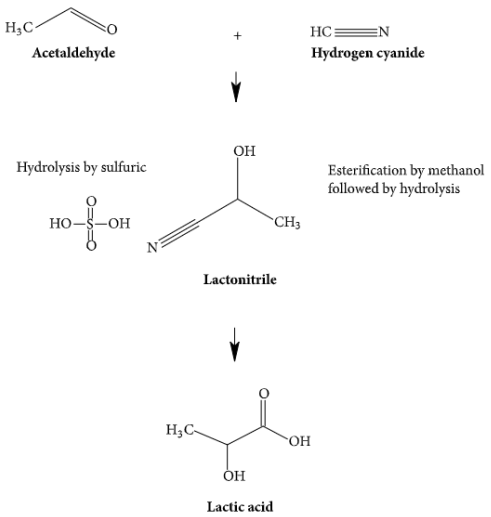

Figure 5. Production of Lactic Acid by chemical process [29].

- *Fermentation method*. Fermentation is a process involving fungi (*Rhizopus* Oryzae) and anaerobic bacteria (*Lactobacillus*, *Pediococcus*, *Lactococcus* and *Streptococcus*), which produce lactic acid through the use of simple sugars, such as glucose, lactose and galactose, without any heating process. Obviously, the yield of lactic acid production will depend on the cell mass and the type of microorganism; the Figure 6 shows the yield of different microorganisms [29,30].

Sr. No.	Microorganism producing lactic acid	Substrate involved	Genetic modification	Yield of lactic acid
1	*T. aotearoense* SCUT27[5]	Lignocellulosic biomass[5]	Engineered to block the acetic acid formation pathway[5]	0.93 g/g glucose with an optical purity of 99.3%[5]
2	*Lactobacillus amylovorus* ATCC 33622[6]	Liquefied corn starch[6]	Nil	20 g l^{-1} h^{-1}[6]
3	*L. helveticus* [6]	Whey[6]	Nil	35 g l^{-1} h^{-1}[6]
4	*Enterococcus faecalis* CBRD01[7]	Glucose[7]	Nil	5 g l−1 h−1[7]
5	*L. delbrueckii* NCIM 2025[8]	Cane molasses concentration of 150 g/L (equivalent to 78 g total sugar). [8]	*adh-ve* mutant by UV radiation[8]	78±1.2 (g/g) [8]
6	*L. plantarum* LMISM6 [9]	Molasses 193.50 g L-1[9]	NIL	94.8 g L-1[9]
7	Thermophilic *Bacillus* sp. XZL4[10]	Corn stover hydrolyzate 162.5 g L-1[10]	NIL	1.86 g L-1 h-1[10]
8	*Lactococcus lactis*[11]	Glucose 60 gl-1 [11]	Nil	35 gl-1[11]
9	Escherichia coliBAD-ldh[12]	1g l-1 of fructose[12]	Overexpression of L-ldh gene derivative[12]	0.62 g l-1[12]
10	Escherichia coli[13]	56 g/L of crude glycerol[13]	Overexpression of GlpK/GlpD gene[13]	50 g/L of L-lactic acid[13]

Figure 6. Table with some microorganisms with their yield of production of lactic acid by fermentation [30].

In its usual state, PLA, which is transparent and colourless, is brittle, so it is additivated (with wood fibers, graphene, marble or bronze powder, etc.) to increase its strength; moreover, it can be processed like other plastics, i.e. as a film or as a fibre.

Although hygroscopic and not very resistant to high levels of relative humidity, as it tends to biodegrade, the polymer is heavier and less deformable than ABS, and can be used to make large objects.

Its extrusion temperature is slightly lower than ABS, between 200°-230°C, and as it does not show shrinkage problems, therefore there is no need to heat the work surface.

FLEX PLA, in addition, represents an alternative to traditional PLA, as it is more flexible due to the use of rubber, and does not show the common characteristics of rigidity or fragility of PLA. Because of this characteristic, FLEX PLA is suitable for producing objects with a good degree of elasticity [31-33].

PLA, therefore, can be compared to traditional thermoplastic polymers due to its good chemical, physical and mechanical properties, such as biodegradability, high stiffness, tensile strength and ease of processing.

At the same time, however, due to its high brittleness, it is unsuitable for some applications and can be improved by blending it with other biopolymers without losing the advantage of biodegradability.

Moreover, being a material of polymeric nature, any chemical reaction or physical action that leads to a change in its molecular weight or chemical structure causes an irreversible alteration and modification of its chemical characteristics, as well as its physical and mechanical properties, to the point of making it unserviceable for the use for which it was designed. Especially polymers of organic nature easily undergo degradation processes due to the action of physical effects (heat, light, high-energy radiation, mechanical deformation) or chemical effects (oxygen, nitrogen, water, atmospheric pollutants). All polymeric materials are therefore exposed to degradation, either during molding, extrusion, and spinning processes, as they are exposed to mechanical stress, heat, and oxygen, or during use, through the action of light, oxygen, and air pollutants [34,35].

In the case of polylactic acid, the degradation process of greatest impact is biodegradation, during which the cleavage of the main or side chains of the macromolecules occurs and could result from different phenomena such as: hydrolysis, thermal activation, photolysis, biological activity or oxidation [36].

This thesis project is focused on the processes of hydrolysis and photolysis, where the main effect is the breakage of polymer chains, which causes a decrease in molecular weight. Specifically, in the case of the photolytic mechanism (Norrish II mechanism), the PLA polymer chain absorbs a photon, causing the chain containing CO bonds to split and leading to the formation of hydroperoxides, from which carboxylic acids and diketone end groups are subsequently obtained. Photolysis of diketones also causes a C-C bond cleavage between two carbonyl groups.

Hydrolytic degradation, on the other hand, occurs by chain scission, the degree of which depends mainly on the amount of water absorbed by the PLA. The process occurs mainly within the molecular structure, where there is a high number of carboxylic acids, which easily undergo ester hydrolysis.

1.1.1.1 Advantages and disadvantages

Like all technologies, FDM has a number of advantages and disadvantages. Firstly, compared to other 3D prototyping methods, the FDM printer is affordable, even for home use. Furthermore, it is considered a 'clean technology', simple-to-use and *'office-friendly'*, requiring minimal user intervention without the need for third-party equipment or special structures; it is also possible to produce complex geometries and cavities that are not easily reproduced by other 3D printing methods [37]. Table 1 summarises all the advantages of FDM printing.

Among the disadvantages, however, it has a lower accuracy and resolution than other techniques, such as stereolithography; in particular, the resolution in FDM depends on the nozzle size and, at the same time, the accuracy is determined by the movements of the extruder on the X and Y axis. Considering other factors, it can also be seen that Stereolithography creates layers that show a higher level of adhesion. In FDM, there is a kind of overlapping of the various layers, and from this point of view, the lowest layers may suffer from the weight of the upper layers, thus compromising the quality of the print itself.
Another disadvantage is that printing times are longer than in other techniques, and the final object requires post-processing, as it does not have a nice or smooth surface aspect [38].

Table 1. Advantages of FDM printing [38].

Standard lead time	Minimum of 4 working days (or 48 hours for models using the Fast Lones service), depending on part size, number of components and finishing degrees.
Standard accuracy	± 0.15% (with lower limit ± 0.2 mm)
Minimum wall thickness – accuracy	1 mm
Layer thickness	0.18-0.25 mm (varies depending on the chosen material)
Maximum part dimensions	Dimensions are unlimited ad components may be composed of several sub-parts. The maximum build envelope so far is 914x610x914 mm.
Surface structure	Unfinished parts typically have a rough surface, but all kinds of fine finishes are possible. FDM parts can be sandblasted, colored/impregnated, painted and coated.

1.1.3 Limits of 3D printing

Although additive manufacturing technologies have led to important developments in a variety of fields, especially in industry, it is clear that these methods have a number of limitations that hinder their use in many sectors. These limitations relate to the various processes involved in additive manufacturing, such as pre-machining, post-machining, quality control and all those processes that are updated to improve the final product; in all these cases, the feasibility of prototyping is affected. Thanks to research, innovation and technological development, these constraints can certainly be overcome in the future.
The main limitations of additive 3D modelling include:

- *Developing technologies*: some of these technologies are still in their infancy; therefore, a tool is only likely to be outdated after a few years.

- *Availability and cost of raw materials*: many of the materials used in 3D printing are very expensive, particularly when looking for specific properties; polymeric material are the most accessible, affordable and simple materials in this respect.
- *Initial investment*: many of the machines have a very high initial cost, especially the large ones.
- *Size of models*: this depends on the size of the worktop; obviously, if the worktop does not allow to make large objects, it is possible to make the various parts of a model individually and assemble them later.
- *Unprofitable mass production*: additive prototyping generally aims to produce limited series of between 1-10 units, so the technology applied to large-scale production is not profitable.
- *Finishing and precision*: If you want to achieve a good finish and precision, you need to carry out a post-processing process, which in some cases means the addition of other, more expensive technologies and machinery.
- *Obtaining digital files*: a good knowledge of CAD software is necessary to use customised and specific models.

More specifically, FDM technology has a limited surface finish and low printing speed compared to other 3D prototyping methods [38].

1.2 USING DIGITAL FABRICATION IN THE FIELD OF CULTURAL HERITAGE

Although digital fabrication methodologies have developed mainly for industrial and medical applications, in recent years, thanks to the increased accuracy of current technologies and the reduction of reproduction costs, they have proposed new opportunities also for the Cultural Heritage sector. 3D scanning is able to offer an essential contribution to the documentation and analysis of heritage, as it can be applied for different purposes: study, diagnosis, repair, protection, conservation, communication-dissemination and use. There are therefore many applications of 3D prototyping in the field of Cultural Heritage.

- *Production of copies in different scales for temporary or permanent replacement*. Traditionally, to produce a replica of a work of art, a cast is made, i.e. a copy of the relief was made using wax, clay or plaster. However, this method requires direct contact and might compromise the state of preservation of the object, in some cases damaging the most fragile parts. For these reasons, digital fabrication can be a valid alternative, as it

allows copies that are very similar to the original, without directly affecting the surface to be reproduced. 3D scanning and photogrammetry, for example, allow definition of copies of high precision, preserving all the various details and duplicating complex geometries that are difficult to reproduce using traditional methods.

Three-dimensional replicas can be used to replace the work of art in a museum if the original object has to be restored or used for a temporary exhibition. Or, on the contrary, the replica could represent a permanent replacement of the good itself, in case the latter is subjected to degradation, which compromises its integrity and, therefore, its preservation. Thus, the original is moved to a protected and controlled environment, while maintaining its concept and value at the original site, by means of the 3D copy [39,40].

An example of a three-dimensional replica, on a 1:1 scale, is the statue of the Prophet, originally placed in one of the entrances of the Florence Cathedral. Due to atmospheric pollution and its consequent deterioration, a copy was first made entirely of polystyrene using a CNC robotized milling machine (Fig.7); subsequently, only the head was reproduced at the request of a private individual, again on a 1:1 scale, using marble, first sculpted using another robotized milling machine (Robostone 3000) and then with manual intervention, to create the details (Fig.8) [41].

Figure 7. A three-dimensional replica of the Prophet's statue, made of polystyrene, thanks to the use of T-scan and Laser Tracker system [41].

Figure 8. A three-dimensional replica of the Prophet's head thanks to the use of FDM [41].

- *Support for visually impaired people and support for tactile paths*. The use of three-dimensional prototyping, in particular the CNC system, can also ensure that visually impaired or blind people can explore works of art through their fingers, without touching the original directly; the technologies have also been adapted to recreate paintings or photographs in three-dimensional models giving interesting results (Fig.9). Concerning tactile representations of paintings, there is a project, the "Tactile Painting", which presents a computer-assisted workflow to build models suitable both for blind and visually impaired people and as learning tools in museums and galleries [42].

  The solution is usually offered by the use of tangible replicas on a small scale, or by adopting a series of methods to improve perception, through the introduction of various details and the use of a material that is quite similar in the tactile feeling to the work itself; studies are being carried out in this regard.

  In some cases, however, in addition to the tactile power, a multisensory experience is proposed, such as the creation of a coloured relief, with the aim of increasing the interest of children and all visitors, since it is through touch that we understand and experience the outside world. An example of multisensory technology is offered by Tooteko (Fig.10), an intelligent device that combines touch and hearing. In this way, tactile models of works of art become 'talking models' through the use of NFC tags, thus ensuring an interactive and independent visit.

  Unfortunately, there are still few museums dedicated entirely to tactile models; among them are: the Museo Omero in Ancona, the Museo Tiflològico in Madrid, the Museo Salvini in Varese and the Tactile Museum ANTEROS in Bologna [39,40,43].

Figure 9. 3D copy of a painting, Raphael, Madonna of the Meadow (Kunsthistorisches Museum, Vienna) [42].

Figure 10. The Tooteko Multisensory System allows to explore the surface of the 3D replica with the fingertips and get audio content in return. It is possible to read NFC tags when the tip of the finger reaches a hotspot [40].

- *Creation of packaging and support structures for transporting or displaying works of art*. Digital fabrication lead to the possibility to create made-to-measure apparatus and support packaging, necessary for the transport, storage or display of works of art. In this way, thanks to the computerised method, an ad hoc structure is created, avoiding all the inconveniences that can be encountered with manual processes (measurement errors, unsuitable material, etc.). Recently, an algorithm has been proposed for the semi-automatic production of customised structures using a CNC milling machine. The algorithm allows the selection of the most suitable material, in terms of chemical composition and softness, for the individual asset to be protected. It also allows the measurement of the optimal laying for the work, maximising the contact surface and the perpendicularity of the normal to the contact surface with respect to the base of the structure.

  In addition to the algorithm, production methods, both additive and subtractive, have been developed to make the packaging required for transport.

  An example of structures built by means of additive manufacturing is given by wireframes, made of a material that should be softer at the surface level, i.e. in the part that comes into direct contact with the work itself (Fig.11) [39].

  A different methodology, based on subtractive prototyping by means of high-precision milling, are Unocad's protective flavours. Thanks to 3D scanning, a high-definition

mathematical model of the work is acquired; then, the weight is estimated in relation to the material and the functional barycentres of the object to be supported are identified in relation to its displacement. Then, on the basis of this information, a negative EPS (Sintered Expanded Polystyrene) stand-in is obtained and here, the work of art is placed, fitting positively. This protective shell is then placed inside a containment box, thanks to which external pressures and tensions are reduced, i.e. any stress or vibration that could damage it is avoided (Fig.12) [44].

Figure 11. Example of a wireframe lattice structured produced to tightly fit around the shape of the artwork [39].

Figure 12. Protective wrapping made for the Saint John of Ubeda attributed to Michelangelo. The sculpture is in the church of San Salvador in Ubeda (Spagna) and was recently restored by the Opificio delle Pietre Dure (Firenze, Italy), needing to be moved from its usual location [44].

- *Museum education and merchandising*. In recent years, museums have tried to modernise, adopting new technologies to digitise their collections and make them available virtually on websites and social networks. The ultimate goal of these institutions is to attract the interest of visitors before they physically reach the site. Therefore, 3D printing is the next step, as by making digital models available to everyone, the file can be downloaded to print. Interesting is, for example, the Smithsonian X 3D project, which makes entire museum collections, and more, available in 3D format via a free WebGL-based explorer plug-in. The user is then able to manipulate the data, interact with the model and visualize all the various details [45]. In other cases, however, the use of an

external website other than the official museum site is proposed, such as Thingiverse [46], where 3D printing experts and enthusiasts upload their virtual 3D models and the files needed for printing. The Metropolitan Museum of Art and the Brooklyn Museum in New York and the Art Institute of Chicago are just some of the museums that have encouraged such projects.

Obviously, there is an artistic and sociological difference between the musealised object, which is immutable and to be preserved, and the 3D printed model, which is open to experimentation and modification. One of the proposed and very interesting initiatives was offered by the Metropolitan Museum of New York, a few years ago: experts could scan and modify some works from the collections, proposing a mashup of different works (Fig.13). From there, some sites offer users the possibility to mix works and create so-called 'hybrid' works, which can be shared online.

In other cases, however, museums focus on interactivity, i.e. on the formation of workshops and educational paths. Museum makerspaces, for example, provide computers, specific software and 3D printers, allowing the public to make small, low-resolution copies of works of art.

Certainly, merchandising in the museum field is also a fundamental aspect; one idea could be to offer visitors the possibility of choosing, during the tour, the object that strikes them most, photographing it and sending the file, for example, via an app or on the museum website, to order a small-scale 3D printed reproduction.

Certainly, the various projects such as Thingiverse and other proposed initiatives could become a business in a society that is increasingly opening up to digitalisation and the use of innovative technologies [22,39].

Figure 13. The unione of Leda and the Marsyas of Moneghan [22].

- *Support for study, research and the different phases of restoration of monuments*. In general, restoration work is extremely complex, involving a variety of professionals, such as restorers, architects, engineers, art historians, chemists, etc. Each of them draws

conclusions about the specific case study, which are then collected in a series of documents. Furthermore, each phase (analysis, study, intervention) has to be documented, as it is essential for experts to have access to data, especially if the asset requires monitoring or future maintenance. Usually, a purely two-dimensional approach based on drawings and images is used for documentation. Only in recent years, however, the use of 3D digital representation has been proposed to collect all the data and to have a global and holistic perspective of the restored monument or architecture. An interesting example is the implementation of a web-based IS (Information System) to restore the Neptune Fountain in Bologna. The technology allows direct interaction with the high-resolution three-dimensional model, consulting all the documents associated with the model and all the phases and interventions carried out. Thanks to the innovative IS system, therefore, it is possible to archive all the operations carried out on the artefact, i.e.: an initial visual analysis, the history of the fountain with any previous restorations, the mapping of the forms of alteration and degradation, the information obtained from analytical investigations, and, finally, an outline of the work carried out. Furthermore, using a graphic user interface, GUI, it is possible to establish, for each phase, the operator who inserted a file, with date and time, the type of activity (maintenance, visual study, chemical analysis, intervention) and the location of the selected element; in addition, attachments can be uploaded, i.e. documents and photos (Fig.14) [47,48].

In general, a 3D model can present several purposes, and for each of them, the final objective is to document all the information. In addition to supporting the research and conservation phases, three-dimensional prototyping, a non-invasive method, can be an important tool to evaluate the effectiveness of different cleaning treatments. This is the case, for example, of several fragments of wall paintings from two archaeological sites: some, from the 2nd century AD, belonging to the Sala del Mosaico de los Amores at the Castulo site (Linares, Jaén province, Spain), others, from the 14th century, belonging to the Alcázar de los Reyes Catòlicos in Córdoba (Spain). The work involved: acquiring the images with a camera; aligning the images with software capable of extracting pairs of equivalent points; constructing the point cloud, i.e. the 3D model; creating the polygonal model and then the texture. The aim of the study was to provide a methodology, absolutely non-invasive and repeatable, able to objectively evaluate the cleaning treatment through the quantification of the thickness of the removed layer (Fig.15) [49].

Another very important use of 3D reconstruction concerns the integration of missing parts in sculptures, which can be reproduced quickly and accurately. Obviously, during the design and realisation of the missing part, it is necessary to respect the total homogeneity of the work, i.e. the part to be added should present a minimum visual impact, as well as

avoiding further damages due to a different mechanical behaviour, thus a different answer to vibrations and stresses.

An example is the integration of a part of a Roman frame from the archaeological site of Castulo (Spain), using photogrammetric techniques, specific software and 3D printing. After selecting the fragment, photogrammetric mapping was performed with Agisoft Metashape software, virtual reintegration of the missing part was performed with Blender and 3D Builder, and finally, the model was 3D printed. As printing technique was chosen FDM, while the material used was PLA, as it is a cheap material, easy to print and has good adhesion properties. Moreover, white PLA was chosen as the printing material because it allows to apply a colored finish, using an acrylic paint and natural pigments to give homogeneity to the whole structure. It was then possible to adapt the missing part to the rest of the frame, which is made, according to physical-chemical analysis, of calcium carbonate and a minimum amount of quartz (about 4%).

Moreover, the applied piece is completely autonomous, i.e. it has not been attached to the original, thus respecting the principle of reversibility. In fact, the 3D Builder software made it possible to create an object that could perfectly match the geometry of the frame (Fig.16) [50].

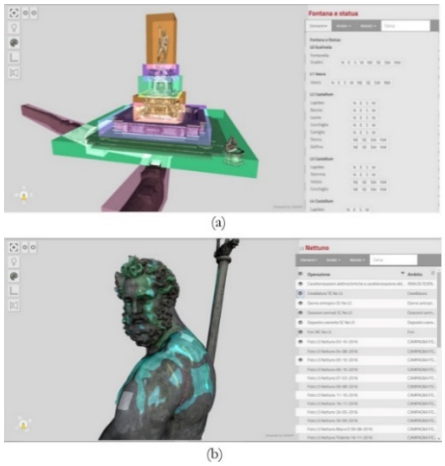

Figure 14. The IS system to restore the Neptune Fountain in Bologna; (a) interactive exploration interface allows you to select the area of interest, (b) and, considering a specific area, there are all the information relating to the operations performed [47].

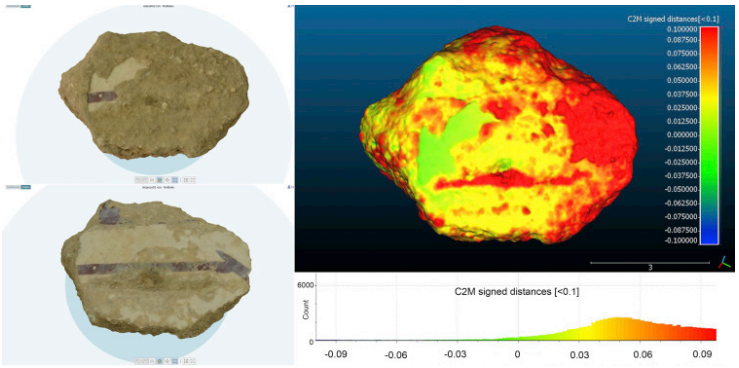

Figure 15. Evaluation of the cleaning treatment of a fragment; on the left the two fragments, before (above) and after (below) cleaning, on the right the distance distribution map with the histogram of the percentage distance distribution [49].

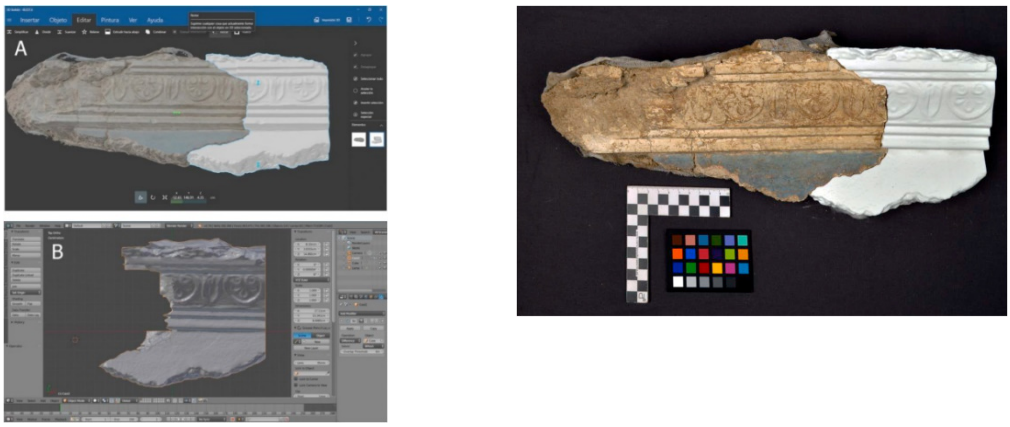

Figure 16. On the left the reconstruction of the missing part of the frame, using 3D Builder; on the right the 3D printed reintegration [50].

1.3 COLD PLASMA AT ATMOSPHERIC PRESSURE

Plasma was first defined in 1928, when Langmuir described it as an ionised gas consisting of free electrons and positive ions in equal numbers, so that the resulting charge is very small. It also contains other chemical species such as negative ions, neutral and radical molecules. Although, from a macroscopic point of view, it is electrically neutral, due to the presence of excited species, the plasma has special electrical properties, proving to be an excellent electrical conductor.

Plasma has been defined as the fourth state of matter and constitutes about 99.9% of all matter in the universe. Therefore, the states of matter progress in the sequence solid, liquid, gas and plasma [51].

The fourth state of matter can be described according to a number of parameters: density of the component species (expressed in $1/m^3$), i.e. electrons (n_e), ions (n_i) and neutral species (n_0); degree of ionisation, given by $a = n_i / (n_i + n_o)$, where a can take values between 0, in the case of weakly ionised gases, and 1, for fully ionised gases. A third parameter is represented by the temperature,

whose value varies according to the average energy of the different species present within it, and is directly proportional to the collisions between the particles; for this reason, plasmas can present multiple temperatures and can therefore be considered as multi-component system.

In general, the temperature difference between the electrons and the heavier particles is proportional to $(E/p)^2$, where E is the electric field generated by the movement of the charged particles that make up the plasma, and p is the pressure. Thus, depending on the type and amount of energy imparted to the gas, both the electronic density and the temperature vary, i.e. two parameters thank to it is possible to distinguish different categories of plasmas.

For low values of the ratio between E and p, a plasma in thermodynamic equilibrium is considered, in which temperatures of the electrons and the heavy particles are similar ($T_e = T_{ions} = T_{neutral}$). This type of plasma is defined as *plasma in thermal equilibrium*, or *plasma in thermodynamic equilibrium* (LTE - Local thermodynamic equilibrium) and is represented in nature by the solar corona. This type of plasma occurs when transitions and chemical reactions are governed by collisions and not by radioactive processes. Moreover, the collision phenomena themselves should be micro-reversible, i.e. each type of collision must be balanced by its inverse: excitation/de-excitation, ionisation/recombination, and so on.

In particular, LTE requires that the local gradients of plasma properties, such as temperature, density and thermal conductivity, are low enough to keep it in equilibrium.

On the contrary, high values of the E/p ratio indicate the so-called "*non-equilibrium plasmas*", "*non-thermal plasmas*" or "*cold plasmas*", or even plasmas in non-LTE (*Non-local thermodynamic equilibrium*), where the electronic temperature, with a value of about 1 eV (about 11605 K), is higher than in neutral species, which have an approximately ambient temperature of about 300 K ($T_e > T_{ions} = T_{neutral}$). Therefore, the plasma is referred to as "cold", since it is the temperature of the heaviest particles that determines the total temperature of the gas. In nature, an example of a non-equilibrium plasma is the aurora borealis.

In the industrial field, both categories of plasma are used: thermal plasma, being more energetic, is applied to make cuts, while cold plasma is mainly used to carry out surface modification.

The main characteristics of LTE plasma and non-LTE plasma are summarised in Table 2.

Table 2. The main characteristics of LTE plasma and non-LTE plasma, considering the name, the properties and some examples [52].

	LTE plasmas	*Non-LTE plasmas*
Name	Thermal plasmas	Cold plasmas
Properties	$T_e = T_h$. High electron density: 10^{21}-10^{26} m^{-3}. Inelastic collisions between electrons and heavy particles create the plasma reactive	$T_e > T_h$. Lower electron density: < 10^{19} m^{-3}. Inelastic collisions between electrons and heavy particles induce the plasma chemistry.

	species whereas elastic collisions heat the heavy particles.	
Examples	Arc plasma (core) $T_e = T_h \approx 10.000$ K	Glow discharge $T_e \approx 10.000$-100.000 K $T_h \approx 300$-1000 K

Finally, the last parameter to be considered is pressure, by which it is possible to distinguish two types of cold plasma: low-pressure or vacuum plasma (*Low Pressure Discharge* or LPD) and atmospheric pressure plasma (*Atmospheric Pressure Discharge* or ADP) [52-54].

1.3.1 Atmospheric plasma sources

A plasma is generally created when energy is applied to a gas, with the aim of rearranging the electronic structure of species, such as atoms or molecules, and thus producing excited species and ions. The energy used may be thermal in nature, or it may be carried by electric current or electromagnetic radiation [52].

The simplest method of generating a plasma is through the use of electromagnetic fields. In particular, the sources of cold plasma at atmospheric pressure can be distinguished according to how the chemical compounds are excited:

- *Direct current (DC) and low frequency discharges*, with a system that can operate in either a continuous or pulsed mode. Generally, DC discharge consists of a circuit system in which there are a cathode and an anode, separated by a gas-filled gap. In this way, it is possible to generate the plasma by applying a continuous voltage to the electrodes, thanks to certain molecules and atoms of the gas are ionised. Arc plasma, corona discharge plasma and dielectric barrier discharge plasma (DBD) are often part of this category.

  Arc sources consist of an electrode (cathode), a nozzle and a flame. The discharge takes place between the two electrodes, where the temperature is very high (approximately 8000-15000 K), as is the electronic density ($10^{21} \div 10^{26}$ m^{-3}). Recently, cooler arc torches have been developed to treat, heat-sensitive surfaces.

  Conversely, where fewer thermal applications are required, it is preferable to use corona discharge plasma and DBD. In these systems, in fact, the densities reached inside the plasma are much lower than in arc plasma, as well as the temperatures reached by the gas. Furthermore, in order to promote the interaction of chemical species with the surface to be treated, it is preferred to apply noble gases or nitrogen [53-55].
- *Plasmas excited by radio frequency (RF) waves*, which can be either high or low power. In the first case, the plasma is generated using frequencies above 1 MHz, and is used above all for spectroscopic analyses, through ICP (inductive coupled plasma)

instruments, and for waste disposal; in this case, high-power RF plasma is able to reach the "local thermal equilibrium" (LTE) where electrons and ions have the same high temperature. Low-power RF plasma, on the other hand, is the most widely used and is represented by several possible configurations like, for instance, the *Atmospheric Pressure Plasma Jet* (APPJ).

The first system is reminiscent of arc torches, and can be made up of two concentric electrodes through which a specific gas (argon or helium) is ionised and then exits the nozzle at a speed of about 12 m/s and a temperature of about 150 °C.

In the latter source, the temperature of the outgoing gas is approximately 400 - 500 °C, whereas the electronic density is 10^{17} - 10^{18} n_e/m^{-3} [53-56].

For this project an innovative plasma device has been used. It is a dielectric barrier discharge (DBD) plasma jet characterized by a dual frequency generation system, able to ensure a low current and low temperature plasma with a high ion content and efficiency (Fig. 17). The plasma device has been provided by Nadir Srl (Italy) and is fully described in part 2.1.2.

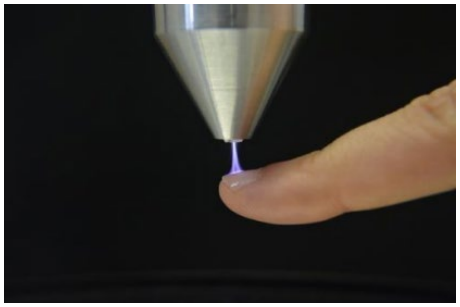

Figure 17. Nadir plasma jet device [54].

- *Microwave discharges or Microwave Induced Plasma (MIP) sources*. A source in the system transmits microwaves, that transmit energy to the electrons in the plasma, resulting in elastic collisions between the electrons and heavier particles. Elastic collisions, which are described according to probabilistic laws, produce a series of inelastic collisions on the electrons, which cause a process of ionisation of the gas, finally transforming it into a plasma. The components of the system are: microwave source, system guiding and transmitting the microwave beam, gas injection system and ignition system for the ionisation process [53,54,56].

A summary of the ionisation potentials and the density of the charged species for the different types of plasma described above is given in Table 3.

Table 3. A general description of the ionisation potentials and the density of the charged species for the different types of plasma [54].

Source	V [kV]	Density [m^{-3}]
Low-pressure discharges	0.2 ÷ 0.8	$10^2 \div 10^7$
Arc and plasma torches	10 ÷ 50	$10^{10} \div 10^{13}$
Corona	10 ÷ 50	$10^3 \div 10^7$
Dielectric barrier discharges	5 ÷ 25	$10^6 \div 10^9$
Plasma jets	0.05 ÷ 0.2	$10^5 \div 10^6$

1.3.2 The different functionalities of atmospheric plasmas

Thanks to its ability to produce a particularly reactive atmosphere, atmospheric cold plasma finds a variety of applications in many fields: in the textile field, as a surface pre-treatment and finishing technique, in the biomedical field, for the sterilisation of surfaces and fabrics and for tissue healing, but also for environmental applications, and in particular in the field of materials science. In the latter case, the treatment can be applied to carry out a cleaning treatments, but also to carry out erosion or activation (or functionalisation) processes; all these modifications take place only at the surface level.

The surface cleaning process consists of removing oils, dust, chemical and biological agents and any other form of contamination present. Of course, the effectiveness of the technology depends on the type of source and the type of contaminant present; however, plasma at atmospheric pressure can remove any type of organic contaminant. An example of this is the restoration work carried out on the "*Capsella Vaticana*," during which cold plasma cleaning was done to convert silver oxides and sulfides into metallic silver. In the areas where it was structurally impossible to reach with plasma, chemical cleaning was used, using calcium carbonate and wooden chisels [57,58].

Erosion, on the other hand, is carried out when helium is applied, introducing a small amount of oxygen, promoting what is known as surface *etching*; this method is mainly used in the field of electronics.

Another function of plasma is activation or functionalisation, aiming 'preparing' the surface for subsequent treatments, for example by improving wettability or adhesion properties. Plasma therefore promotes the introduction of new functional groups at the surface, the nature of which depends mainly on the gas used: gases or gas mixtures containing oxygen increase the hydrophilic character of the surface, introducing a series of polar groups (-COOH, -OH, $-NH_2$) and/or radicals, and also lead to an increase in adhesion, thanks to the introduction of functional groups related to the material, or in any case capable of interacting chemically with it; while fluorinated gases or

CF_4 or SF_4 give a hydrophobic and anti-adherent character to the material. The effectiveness of the treatment can be measured by contact angle ($\alpha > 90°$: hydrophobic surface, $\alpha < 90°$: hydrophilic surface) to be carried out immediately before the next treatment.
Plasma can also function as a reactive chemical agent, as it can initiate polymerisation reactions, forming surface functional deposits, with the aim of obtaining specific properties from the material.

Despite the numerous functionalities offered by plasma, the focus of this thesis will be on improving the surface wettability and adhesion properties of polymeric materials.
Nowadays, plasma methodology ranges from the textile industry to printing on synthetic coating materials. In the specific case of polymers, the application of atmospheric plasma can produce ablation, cross-linking and activation effects at the surface level.
Therefore, when non-LTE plasmas are applied to a polymer surface, a number of changes are induced to the surface energy, wettability, adhesion, surface electrical resistance, dielectric permectivity, gas absorption and permeability characteristics. Generally, the most common methodology involves non-LTE discharges at low pressure, or atmospheric pressure, which is required to carry out surface cleaning and wettability modification treatments. The interaction between plasma and polymer surface can cause both the breaking of chemical bonds between polymer macromolecules and new molecular recombinations. Obviously, the effects of non-LTE plasma can only be seen at the surface.
The most important resulting changes, however concern, as stated above, both the surface wettability and the adhesion properties of the material. If the plasma, for example, contains a certain amount of oxygen, it causes an increase in the wettability of the material. At the chemical level, the plasma-polymer interaction results in the formation of polar groups, which leads to an increase in surface energy, adhesion to organic compounds and metals and, in particular, wettability. Using photoelectron spectroscopy, it is possible to justify this behaviour, since, due to the presence of oxygen, oxidation of the polymer occurs, i.e. the oxygen forms, for example, peroxides, alcohols, carboxy-acid groups and aldehydes. The various functional groups formed are of low molecular weight, which is why, at the end of the process, a substantially cleaner surface is achieved.
Obviously, the effects obtained as a result of plasma treatment will depend on the nature of the gas applied: in presence of air, oxygen, nitrogen and ammonia, the surface changes from hydrophobic to hydrophilic; on the other hand, in contact with fluorine, the hydrophobic character of the material increases. Furthermore, wettability is directly proportional to gas pressure, treatment time and discharge current.
Wettability, as already mentioned, is accompanied by adhesion, which tends to increase with the surface energy of the material undergoing treatment.

The methods most commonly used for these purposes are: Corona Discharge Treatments (CDT) and cold plasma treatments at atmospheric pressure, by means of dielectric barrier discharges (Atmospheric Pressure Plasma - Dielectric Barrier - APP-DB). Although final results depend on plasma power and exposure time, the APP-DB methodology ensures good efficiency, greater control over the final chemistry and improved surface wettability [54, 59-62].

1.4 APPLICATION OF PLASMA IN 3D PRINTING

The use of additive manufacturing, or 3D printing, coupled with cold plasma treatment at atmospheric pressure, as well as representing a completely innovative and still little-known technology, constitutes one of the main objectives of this thesis.

In particular, the project aims at studying the durability of printed specimens based on polylactic acid (PLA), a polymer that, as mentioned in the previous paragraphs, has undergone significant development for its biodegradability, compostability and sustainability.

PLA, a polyester made from 100% renewable raw materials, has been used, especially in recent years, in the industrial and medical sectors as a primer for printing or inks, as an adhesive or to create surface finishes. However, since it is inert and quite hydrophobic, forming a contact angle of around 80° with water, various types of treatment are often used to chemically and physically modify the surface.

Chemical treatments are generally discouraged, as they tend to produce waste and environmentally harmful waste. Therefore, the application of plasma is generally preferred, which, in addition to not being harmful to the environment, manages to selectively modify the surface layer of the material, without damaging or altering it. In fact, by appropriately selecting the parameters, such as the pressure and the chemical composition of the gas, a specific modification of the object is carried out, for example: generation of highly reactive functional groups, change in free surface energy, increase in the hydrophilic or hydrophobic surface character, removal of organic impurities and modification of polymer cross-linking and surface morphology [63-67].

Argon plasma has been shown to significantly improve adhesion and lead to a significant increase in surface roughness by forming free electron pairs in carbon atoms. According to a study, conducted by J. Podsiadly and E. Dörsam [63], it was found that Ar plasma improved the hydrophilic character of a PLA film; however, the surface modification is not permanent, as the contact angle measured for the samples tends to increase over time. In addition, the treatment led to an increase in surface roughness and increased resistance to ageing.

The same results are also confirmed by A. Vilaplana et al [64], who demonstrate, thanks to FTIR analysis, the cross-linking of the polymer chains, i.e. the fragmentation of the compound with the

formation of low molecular weight fractions. Moreover, they claim that the best results obtained with surface treatment using atmospheric plasma are obtained at low feed rates, around 100÷300 mm s-1, and with a nozzle-substrate distance of 10 mm.

From a chemical point of view, when Argon plasma interacts with the polymer surface, it causes the cleavage of the C-H and C-C bonds and leads to the formation of a series of carbon radicals both in the center and in the two terminal positions of the chain. The radicals, being highly reactive species, tend to oxidize, forming different functional groups: hydroxyl, carbonyl, carboxyl, etc. The oxidation process, however, is accompanied by degradation reactions, during which the carbon radicals in the terminal positions give rise to low molecular weight compounds, i.e. monomers that separate from the polymer chain.
The figure 18 summarises the possible reactions that can occur on a PLA film when exposed to Ar plasma.

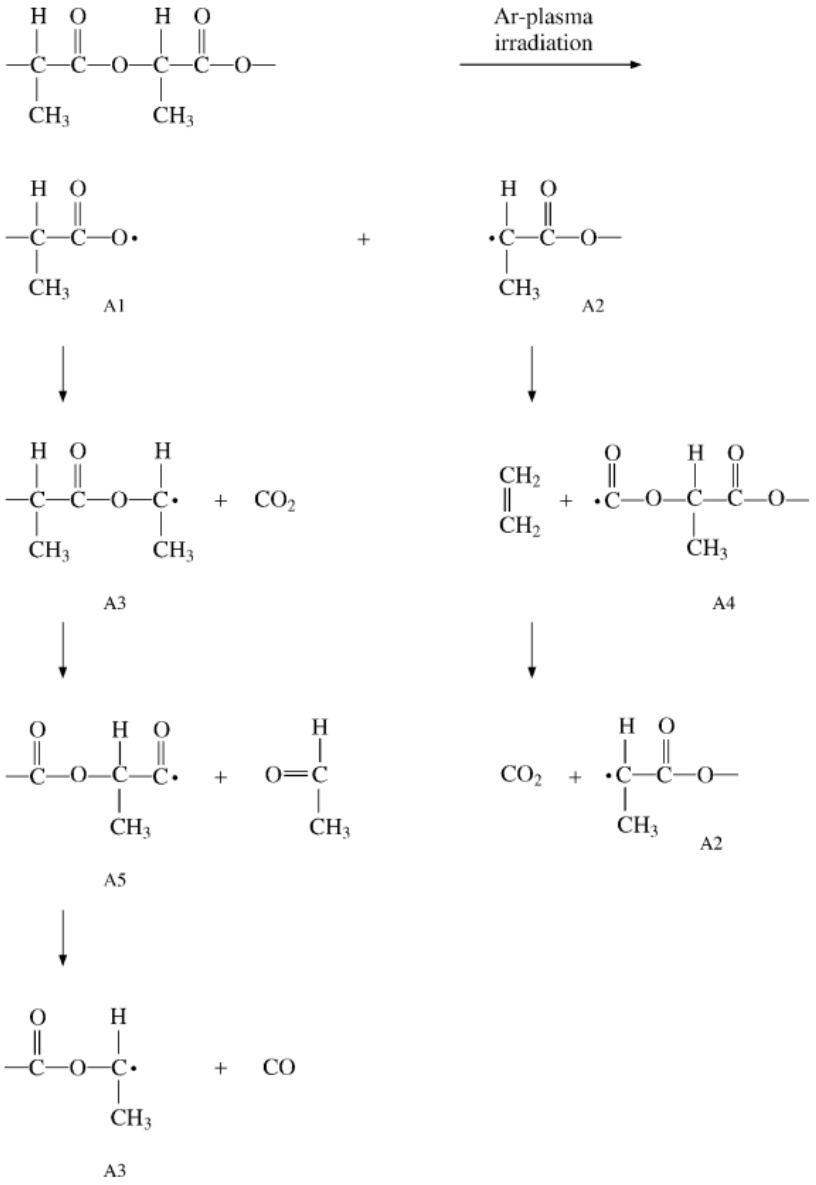

Figure 18. Possible reactions on a PLA film when exposed to Ar plasma [65].

Exposure to Ar plasma causes the C-O bond to split, resulting in two radicals (A1 and A2), which in turn, being particularly unstable, tend to eliminate CO_2 and CH_2=CH_2 to form A3 and A4 radicals. Subsequently, the A3 and A4 radicals are transformed into A5 and A2. From here, the A5 radical will become A3, eliminating a CO molecule. Therefore, from the initial splitting of the CO bond, the various radicals will begin to form, and at the same time low molecular weight molecules (CO_2, CH_2=CH_2, CHO-CH_3 and CO) are eliminated until two radicals react.

At the end of the Ar plasma treatment, no more radicals remain on the PLA surface; moreover, the formation of oxygen functional groups could be due to post-oxidation of the radicals present on the material [65].

Considering a situation similar to the previous one, when the treatment of polylactic acid with a plasma stream is prolonged, a destruction of polymer bonds occurs with a consequent formation of volatile gases.

Figure 19 shows oxidation, a reaction also described by Figure 16, and the subsequent destruction of the thermoplastic polymer due to prolonged plasma treatment. The interaction between the radicals and the oxygen leads, therefore, to the formation of the peroxide group, which is highly unstable and for this reason there is the destruction of some bonds with the formation of new radicals, from which new crosslinks are eventually obtained [68].

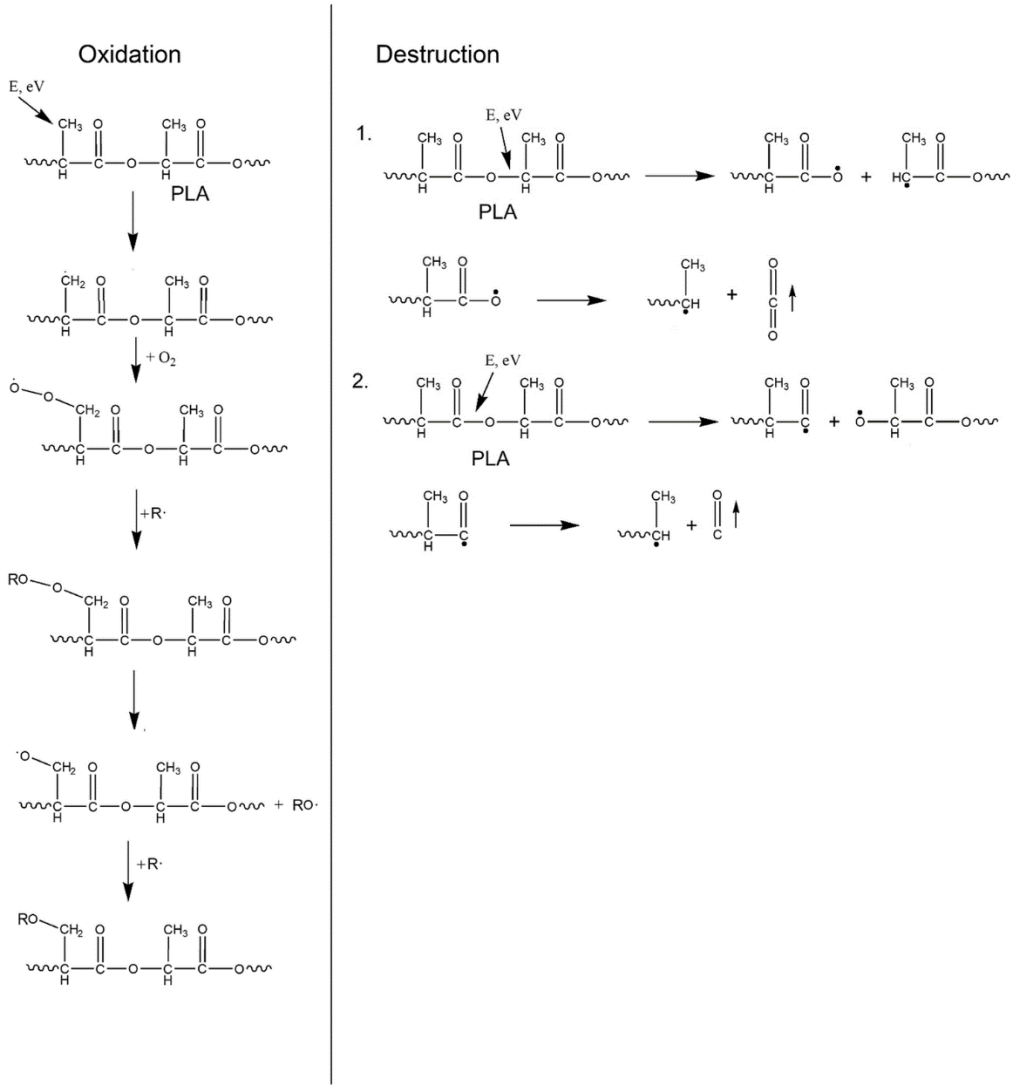

Figure 19. Two reaction processes that occur in PLA during plasma treatment. On the left is an oxidation reaction (also described by Figure 16); on the right is a destruction reaction, in which free radicals and volatile compounds are formed [68].

During the fabrication of the specimens, vapours of a chemical precursor have been added to the Argon gas. The precursor used is tetraethyl orthosilicate (TEOS), an organosilicate having formula $Si(OC_2H_5)_4$ and a three-dimensional tetrahedral structure, where each vertex is occupied

by an ethyl group, bonded to the central SiO_4^{4-} orthosilicate ion (Fig.20). TEOS at room temperature appears as a colorless liquid having a low surface tension [69].

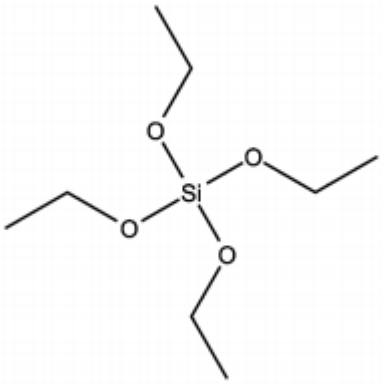

Figure 20. Chemical structure of TEOS.

Traditionally, siloxane-based precursors were applied using O_2/SiH_4 or N_2O/SiH_4 plasmas, although they soon began to be replaced by TEOS, as it is non-toxic, easier to handle and provides good deposition and thus surface coverage [70].

Therefore, the coating of tetraethyl orthosilicate, applied by plasma polymerization, involves a number of changes to the material, which will depend on the number of steps performed above the material.

From the chemical point of view, however, there is an increase in the degree of surface oxidation, with a consequent increase of oxygen-containing functional groups (C-O, O-C=O) and decrease of carbon groups (C-C/C-H); the effect is due to both the energy of the plasma and the oxygen present in the atmosphere. The application of TEOS also tends to increase the concentration of silicon, forming Si-Si and Si-O groups.

Obviously, the increase in the O/C ratio confirms the hydrophilic character of the deposited coating [72].

From a structural point of view thanks to a series of studies conducted by Nadir Srl [71], the precursor is able to increase the adhesiveness between polymer layers and thus improve the material resistance to tensile and stress movements. In previous experiences, in fact, it has been verified that the deposition of the siloxanic coating increases the resistance of the printed material if placed in an acidic or invasive environment. Below is an example about the durability of the polymeric material; for the test carried out, in fact, were made of cubes, some of which had undergone a process of deposition of TEOS. Therefore, the treatment parameters followed are reported:

- Plasma power: 30 W
- HMDSN precursor vapors at 0.5 ml/min

- Printing speed: 30-50 mm/sec

During the test, two cubes were immersed in formic acid, a not very aggressive organic acid, and two in acetone, also an organic solvent.

The results are shown in Figure 21

.

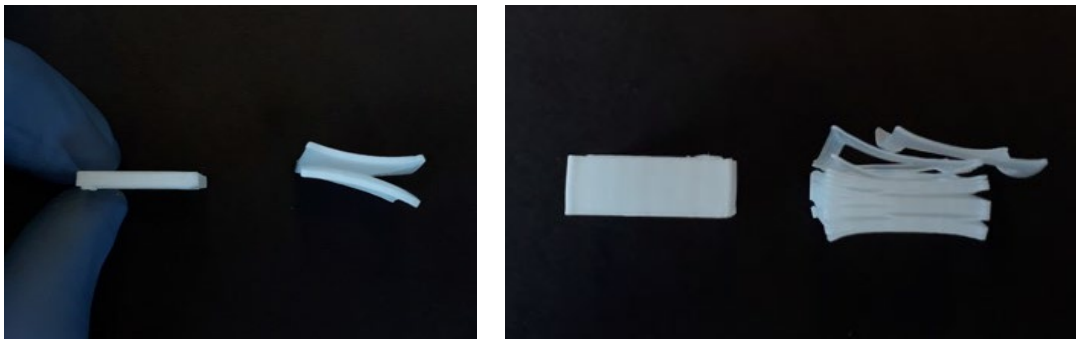

Figure 21. Results obtained following immersion in formic acid (left) and acetone (right): for each image, on the left there is the cube with TEOS, on the right the cube without TEOS.

From the results obtained, it is observed that in the case of the samples consisting of a silazane, the layers remained well adhered, and no signs of detachment or cracking are visible; on the contrary, in the case of the sample without precursor, there is a detachment along the different printed layers, which therefore appear decohesive and inconsistent [71].

1.5 LCA: "LIFE CYCLE ASSESSMENT"

Life Cycle Analysis (known as LCA) is an investigation methodology that allows to evaluate the environmental and energy impacts of products or services in a context well defined by its life cycle. Precisely for this reason, the first step is to clearly delineate the boundaries of the system on which you want to act.

To clarify the functionality that the software can offer, the definition of "Life Cycle Assessment" of 1993 is reported, proposed by SETAC ("Society of Environmental Toxicology and Chemistry"), according to which a LCA is "*an objective process of evaluating the environmental loads associated with a product, process or activity, through the identification and quantification of energy, materials used and waste released into the environment, to assess the impact on the environment and opportunities for environmental improvement for its reduction*".

Thus, to carry out this analysis it is a must to draw up an inventory establishing the materials, raw materials, transportation, disposal of by-products and materials and all other detailed flows that characterize the process.

The basic idea is to characterize a system through life cycle analysis, starting from the creation/extraction of raw materials up to the disposal of the system and the products formed (*cradle-to-grave* approach). The LCA technique also allows impact assessments of different end-of-life scenarios to be presented early in the design stages, such as partial or total recycling of end products. For scenarios where recycling is considered, it is referred to as the "*cradle-to-gate*" approach, in which the life cycle is evaluated starting from the production of materials until recycling.

Therefore, LCA was created with the objective of assessing the maximum useful life of materials, estimating their impacts during their life cycle; for these reasons, especially in recent years, it has become a particularly widespread technique in various scientific circles and a valid tool for the development of policies aimed at environmental protection.

The Life Cycle Assessment is regulated by ISO 14040 and is based on four study phases (Fig.22):

1. *Definition of aims and objectives*, in which the temporal, technological and geographical area of the system is established. During this first phase, the functional unit to be referred to according to the type of process is proposed, and the system boundaries are defined by identifying the necessary data.
2. *The Life Cycle Inventory (LCI),* in which all data relating to emissions, resources used, and products are presented, specifying them as input and output flows.
3. *Life cycle impact assessment (LCIA),* in which potential environmental impacts on the environment and humans are correlated with the cause/effect of each phase of the cycle; then, these relationships are classified using standard units to identify impact categories.
4. *Interpretation of results (LCI),* as the life cycle analysis concludes with the drafting of a report, in which the results are reported. During this phase, it is also possible to include a set of recommendations for improving environmental performance [73-79].

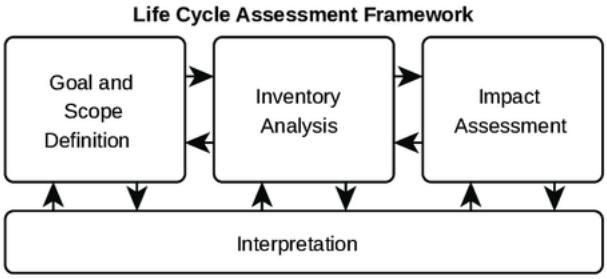

Figure 22. Four study phases of LCA.

1.5.1 Phase 1: Goal and scope definition

The first phase is very important, as it outlines the quality of the work that will be done, defining the data, the parameters, the level of depth of the study and the possible final interpretations. In addition, during this phase it is imperative to establish an objective, functional unit and boundaries.

Going in order, you have:

- The *functional unit* is defined as the unit of measurement to which the analysis refers. Generally, it can be understood as an index of the performance performed by the system or the service rendered to the user. Therefore, in this way it is possible to have a basis of comparison between different products having the same unit.
- *Boundaries*, on the other hand, define the system through the creation of a flow chart, in order to order and collect all the various information of the case you want to consider. During the LCA analysis, moreover, it is important to clarify what is considered and what is discarded as input/output, justifying such choices [73-79].

1.5.2 Phase 2: Life Cycle Inventory (LCI)

During the second phase, the inventory is compiled, including all the various flows required. Precisely for this reason it is a very delicate phase, as it determines the reliability of the system that is to be analysed. In fact, during this phase the flows that have a particular weight in the studied process, and therefore a significant environmental impact, are evaluated. The incoming and outgoing flows are identified as energy consumption (thermal and electrical), resources (raw materials, recycled products and water), emissions into water, soil and air. All values are expressed using physical units, mass and energy units, and normalized according to functional unit. Depending on how the data are collected, they can be classified into:

- Data directly collected in the field are called primary;
- Data derived from literature or databases are called secondary;
- Data taken from other sources are referred to as tertiary.

Whatever the type of data, they will be associated with their respective process units [73-79].

1.5.3 Phase 3: Life Cycle Impact Assessment (LCIA)

LCIA provides a correlation between cause and effect of the individual phases identified by assessing potential impacts. During this phase, in fact, the environmental effects of the analysed systems are estimated in terms of effects on human health, the environment and ecological disturbances of natural resources.

The ISO standard defines environmental impact as "*any change caused by a given environmental aspect, i.e. any element that may interact with the environment*". So LCA is able to calculate environmental loads (e.g. it calculates CO_2 equivalent kg and not average temperature rise), but it does not define the actual changes that occur in the environment.

According to ISO 14040 and ISO 14044 LCIA is distinguished in the following steps:

- *Choice of impact categories and classification*: impact categories are used to define the effects on the environment and on humans, while the term "classification" is used to label inputs and outputs to one or more impact categories. Among the most common and widespread impact categories, there are: Acidification (AP), Global warming (GWP), Eco-toxicity (ETP), Eutrophication (NP), Ozone depletion in the stratosphere (ODP).
- *Characterization*: systems are modeled based on characterization factors for each individual substance. These factors are multiplied by the fluxes present, thus identifying the possible environmental impact. It comes, then, to a limited number of inventory items that represent the "eco-profile", shown graphically through histograms.
- *Normalization*: to compare possible impacts or products, the potential impact is related to a reference unit within the same area.
- *Attribution of weights (weighting) to emphasize the most relevant impacts*: the effects, multiplied by their respective weights, provide "eco-indicators" that quantify the environmental performance of the system.

According to ISO standards, the last two points are optional [73-79].

1.5.4 Phase 4: Life Cycle Interpretation (LCI)

During this phase, an attempt is made to explain and evaluate the results obtained, which should be sensitive, complete and consistent, and in particular, recall the hypotheses proposed in the first phase. Depending on the results obtained, you then try to consider the significant environmental factors in order to provide solutions for improvement [73-79].

1.5.5 Possible disadvantages in using LCA

In some cases, the use of the LCA methodology can be burdensome, non-productive and laborious, as it is essential to acquire a large amount of data, entering in detail all the existential phases. In addition, if specific case studies are examined, as in this case, there is a risk of not finding the specific inputs, thus leading the user to make different choices regarding the input of values [73-79].

Chapter 2

2.1 MATERIALS

The aim of this thesis project is to study and analyse the outdoor stability of PLA, the filament most commonly used in three-dimensional prototyping to create design models and to document and safeguard cultural heritage. In particular, the aim is to verify a possible use of the filament, under the mechanical aspect, for the creation of virtual reconstructions, the realisation of sculptural integrations and the production of copies of artifacts that can be used in museums.
The main characteristics of the material under examination, the methodology and the printing parameters of the samples and, finally, a description of the 3D modelling process coupled with atmospheric pressure plasma technology are reported.

2.1.1 Filament and specimens

For this study, a transparent PLA-based Eumakers filament with no additives and a diameter of 1.75 mm was selected (fig.23).

Figure 23. On the left the chemical structure of PLA; on the right the coil of PLA-based Eumakers filament.

The material selected for the study is the biopolymer Ingeo 4043D, which is suitable for various types of printers and a wide range of printing applications. The filament, which is available in pellet form, demonstrates good melt stability and has excellent printing properties, i.e. it allows the creation of precise details, offers good adhesion to the build plates (so there is no need to heat the work surface) and, during three-dimensional modelling, does not have a strong odour, as it does not release volatile organic compounds and therefore is not harmful to human health (fig.24). Furthermore, the biopolymer can be recycled through a composting process, in which lactic acid, the main constituent of PLA, is degraded and broken down into polymers of lower molecular weight, which are used as nutrients by microorganisms in the soil (bacteria and fungi) [80].

The choice of a pure PLA, i.e. without additives, offers the possibility of investigating only the durability of the polymeric matrix, so as to promote its diffusion in the field of restoration and in the production of copies for museum and educational routes.

Typical Material Properties [1]		
Physical Properties	**Ingeo Resin**	**ASTM Method**
Specific Gravity, g/cc	1.24	D792
MFR, g/10 min[2]	6	D1238
Relative Viscosity[3]	4.0	D5225
Clarity	Transparent	-
Peak Melt Temperature, °C	145-160	D3418
Glass Transition Temperature, °C	55-60	D3418
Mechanical Property		
Tensile Yield Strength, psi (MPa)	8700 (60)	D882
Tensile Strength at Break, psi (MPa)	7700 (53)	D882
Tensile Modulus, psi (MPa)	524,000 (3.6)	D882
Tensile Elongation, %	6	D882
Notched Izod Impact, ft-lb/in (J/m)	0.3 (16)	D256
Flexural Strength, psi (MPa)	12,000 (83)	D790
Flexural Modulus, psi (MPa)	555,000 (3.8)	D790
Heat Distortion Temperature, °C 66 psi (0.45 MPa)	55	E2092

Processing Temperature Profile [4]		
Melt Temp.	410°F	210°C
Feed Throat	113°F	45°C
Feed Temp.	355°F	180°C
Compression Section	375°F	190°C
Metering Section	390°F	200°C
Adapter	390°F	200°C
Die	390°F	200°C
Screw Speed	20-100 rpm	
Filament Diameter Inspection (on-line)	Essential for quality monofilament (+/- 3% max. deviation)	
3D Printing Temp.		190-230°C
Print Bed Temp.		None needed. (or 50-70°C if applicable)

Figure 24. Information regarding physical and mechanical properties and printing conditions taken from the filament datasheet [80].

With the aim, therefore, to obtain statistically valid results (in the case of dynamometric tests, a more reliable result is guaranteed with at least three specimens) and on the basis of the methods of investigation chosen to evaluate the material, 30 specimens were realised, half of which were treated with plasma at atmospheric pressure.

Considering the 15 treated specimens, indicated by the letter "t", and the 15 untreated specimens, indicated by "n-t", it must be specified that: ten are considered as a reference for the proposed analyses and tests (5 t + 5 n-t), ten for artificial ageing (5 t + 5 n-t) and then for dynamometric tests, whereas the remaining ten are subjected to artificial ageing under an incandescent lamp, also followed by the dynamometric test. During the tests, the specimens are subjected to a series of analytical investigations in order to characterise any structural changes.

Moreover, the parameters followed during the manufacture of the specimens comply with the ISO 527-2 standard from 2012, which deals with the tensile properties of plastic materials and provides a description of the test conditions for moulding and extrusion of the same [81]; the dimensions, therefore, are suitable to facilitate the analysis of mechanical strength.

The model of interest is 5B (fig.25), whose measurements are shown in the table 4.

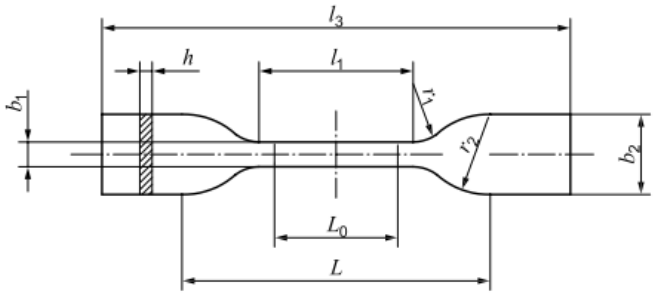

Figure 25. Sample sizes following the ISO 527-2 standard of 2012 [81].

Table 4. Sample size of type 5B, according to ISO 527-2 standard of 2012 [81].

	Specimen type	**5B**
l_3	Overall length	≥35
b_2	Width at ends	6 ± 0,5
l_1	Length of narrow parallel-sided portion	12 ± 0,5
b_1	Width at narrow portion	2 ± 0,1
r_1	Small radius	3 ± 0,1
r_2	Large radius	3 ± 0,1
L	Initial distance between grips	20 ± 2
L_0	Gauge length	10 ± 0,2
h	Thickness	1 ± 0,1

Subsequently, two cubes with a surface area of 1 cm^2 were produced, one of which underwent plasma treatment. The cubes were made to test the resistance of the PLA filament in acetic acid, which, according to the "like dissolves like" rule, should be able to easily hydrolyze the polymer [82]. Obviously, the test puts the material in a totally extreme condition, and, in general, even if subjected to the elements (acid rain, pollutants, etc.), it will never suffer a similar impact to the proposed treatment. Therefore, in addition to assessing the strength of the PLA, differences between the cube treated and not cold plasma are verified, in terms of durability and structural strength.

In order to create the samples, it was first necessary to create a digital model in stp format. An image taken from an open source online programme (3D STP Viewer [83]) describing the structural lines followed during the three-dimensional modelling is shown (fig.26).

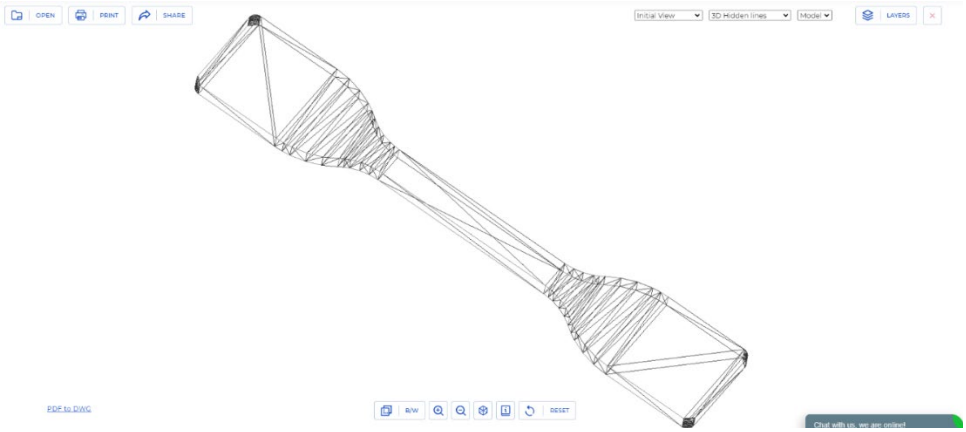

Figure 26. Digital model in stp format of sample [83].

The digital model is then used to 3D print the samples, that are made up of a first base layer, also known as the bottom layer, several filling layers and a final layer, or top layer. Obviously, the higher the number of layers, and therefore the higher the level of filling, the longer it takes to form the object, and at the same time, the better the strength of the material.

For this thesis project, dog bones were made with the DeltaWasp 3MT (Fig.27), an innovative large-format 3D printer capable of creating objects using the FDM technique. The DeltaWasp 3MT printer allows objects to be produced from a variety of thermoplastic materials, such as PLA, ABS, Nylon, TPU and Polystyrene [84].

The tool has been made available by Fab Lab of Venice, located at the Vega - Science and Technology Park, a place where it is possible to do research on digital fabrication and computational processes [7].

The printing area of the instrument is 1m in diameter by 1m in height, whereas the diameter of the extruder nozzle is 3mm. All samples were made with constant printing parameters, as shown below:

- Temperature: 210°C
- Filling: 80% for dog bones, 100% for cubes
- Printing speed: 60 mm/min for dog bones, 40 mm/min for cubes
- Layer thickness: 0.1 mm

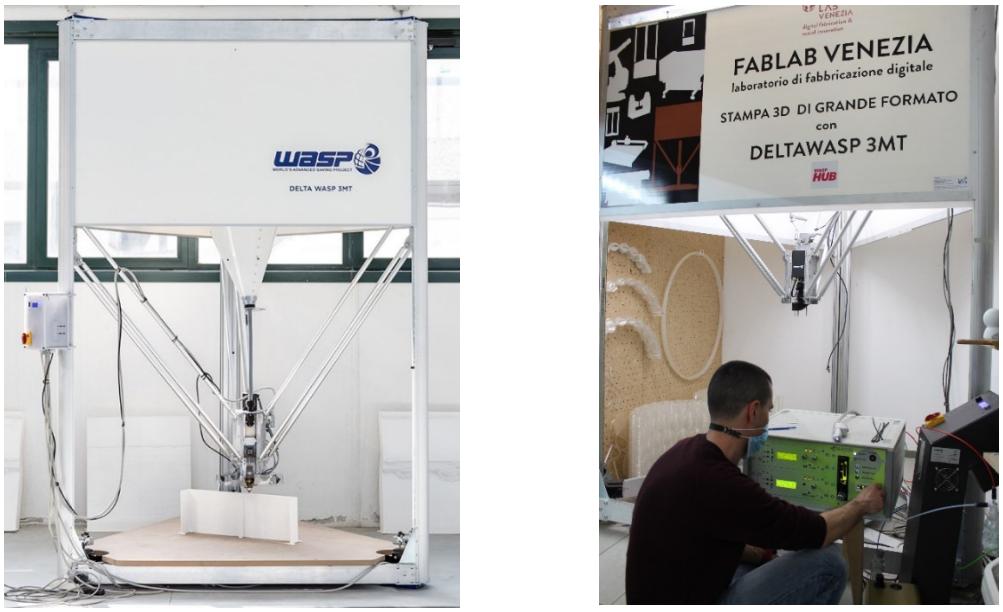

Figure 27. DeltaWap 3MT 3D printer at FabLab in Venice, Italy [85].

Each specimen took about six minutes to be printed and weighed an average of 0.15 g (Fig.28).

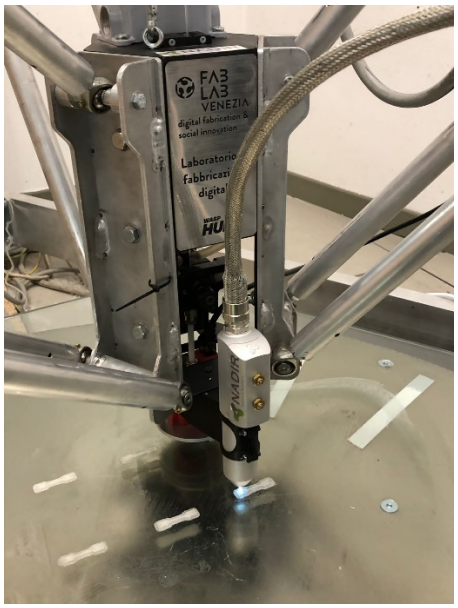

Figure 28. Sample printing phase (on the left) and cold plasma treatment (on the right).

2.1.2 Plasma torch

In order to improve mechanical properties and chemical resistance of the PLA layer, the use of plasma at atmospheric pressure and the deposition of a siloxane-based coating (TEOS) is proposed (Fig.29).

Figure 29. Plasma torch coupled with 3D printer. The torch has been provided by Nadir-tech, a company present at the scientific campus of Ca' Foscari University.

In addition, the proposed surface treatment is based on the deposition of a specific precursor, based on low molecular weight monomers, thanks to which reactive ions and radicals are created that initiate a polymerisation process. As already mentioned, the application involved half of the samples produced by 3D printing.

In more detail, the instrument used in this study is the Stylus Plasma Noble (Fig.30) patented by Nadir Srl (Italy), which consists of a DBD (Dielectric Barrier Discharges) plasma jet, in which the plasma is not in direct contact with the electrode, thus guaranteeing clean processes in which no undesirable deposits are formed.

The electrodes, therefore, are located outside an alumina tube (~6 mm) where argon is purged through, allowing the plasma to be ignited. In addition, the device consists of two other conduits, one internal and one external: the first allows the precursors to enter in the form of gas or aerosol, whereas the second controls the atmosphere outside the torch, where air or nitrogen is generally used [86].

A key feature of the instrument is its low processing temperature thanks to the use of a double pair of electrodes: the first pair upstream has a high-voltage (HV) supply, in the order of kilohertz (~ 17 kHz), and allows low-power stability to be checked, while the second pair upstream has a radiofrequency (RF) supply of 27 MHz and checks plasma stability.

The gas chosen for is argon, as it enables to work with a plasma characterised by a low temperature ($T < 50°C$) and, moreover, avoids thermal thermisation caused by dissociation/recombination reactions or molecular vibrational motion. The low temperature of the plasma, which interacts with the material both chemically and physically scale, means that the surface being treated is not heated, thus avoiding damage, surface expansion or phase changes.

The coating used is based on siloxane, i.e. TEOS (TetraEthyl Orthosilicate), applied during the 3D printing of the dog bones: while the printer realized on one side a sample, on the other side the plasma flashlight, directly attached to the printer, performed the treatment depositing the precursor (fig.27,28).

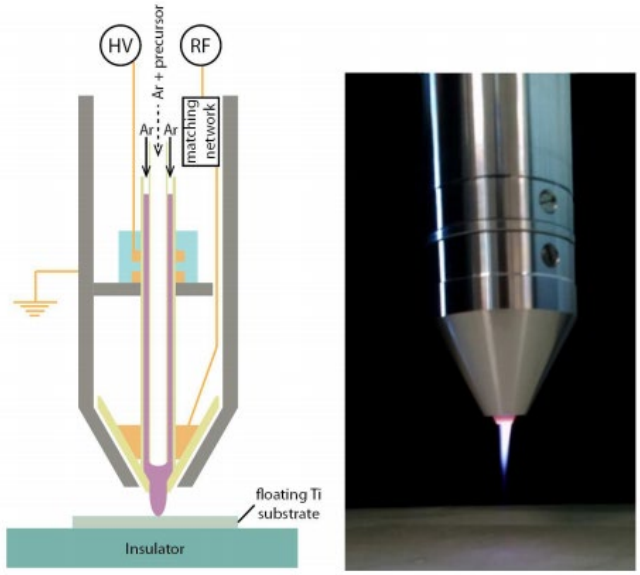

Figure 30. On the left a scheme of the atmospheric plasma jet characterized by the double couple of electrodes RF and HV; on the right a photograph of the device [86].

Table 5 shows the technical characteristics of the Noble Plasma Stylus.

Table 5. Technical specifications of Plasma Stylus Noble [87].

MECHANICAL DIMENSION	
Control unit	3 U dimension rack, trolley or benchtop
Plasma jet	20 cm long, 250 g
Connection cables	2 m
SUPPLY	
Power	30÷100 W, 220 V
Gas 1	Ar 5÷10 slm
Gas 2	Carrier for chemical precursor vapour or reactive gas (0.2÷5 slm)
Gas 3	Cooling/shell (Air or N_2 10÷20 slm)
TREATMENT	
Spot size	1 cm^2
Surface actiovation rate	1-10 cm^2/s
Deposition rate (cm^2)	10 nm/s
Pulsing system	T_{on} (30÷10.000 µs)

	T_{off} (50÷10.000 μs)
OPTIONS	
Interchangeable heads for different spots size: 5 -	10 or 50 nm^2
Aerosol precursor feeding systems	
Table top robot with controlled atmosphere	

2.2 INVESTIGATION METHODS

Below is a description of the analytical techniques used for the characterisation and study of the polymeric material under analysis. The same techniques are also use to follow accelerated ageing, so that the stability and durability of the filament can be assessed.
The analyses carried out offer also a direct comparison between treated and untreated samples at atmospheric pressure plasma, both in terms of chemical properties and mechanical characteristics.

2.2.1 Colourimetric analysis

Colorimetric analysis has a wide field of application in cultural heritage, from analytical laboratories to *in situ* investigations, and is applied with the aim of measuring the absorption of visible radiation. Colorimetry appears, therefore, as a valid tool to measure possible chromatic alterations, after accelerated ageing or following possible surface degradation of the materials.
During the analysis, thanks to the colorimeter, it is possible to measure the tristimulus values, based on the CIELab system, or CIE 1976, which define the color based on the percentage of the three primaries, i.e. red (R), green (V) and blue (B) present, and whose sums (R+V+B) give the total brightness. The three coordinates are described by the following equations [88]:

$$r = \frac{R}{R+V+B} \qquad v = \frac{V}{R+V+B} \qquad b = \frac{B}{R+V+B}$$

The three coordinates are described graphically by means of Maxwell's triangle, also called chromaticity triangle (fig.31), and subsequently represented by the CIE chromaticity diagram (fig.32). The CIE (International Commission on Illumination) diagram is based on the three values of the tristimulus (fig.33), i.e. on three "imaginary" primaries, thanks to these it is possible to obtain all possible colour hues.

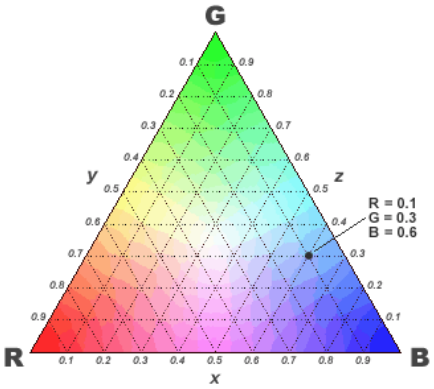

Figure 31. The representation of the chromaticity coordinates r, v and b in Maxwell's triangle. At the vertices are red, green and blue, and at the midpoints of the sides are yellow, cyan and magenta. The pure colors are located along the perimeter, while in the center are all the colors resulting from the combination of the three variables [88].

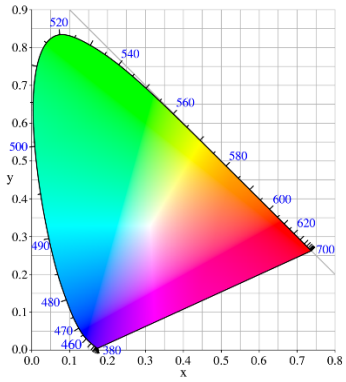

Figure 32. CIE chromaticity diagram, where the spectral colors fall along the "bell-shaped" perimeter, while the non-spectral colors (violet, purple) are on the base, joining the blue and red [88].

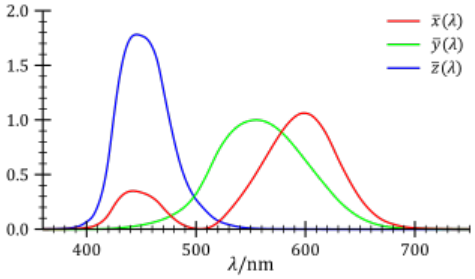

Figure 33. Three values of the tristimulus established by the CIE, the International Commission on Illumination [88].

The colorimetric measurements carried out for this thesis project were performed with the Konica Minolta CM 26d portable spectrocolorimeter (fig.34), using a D65 illuminant and a standard 10° observer. With the instrument, it is possible to obtain information in either SCE (Specular Component Excluded) mode, where specular reflectance is excluded and therefore the colour assessment is akin to the observer's perception, or SCI (Specular Component Included) mode, where specular reflectance is included in the colour measurement.

The reflectance curves and data were then processed using Spectra Magic NX software. The values, which are based on the CIE L*a*b* system, are defined on the basis of hue, brightness and saturation. Specifically, L*, which represents brightness, can take values from 0 (black) to 100 (white), while a* and b* can take both infinite positive and negative values: in the case of a*, a positive value expresses red component and a negative value green, whereas positive values of b* describes yellow and negative ones blue.
In the CIE space L*a*b*, when considering the colour difference between two points, (L_1*, a_1*, b_1*) and (L_2*, a_2*, b_2*), it is possible to calulate the Euclidean distance ΔE, which is given by (1):

$$\Delta E^*_{a,b} = \sqrt{(L^*_1 - L^*_2)^2 + (a^*_1 - a^*_2)^2 + (b^*_1 - b^*_2)^2} = \sqrt{(\Delta L^*)^2 + (\Delta^*_a)^2 + (\Delta b^*)^2} \qquad (1)$$

The values that can be obtained range from 0 to infinite: 0 indicates that no difference in colour is perceived, values between 1 and 3 indicate that there is variation but can be considered negligible, whereas values greater than 3 indicate that there is a perceptible variation [89].
With the data obtained through the analysis, the difference in colour of the samples before and after ageing was measured in order to verify possible aesthetical changes, due to chemical and/or morphological modifications in the material.

Figure 34. Konica Minolta CM 26d portable spectrocolorimeter [90].

2.2.2 Fourier transform infrared (FT-IR) spectroscopy in attenuated total reflectance (ATR) mode

FT-IR spectroscopy is an analytical technique to identify compounds present in samples and is used, in this study, to characterize any differences in cold plasma treated and non-treated samples. The technique was used in combination with ATR in order to analyze the chemical composition, and in particular the molecular species, of the samples [91-94].

In addition, the spectra are compared with data that can be found in the literature in order to associate the peaks with the different chemical compounds and functional groups belonging to polylactic acid. Since PLA is an aliphatic polyester consisting of lactic acid, in addition to the methyl groups (-CH_3, -CH_2), it is expected to find peaks characteristic of the functional groups -OH, -COOH and COC.

Table 6 shows the characteristic peaks of polylactic acid [95-100].

Table 6. Characteristic peaks of polylactic acid in ATR FTIR spectroscopy [95-100].

Frequencies cm^{-1}	**Association**
≈ 3000-2800	CH_3 symmetrical and asymmetrical stretching
≈ 1750	Carbonyl peak, stretching C=O
≈ 1455-1360	CH stretching of methyl groups
≈ 1300	CH+COC group COC stretching
≈ 1270	
≈ 1210	COC+CH_3 group COC stretching
≈ 1180	C-O- bond stretching vibration in -CH-O- group
≈ 1130	Stretching CH_3 Or 1/3 characteristic peaks related to -C-O- stretching of the -O-C=O group
≈ 1080	Stretching CH_3 C-O-C stretching Or 1/3 characteristic peaks related to -C-O- stretching of the -O-C=O group
≈ 1045	Stretching CH_3 Or 1/3 characteristic peaks related to -C-O- stretching of the -O-C=O group
≈ 955	CH_3 and CC rocking (association with amorphous phase)
≈ 890	C-COO stretching
≈ 870	C-COO stretching (association with amorphous phase)
≈ 755	CO bending (association with crystalline phase)
≈ 700	CO bending

In particular, for the plasma treated samples it is assumed the presence of the characteristic peaks of the deposited coating (TEOS), siloxane based (tab.7) [101].

Table 7. Characteristic peaks of TEOS in ATR-FTIR spectroscopy [101].

Frequencies cm^{-1}	**Association**
≈ 3678	Stretching vibration of OH
≈ 2990	Stretching vibration of CH
≈ 2145	Stretching of CO
≈ 1776	Stretching of C=O
≈ 1747	
≈ 1115	Stretching of CO
≈ 1070	
≈ 800	Bending vibration of the Si-O-Si
≈ 656	Stretching vibrations of Si-O

Then, this technique is used to identify the presence of changes before and after accelerated aging of PLA samples.

From a chemical point of view, the hydrolytic process should lead to an increase in carboxylic acids, which easily undergo ester hydrolysis. While the photolytic process should lead to the formation of hydroperoxides from which carboxylic acids, diketone end groups, carbonyl and vinyl groups are subsequently obtained, which appear in the carbonyl region of the spectra and tend to increase over time.

According to the literature [102-107], all these chemical changes resulting from weathering or accelerated aging could be confirmed by studying an IR spectrum. The analysis, in fact, could show a decrease in the intensity of the signals belonging to the ester groups and an increased intensity of the carbonyls. In order to be able to state any changes in the peaks, it is possible to calculate the carbonyl index (CI), a dimensionless parameter that relates the intensity of the peak of the carbonyl groups (≈1750 cm^{-1}) with the intensity of the stretching band of the methyl group (3000-2800 cm^{-1}, 1450 cm^{-1}), thus determining the extent of degradation of the polymeric material. Generally, the greater the degradation of PLA, the higher the carbonyl index value.

Therefore, with exposure time the carbonyl band should widen slightly, forming a shoulder at about 1845 cm^{-1}, attributed to the formation of anhydride groups. In addition, in the hydroxyl region there should be growth of a broad absorption band, having a maximum at 3400 cm^{-1}, which corresponds to hydroperoxides and alcohols.

The spectroscopic analyses were carried out by means of the Thermo Nicolet FTIR NEXUS 750 instrument, supplied at the scientific campus of the Ca' Foscari University, consisting of a Smart Endurance ATR accessory with a diamond tip and having an investigation area of 0.75 mm^2. The FTIR-ATR spectra have been recorded through 64 scans, considering a spectral range between 4000 and 400 cm^{-1} and a resolution of 4 cm^{-1}. Then the spectra were processed with OMNIC 6.0a software, which allowed baseline correction, peak evaluation, and comparison of spectra.

2.2.3 Raman spectroscopy

Raman spectroscopy is a non-invasive and non-destructive vibrational technique that allows you to trace the structure of molecular vibrational energy levels, which represent a kind of "fingerprint", because they are specific to each molecular type. The analytical technique is widely used in the field of Cultural Heritage, as it allows to identify substances of crystalline nature,

pigments and dyes, both organic and inorganic, as well as to identify restoration materials and products of degradation [108-111].

In this study, the methodology of investigation is applied to identify any variations between treated and untreated samples.

Spectra identification is performed by comparing the results with online databases and data reported in the literature. Typically, one would expect to find peaks related to methyl (-CH_3, -CH_2), carbonyl (-CO), carboxyl (-COOH) and ether (-COC) groups [112,113].

Table 8 shows the main peaks for polylactic acid.

Table 8. Characteristic peaks of polylactic acid in Raman spectroscopy [112,113].

Raman intensity cm^{-1}	**Association**
≈ 3002-2995	CH_3 asymmetric stretching
≈ 2947-2944 ≈ 2889-2878	CH_3 symmetric stretching
≈ 1773-1769	C=O stretching/ CH stretching
≈ 1456-1454	CH_3 symmetric deformation
≈ 1388	CH_3 simmetrico
≈ 1298	CH + COC
≈ 1128	CH_3 rocking vibration
≈ 1046-1042	C-CH_3 stretching
≈ 873	C-COO
≈ 742	C=O
≈ 408-399	C-CO

Also in this case, for the plasma treated samples it is assumed the presence of the characteristic peaks of the deposited coating (TEOS), siloxane based (tab.9) [114].

Table 9. Characteristic peaks of TEOS in Raman spectroscopy [114].

Raman intensity cm^{-1}	**Association**
≈ 1049	Si-O-Si stretching vibration
≈ 980	Si-O-C stretching vibration
≈ 880	C-O-C stretching vibration
≈ 675	SiO_4 stretching vibration
≈ 484	Si-O-Si bending vibration
≈ 435	

Then the technique is used to assess whether there have been changes at the molecular level after the accelerated aging process.

Also, in this case it is valid what has been said in the ATR FTIR spectroscopy about the degradation of PLA. Therefore, in general, during accelerated aging the polylactic acid has undergone both hydrolysis and photolysis. In the former case, hydrolysis of the esters comprising the carboxylic acids occurs, while in the latter case, hydroperoxides are formed.

In particular, the peak related to the stretching of the C=O group of the ester, located at about 1768 cm^{-1}, should decrease with aging, due to the cleavage of the COO group.

In this case, was used the BRAVO Raman spectrometer, a portable instrument that allows to acquire Raman spectra at different energies using laser diodes with controlled and variable temperature and with good spectral accuracy due to the neon lamp integrated in the instrument. The spectra obtained were recorded considering the region between 3200 cm^{-1} and 400 cm^{-1} and were then processed and analyzed using OPUS and OMNIC 6.0a software.

2.2.4 Thermogravimetry (TGA) and Differential Scanning Calorimetry (DSC)

Differential scanning calorimetry (DSC) is an analytical technique for determining and characterising polymeric materials, glass, ceramics, etc.
The instrument used is the DSC calorimeter, which measures the heat flows associated with thermal transitions of a sample when it is heated/cooled or when it is maintained at a constant temperature. Therefore, this technique allows the identification of the temperature during which particular transitions occur in the sample, which will depend on the chemical nature of the material itself.
In the particular case of polymers, DSC makes it possible to determine: the glass transition temperature (T_g), the melting temperature (T_m), the crystallisation temperature (T_c), the enthalpy of melting (ΔH_m) and crystallisation (ΔH_c), the degree of crystallinity (X_c) in the case of semi-crystalline polymers, polymorphism and solid-solid transitions.
Usually, one of the most visible transitions in polymeric materials is the glass transition, which, according to a general definition, indicates the temperature during which an amorphous polymeric material passes from the glassy state (rigid and brittle) to the highly viscous liquid, or rubbery state. Therefore, the glass transition temperature indicates a change in the specific heat ΔC_p, corresponding to a change in the concavity of the DSC curve. From a practical point of view, the T_g corresponds to the inflection point, also referred to as the *midpoint* temperature.
Generally, the glass transition temperature depends on the molecular and microstructural nature of the polymer under analysis; therefore, the presence of other polymers or additives, such as fillers or plasticisers, can certainly modify the value of the parameter.
Another transition to be considered concerns crystallisation (T_c), the value of which depends mainly on the cooling rate: the higher the rate, the lower the T_c measured. Furthermore, for high cooling rates, macromolecules may not have time to crystallise, leading to the formation of an amorphous material, which, on subsequent heating, may show the phenomenon of cold crystallisation, whose temperature is called T_{cc} (cold crystallisation), between T_g and T_m.

In general, it is important to know the glass transition, crystallisation and melting temperatures of a polymeric material, as it is possible to estimate the optimum processing conditions depending on the application of the material besides the working condition themselves.
Among the quantities that can be measured through DSC there is also the enthalpy of fusion (ΔH_m) which indicates the heat necessary to transfer a mole of substance from the solid state to the liquid or liquid-viscous state, while the enthalpy of crystallization (ΔH_c) indicates the heat developed in the opposite passage. During the analysis, the degree of crystallinity of the samples examined was also calculated, according to the formula:

$$\chi_C = 100 \times \frac{\Delta H_m - \Delta H_c}{\Delta H_0}$$

where ΔH_m is the enthalpy of fusion (J/g), ΔH_c is the enthalpy of crystallization (J/g) while ΔH_0 is the heat of fusion of the 100% crystalline polymer (J/g), which for PLA is 93.1 J/g.
Under isothermal conditions, DSC analysis allows thermal or thermo-oxidative stability tests to be carried out, and also studies the kinetics of crystallisation and phase transition, i.e. polymerisation, cross-linking and curing.
Among the advantages, differential scanning calorimetry is a non-destructive technique (in case the thermal degradation threshold of the material under analysis is not exceeded) and it does not require large quantities of material.
DSC analysis was applied both to the pure PLA filament and to the PLA filament after annealing process (oven, T≈80°C); also, n-t and t samples, before and after aging, were subjected to the analysis.
According to the literature, the thermogram of pure PLA should show the following temperatures:

- Glass transition temperature, T_g, around 61°C;
- Cold crystallization phenomenon, T_{cc}, around 100-130°C, which consists in a change in the physical structure of macromolecules, leading to an increase in the degree of crystallinity of the polymer;
- Melting temperature, Tm, around 160-170°C, which is the thermal threshold at which the transition from solid to molten polymer occurs [96,97, 115, 117].

Then the polymeric material is heated to such a temperature that it cannot melt and there is not a forced stretch of the polymeric chains as with the extrusion, thus macromolecules can rearrange in space; by absorbing thermal energy, they can move, stretch, realign and have the time in the cooling phase to partially recrystallize, forming a stabler internal matrix. Therefore, the objective of the analysis is to investigate the effect of the "annealing" process on the thermal stability of the PLA filament.

Thermogravimetric analysis (TGA), on the other hand, records the variation in the mass of the sample when it is subjected to a programmed temperature scan over time. The instrument consists of a microbalance that is sensitive to any change in the mass of the sample (in the order of a μg or a tenth of a μg), a sample crucible, a furnace, a system of purging gases that controls the flow and nature of the gas, and a data processor. The sample is placed in the furnace, where the temperature (25°C to 1500°C) and atmosphere parameters are highly controlled.
In the specific case of the atmosphere, it is possible to subject the sample to both inert and reactive atmospheres, with the aim of obtaining information about the stability and reactivity of the materials under analysis.
At the end of the analysis, a thermogram is obtained where the abscissa shows the temperature and the ordinate the percentage or absolute change in mass. From the TG curve it is possible to determine the degradation temperature of the material, defined as the onset temperature, $T_{onset-i}$, resulting from the intersection of the tangents to the point of deviation from the initial weight and the inflection point of the curve. In some cases, the temperature at which 10% degradation of the material occurs, $T_{10\%}$, the temperature at which 50% degradation occurs, $T_{50\%}$, and the end of degradation temperature, $T_{onset-f}$, are also indicated. Finally, another temperature that is indicated in the graph and that defines degradation is the temperature of maximum degradation rate, T_{vmax}, corresponding to an exotherm in the curve and an inflection point of the TG curve.
Thermogravimetric analysis is used to analyse the composition of polymer mixtures and the presence of inert fillers in organic-based compounds, such as in the case of filled epoxy or polyurethane resins [117-119].
With reference to polymeric materials, for example, the information obtained concerns: thermal stability, thermo-oxidative stability, stability in corrosive or reactive atmospheres, etc. On the contrary, it is not possible to obtain information about the possible presence of chemical or structural modifications that do not involve mass changes, and it does not allow to trace the nature of degradation products, as it is not a qualitative analysis, but on the contrary it allows to quantify the presence of certain products already known.
TGA analysis was also applied to both pure PLA filament and PLA filament after annealing process (oven, T=80°C); in addition, n-t and t samples, before and after aging, were also subjected to the analysis. Typically, PLA degradation occurs in a single step, above 300°C to about 400°C. Typically, PLA degradation occurs in a single step, above 280/300°C to about 350/400°C, regardless of the process immediately prior to analysis [120].

During this thesis project it was decided to couple the two techniques TGA-DSC, in order to correlate the mass losses of the sample to the variations of the heat flux and the physical transitions. In particular, as previously mentioned, the technique allows the definition of optimal processing conditions for 3D printing of PLA.

The instrument used is Netzche Termische Analyse TASC 414/3 Controller - model STA 409 cell (fig.35). The sample used as a reference is alumina, given its stability at high temperatures (30°C-1000°C). The samples submitted for analysis underwent a temperature ramp of 10°C/min, considering the following temperature range: from room temperature (≈ 30°C) to 700°C. In the case of DSC, however, it was preferred to consider a 30-400 range, within which the temperatures, and thus the typical peaks of the polymeric material, are concentrated. The gas applied is nitrogen, so no oxidation reactions are expected, which occur in the presence of nitrogen and air. The same parameters were applied during the analysis of both the PLA filament after annealing and two samples (n-t + t) before aging, i.e., at time 0.
Subsequently, oxidative tests were also performed, applying a flow of N_2/air gas 40/80 ml/min, on dog bones both before (t0) and after 2000h of artificial aging and dynamometric tests.

Figure 35.Netzche Termische Analyse TASC 414/3 Controller - model STA 409 cell.

2.2.5 Dynamometric tests

Dynamometric tests, or tensile tests, allow the mechanical properties of a material to be tested, depending on how it reacts in the presence of a stress. Therefore, depending on the type of tension and deformation that the specimen undergoes, one can have a behaviour:

- *Linear*, if the deformation is proportional to the applied stress;
- *Elastic*, if the deformations cancel out when the tension is no longer applied;
- *Plastic*, if permanent deformations remain when the applied tension ceases.

Generally, elastic deformation is related to the stretching of interatomic bonds in solids, which fails when stresses, i.e. external forces applied to them are removed, so it is reversible and not permanent. This type of deformation depends on the chemical bonds of the substance, which

should be able to stretch or bend temporarily; however, over time, the substance deteriorates, becoming more brittle and thus losing ductility.

Plastic deformation, on the other hand, occurs in the presence of high tensions and is related to the slippage between planes of atoms in the crystalline grains that goes to cause dislocation of atoms, and then the breakage of a limited number of chemical bonds; compared to elastic deformation, it is irreversible and permanent. In the case of ductile substances, the elastic limit represents the maximum limit to which the solid can be stretched without undergoing permanent alterations and beyond which, instead, it suffers a plastic deformation (fig.36) [121].

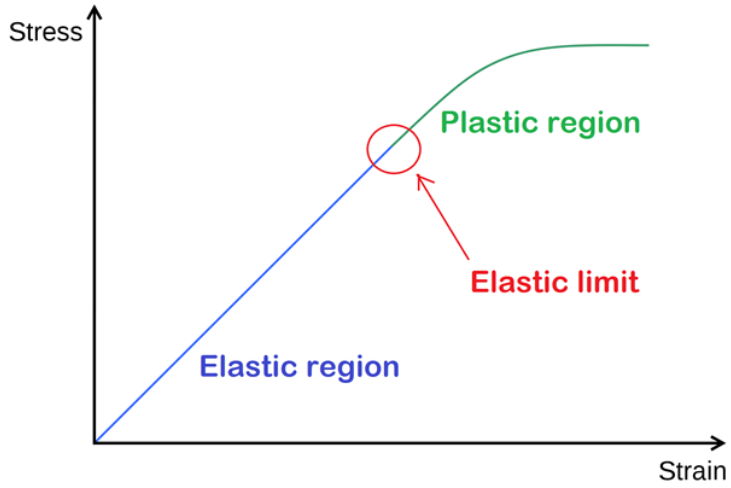

Figure 36. Stress-strain curve for a ductile material. In the first part of the curve there is the elastic region (elastic deformation), beyond which the materiale will undergo plastic or permanent deformation, after the elastic limit [121].

Therefore, to determine the physical-mechanical properties of the material, tensile tests are carried out, which will obviously be unrepeatable.

The specimens have a standardised geometry and dimensions according to ISO 527 and, during the analysis, they are subjected to a unidirectional tensile force F increasing from a value of 0 N to a value that determines their breakage, in order to measure the total applied force and deformation reached [122].

The procedural steps for the tensile test are given in ASTM D 638 "*Standard test method for tensile properties of plastics*" [123], which states that information about tensile strength, yield strength, elongation at yield, elongation at break and modulus of elasticity can be obtained [124].

More specifically, the specimen is connected to the instrument at both ends by means of grips, one of which is fixed whereas the other is attached to the movable crosshead, also called the actuator piston. The distance between the two grips is indicated by *h*.

During the dynamometric test, the force applied to the specimen is measured using a transducer, or load cell, and the displacement of the moving element (Δh) using a device called Linear

Variable Differential Transformer or LVDT. Before applying the force and causing the displacement, a minimum load is applied to the sample so that it settles at the two grips of the machine.
Next, a strain gauge can be used to measure localised elongation, or a strain gauge can be used to measure strain [111].
Finally, data collected are reported in a graph where the strain is indicated according to the stress. In other cases, however, the load versus elongation data can be reported in the graphs.
The instrument used for the following work is the MTS Insight System Corporation 50kN Extended Length extensometer (cell model 569332-01), with stationary face grips (MTS Advantage, Wedge Action Grips) [125]. A speed of 0.050 mm/s was set during the tests, setting the parameters for the printed specimen, then considering the thickness (1 mm) and the height for the jaws (12 mm). The load applied on the samples is 10 kg. In addition, the samples considered are 5 for each type, although in the case of samples n-t before aging are considered 6 (one more for a printing error), while for samples t are considered 4, because one is broken.

2.3 ACCELERATED AGING

Accelerate ageing allows the effects of degradation agents to be assessed by simulating natural degradation, thus determining the most appropriate conservation and restoration processes to counteract them. The test therefore offers the possibility of controlling degradation agents at the same time, such as irradiation, temperature and relative humidity [126].
During the accelerate aging, the material under analysis is subjected to different conditions of temperature and relative humidity, in order to simulate the conditions of a hypothetical outdoor environment, given the proposal to use the filament to integrate and restore works of art in an outdoor environment, and to produce copies of wear-resistant artefacts.
Afterwards, the effects and possible changes resulting from accelerated aging are verified by comparing the results obtained from colorimetric analysis, ATR FT-IR and Raman spectroscopies, TGA-DSC curves and dynamometric tests.
Furthermore, in this work, ageing was carried out in two steps: in the first step, the process was carried out using an ageing chamber, while in the second step, a more traditional methodology was followed due to a series of technical problems encountered in the chamber during the analysis.

Generally, when considering the climatic chamber, in most of the tests UV radiation is combined with rain or condensation (according to ASTM G 154, EN 1297, ASTM D 4799: 2008, ISO

11341: 2004, UNI EN 14509: 2006 [127-131]), or solar radiation, thanks to the use of a Xenon lamp, and rain (ASTM G 155 [132]). One of the limitations of the chamber, however, is the impossibility of proposing a freeze-thaw cycle, precisely because the UV or Xenon lamps tend to be damaged at low temperatures; therefore, in the case of wanting to introduce freeze phases, separate chambers or cold rooms can be used [133]. No freeze-thaw cycles were performed on the specimens during aging because, being composed of a thermoplastic material, exposure in an outdoor environment to temperatures where water can change from a liquid to a gaseous state, or the reverse, should not cause structural deformation or fracture.

During the initial step, a cyclic ageing process was chosen using the Q-SUN Xe-3 tester (fig.37), a full-featured chamber for testing lightfastness, colourfastness and photosensitivity. The instrument uses three xenon lamps, and features a removable sample tray, which measures 451 mm x 718 mm, and is capable of carrying large samples. The Xe-3 models are very versatile, as they offer the possibility to control the relative humidity, and have several options available, including a water spray system, a back spray system and a chiller [134].

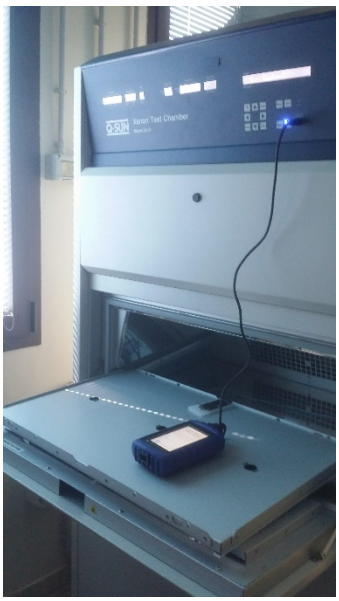

Figure 37. Q-SUN Xe-3 tester.

The initial objective was to evaluate the behaviour of the test specimens exposed for 500h to light radiation and another 500h to a combination of light radiation and humidity, for a total of 1000h. Therefore, the initial parameters set in the climatic chamber were:

- T_{aria}: 45°C.
- $T_{black\ panel}$: 68°C.
- RH: 60%.

The specimens were adhered to a net, so that they would not move during treatment (fig.38).

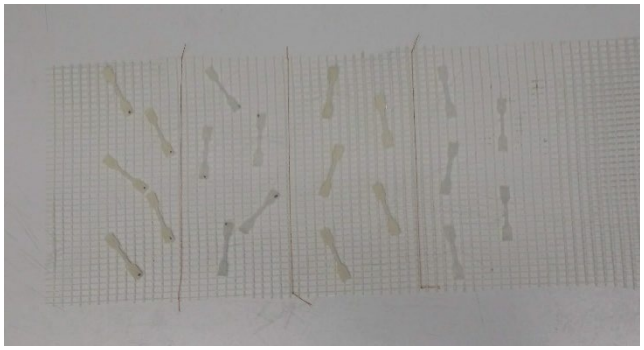

Figure 38. Preparation of samples for treatment.

Accelerated aging continued for 87 hours and about halfway through the cycle the specimens were rotated with respect to their initial position in order to provide a treatment that was somewhat more homogeneous.

Subsequently, due to a number of technical problems, it was decided to continue the aging process outside the chamber, adopting traditional methods, i.e., proposing the use of an incandescent lamp for thermal aging and a dryer consisting of an oversaturated solution of potassium iodide, in order to maintain a constant RH level (≈69%) (Fig.39).

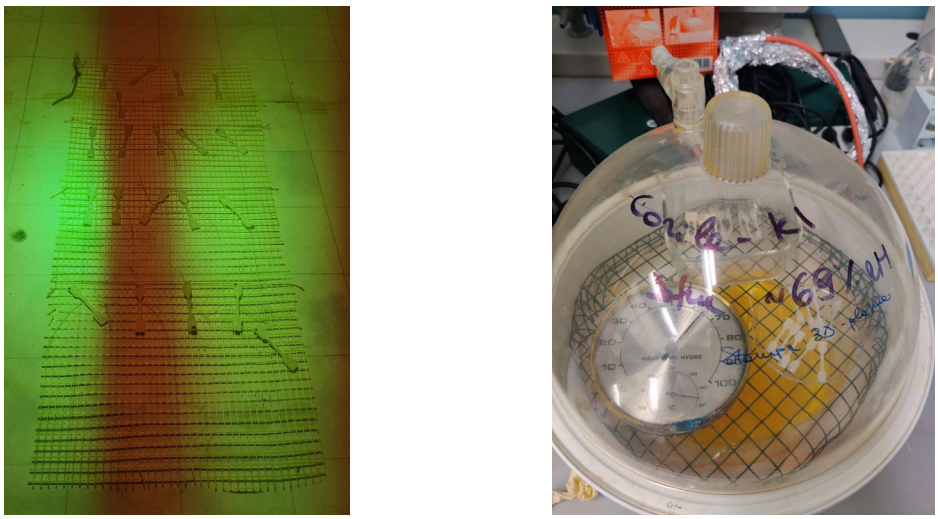

Figure 39. On the left, samples under an incandescent lamp; on the right the samples into a dryer.

In this case, the 10 specimens (t+nt) in the climate chamber were placed in the dryer, while another 10 specimens (t+nt) were placed in a fume hood under an incandescent lamp. In the latter case, a luxmeter (Lux Meter model LX1010BS) was used to check the illuminance level of the work environment. The table 10 shows the grid used to collect the average lamp brightness values.

Table 10. Luminous flux between the UV lamp and the grid; values are given in the lux (lx) unit of measurement.

	11	12	13	14	15	16
E	5090	8963	21700	36267	19000	9100
F	4943	8667	21667	35700	18900	8780
G	4160	6827	12000	14533	10433	6517

The total 20 specimens were left until the cycle was completed (2000h); thus:

- the 10 specimens that had been placed in the chamber were left in the dryer for approximately 1913 h;
- the 10 samples that had not been placed in the chamber, were left under lamp for 2000h.

2.4 DURABILITY OF THE FILAMENT

The aim of these tests is to evaluate any transformations of the material following contact with the acid and, in particular, the possible release of chemical compounds.

2.4.1 Acid attack resistance tests

The aim is to evaluate the resistance of the material when it is placed in direct contact with both inorganic and organic acids over a longer period of time, so that it can be shown to be resistant in an aggressive environment.

Generally speaking, when a polymer comes into direct contact with an acidic substance, it tends to swell or soften as the acid molecules diffuse between the polymer chains, pushing them apart. In particular, organic chemicals, as opposed to inorganic chemicals, tend to cause dissolution, swelling the polymer [135].

For this reason, two samples of the Eumakers filament was initially placed directly from the bobbin in a test tube containing HNO_3, nitric acid at pH≈2 and diluted at 70 % (tab.11) and glacial acetic acid (CH_3COOH) respectively (tab.12). From the information obtained from the literature, the acid that should present a more aggressive action towards PLA is acetic acid, since, compared to the former, it is organic in nature and therefore similar to the polymeric material.

Precisely for this reason, therefore, the two PLA cubes (t+nt) were also placed in two test tubes and covered entirely with acetic acid. The two cubes were left inside the tubes for about 840 h,

after which, in order to verify the effects produced by the acid, they were analyzed by ATR FTIR spectroscopy.

2.5 LIFE CYCLE ASSESSMENT OF A COMPARATIVE ANALYSIS

In this thesis project, an evaluation about the environmental impact of two cases of integrative restoration is presented, focusing in particular on the materials to be applied. For this reason it has been chosen to use SimaPro [138, 139], a professional software that allows to collect, analyze and evaluate the environmental performances of different materials and processes. Basing then on the ISO 14040 (Environmental management, Life cycle assessment, Principles and framework) and 14044 (Life cycle assessment, Requirements and guidelines) standards, it is possible to analyze and model life cycles, even complex ones, in a practical and systematic way. In general, with SimaPro it is possible to propose Life Cycle Assessment (LCA) analyses, to calculate the Environmental Product Declaration (EDP), to calculate the carbon footprint and the water footprint and much more [140, 141].
Obviously, before delving into the software, it is necessary to establish the objective of the study, thus defining the functional unit, the system boundaries, the inventory and the methodologies used to assess the environmental impact.

2.5.1 Comparative analysis

The purpose of this work is to analyze the life cycle contribution of two hypothetical cases of integrative restoration, through the software SimaPro, in order to offer an assessment in terms of sustainability and environmental impact. The first case is based on the use of a PLA-based filament, printed through FDM additive technology and treated with cold plasma at atmospheric pressure, while in the second case more traditional materials are proposed, namely the use of plaster, for the integration, and silicone rubber, for the realization of the cast.
Therefore, the objective is to offer different scenarios to carry out an integrative restoration, in order to choose the intervention, traditional or innovative, that best suits in terms of environmental sustainability.
To this end, it is necessary to identify the functional unit, i.e. the reference against which all data (input and output) are normalized; in other words, it represents the product, the service or the function on which to set the analysis and comparison of possible alternatives.

2.5.2 Definition of the functional unit

In order to adequately compare the two types of intervention, for this study the volume of the cube is considered as a functional unit, so that the total values of the inputs considered in the two

cases can be compared. By proposing two cases of integrative restoration, which involve the use of different materials, it is believed that the most appropriate functional unit is the volume, since during a restoration intervention, in addition to the products that are applied, which usually tend to penetrate inside the surface becoming part of the structure, the materials that are used for the integration become a constitutive part of the artifact itself. Therefore, the functional unit is 1 cm^3.

2.5.3 Definition of boundaries

The system boundaries determine the unit processes that must be included in the LCA, from which the inventory, which is the focus of the study, will later develop. It is important, therefore, to define which unit processes to include in the study and the level of detail with which those processes are to be analyzed. Obviously, the selection of the system boundary must be consistent with the objective of the study, which is to analyze the environmental impact and sustainability of the hypothetical integrative restoration case described above.
For this reason, in both cases only the cube formation process is considered, reporting all materials and chemicals applied, followed by the time of use and final disposal process.
The quantities presented in the two cases of application represent indicative values, with which we have tried to estimate the real values as much as possible, also on the basis of the experience carried out for the thesis work and on the data reported in the literature.
Moreover, the output of each system will be given by the cubes, indicated according to a volume of 1 cm^3, and with a normalized temporal boundary in order to compare the two cases.

2.5.3.1 Case 1

Figure 40 describes the boundary diagram of the first integration case using PLA. The first input is the polylactic acid filament, presents on the left, to the formation of the cube on the right, which is the output of the system. Each phase and material needed to produce the cube is reported, with some values: quantity (mg, kg), density (kg/m^3), transport (km), time of use in minutes and duration of the material in years.
The duration of the cube was estimated on the basis of a study carried out by analyzing a white PLA covered with a bronze-based paint. The material was, in fact, used to reproduce, with 3D printing and in 15:1 scale, the Isadora belt, an artifact exposed in a square, and therefore in direct contact with atmospheric degradation (rain, solar radiation, pollution). The various investigations carried out showed that the material presented problems of mechanical strength, perhaps due to

recent transport, while on the contrary it showed good chemical resistance [142]. Therefore, in this analysis, it is assumed that the durability of the thermoplastic polymer is increased, due to the cold plasma treatment at atmospheric pressure, which should improve the mechanical strength of the material. While the spatial boundaries considered in the system refer to the city of Mestre, where it is assumed the realization of the cube at the FabLab, located in the Vega science park; for this reason, they are indicated under the voice “local environment”.

Next, for electronic equipment, electrical energy is reported, where the unit is kWh.

Then, after the inputs, there is the waste product, which comes from the printing process and consists of plasma-treated PLA.

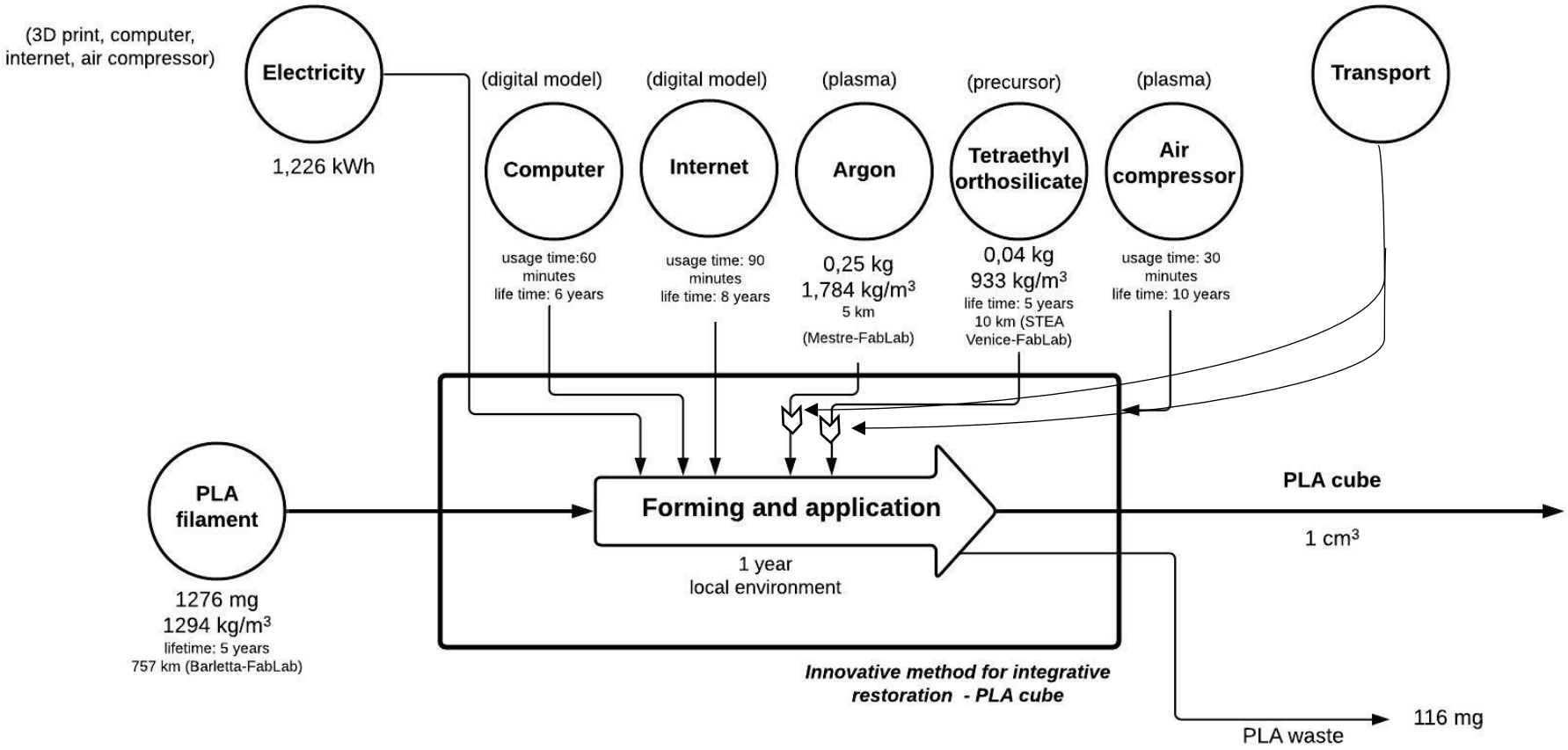

Figure 40. System boundaries of case 1.

2.5.3.2 Case 2

Figure 41 shows the system boundaries of the second reinstatement intervention. As before, there are the materials used to make the mould and the reintegration, considering the quantities (mg, kg), densities (kg/m3), transport (km) and duration in years. As in the case of PLA, the durability of the gypsum depends mainly on the microclimate of the place and its position, since different effects can be observed depending on whether the object is in direct contact with the weather or protected by canopies or other coverings. The main degradation actions that can be found in this material are: solubilization of calcium sulphate with consequent disintegration of the material, due to humidity, and deposition of dust on the surface, which, being porous and sensitive to mechanical actions, appears as a problem not to be neglected [143].

In addition, as in the first proposed case, the Mestre area is considered, thus the FabLab as the center of realization of the integration.

At the end, among the waste products there is only the silicone rubber, which, following the realization of the cube, does not find a further functionality.

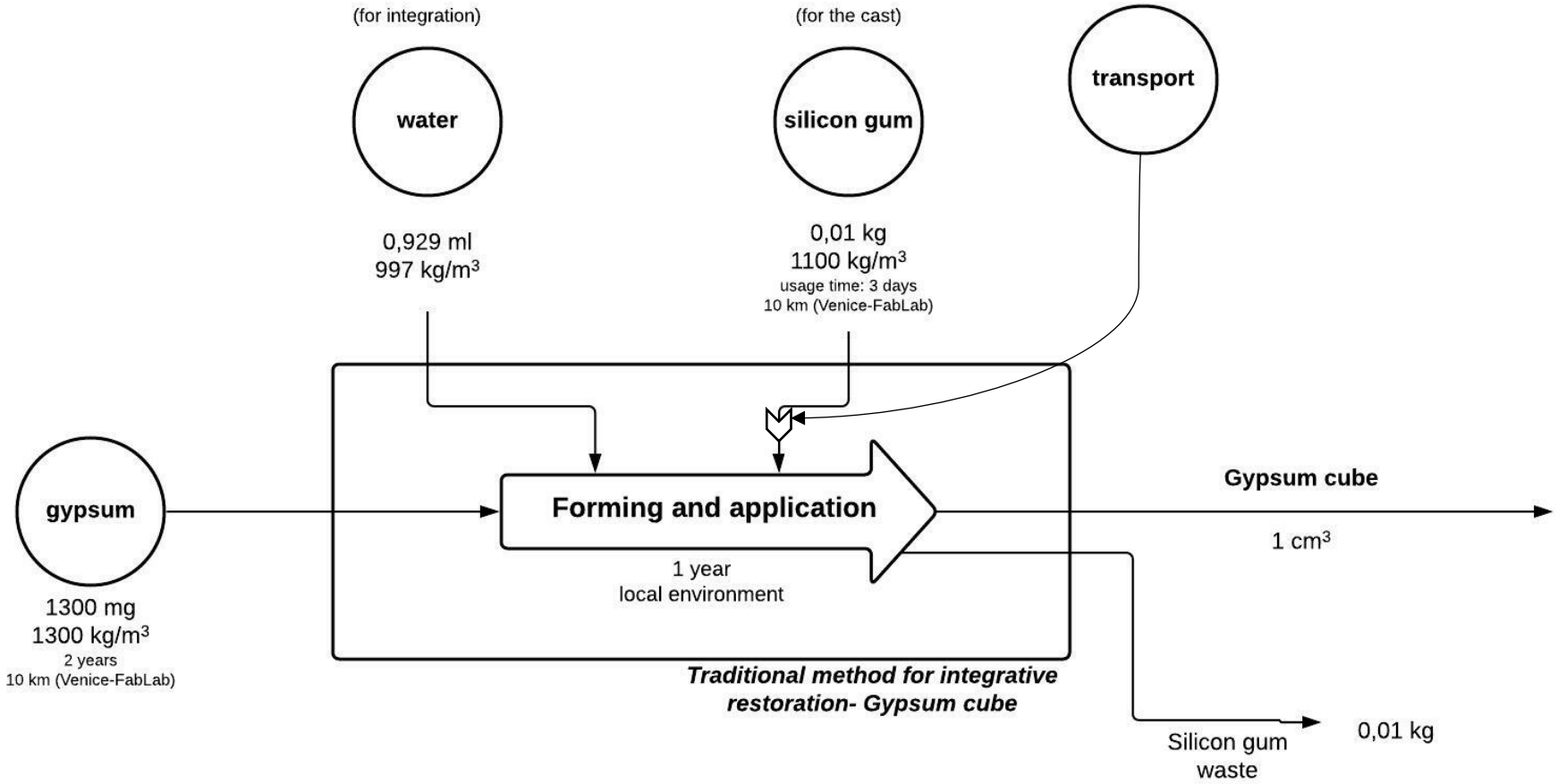

Figure 41. System boundaries of case 2.

2.5.4 Life Cycle Inventory (LCI)

The materials and chemicals used during the two hypothetical cases of integrative restoration must be considered in an LCA analysis through an appropriate inventory phase.
Therefore, in order to select products that are somewhat more consonant with the materials considered in the study, it is appropriate to refer to specific databases, such as "Ecoinvent 3 - allocation, cut-off by classification" and "Methods". The Ecoinvent database covers almost 4000 processes in various industrial sectors, such as energy, transport, chemicals, building materials, agriculture, pollutant treatment, etc [144].
All processes consist of extensive documentation, followed by a description of the data, such as name, unit of measurement, category and subcategory to which they belong.

2.5.4.1 Case 1

In the first case of integrative restoration, the initial input is pure PLA filament, that is a material similar to the one taken under analysis for this thesis project.
Therefore, the material was entered under "*Polylactide, granulate {GLO}| production | Cut-off, S*", which considers polylactic acid in granulate form. For the purposes of this work, it was not necessary to consider the preliminary processing step of the thermoplastic polymer, i.e., the process of extruding the filament to create the spool, the impact of which is considered negligible.
The PLA cube is then entered with a mass of 1276 mg, where 10% of the total value is discarded as it constitutes the basis on which the sample is made; therefore, about 116 mg of PLA are entered in the software under the category of "waste treatment", marked as "*Municipal solid waste {IT}| treatment of, incineration | Cut-off, S*".
Next, from the initial input, all other inputs are reported, described following the order of the various intervention steps (tab.13).

Table 11. Input and waste scenario of case 1: for each one product in SimaPro, quantity, density, transport, lifetime, electricity and allocation waste are indicated.

INPUT								
Phase	**Materials**	**Inventory**	**Quantity (g)**	**Density (kg/m^3)**	**Transport (km)**	**Lifetime Using time**	**Electricity (kWh)**	**Waste and allocation (g)**
Digital model processing	Computer	*Computer, desktop, without screen {GLO}| production | Cut-off, S*	1 p	-	-	6 years 60 min	0.2	-
		Display, liquid crystal, 17 inches {GLO}| production | Cut-off, S	1 p	-	-	6 years 60 min	0.05	-
	Internet	*Router, internet {RoW}| processing | Cut-off, S*	1 p	-	-	8 years 90 min	0.006	-
3D-printing	3D printer	*Electricity, low voltage {IT} | electricity voltage transformation from medium to low voltage | Cut-off, S*	-	-	-	-	0.66	-
Filament	PLA	*Polylactide, granulate {GLO}| production | Cut-off, S*	1.276	1294	-	5 years	-	-
		Municipal solid waste {IT} | treatment of, incineration | Cut-off, S	-	-	11	-	-	0.116 (10%)
		Transport, freight, light commercial vehicle {Europe without Switzerland} | market for transport, freight, light commercial vehicle | Cut-off, S	-	-	757	-	-	-
Plasma treatment	Argon gas	*Argon, liquid {RoW} | production | Cut-off, S*	250	1.784	-	-	0.06	-
		Transport, freight, light commercial vehicle {Europe without Switzerland} | market for transport, freight, light commercial vehicle | Cut-off, S	-	-	5	-	-	-
	TEOS	*Tetraethyl orthosilicate {GLO} | production | Cut-off, S*	20	933	-	5 years	-	-
		Municipal solid waste {IT} | treatment of, incineration | Cut-off, S	-	-	11	-	-	2 (10%)

		Transport, freight, light commercial vehicle {Europe without Switzerland} | market for transport, freight, light commercial vehicle | Cut-off, S	-	-	10	-	-	-
	Air compressor	*Air compressor, screw-type compressor, 4kW {RoW}| production | Cut-off, S*	1 p	-	-	10 years 30 min	0.25	-
WASTE SCENARIO								
End-of-life	PLA waste	*Municipal solid waste {IT} | treatment of, incineration | Cut-off, S*	1.160	-	-	-	-	90 %
		Transport, freight, light commercial vehicle {Europe without Switzerland} | market for transport, freight, light commercial vehicle | Cut-off, S	-	-	11	-	-	-
	TEOS waste	*Municipal solid waste {IT} | treatment of, incineration | Cut-off, S*	18	-	-	-	-	90 %
		Transport, freight, light commercial vehicle {Europe without Switzerland} | market for transport, freight, light commercial vehicle | Cut-off, S	-	-	11	-	-	-

- Modeling phase and printing process. During the first phase of intervention a .stl file is realized in order to create the digital model of the cube that you want to print. For this reason, therefore, it is opportune to consider the computer, the desktop and the internet, whose voices are brought back together with the time of use, for the elaboration of the model, that is compared to the time of life of the electronic object. For the computer and the desktop, introduced according to the items "*Computer, desktop, without screen {GLO}| production | Cut-off, S*" and "*Display, liquid crystal, 17 inches {GLO}| production | Cut-off, S*", a time of about 1 hour is established, while for the internet, introduced through the item "*Router, internet {RoW}| processing | Cut-off, S*", 1 hour and a half, whose connection is also used to send the digital model file to the 3D printer. Regarding the lifetime, instead, it has been tried to make an estimate about the duration of the electronic apparatus, inserting a time of 6 years for the computer and 8 years for the internet.

  Of these objects, moreover, is also considered the electrical energy required for their operation, reported according to the unit of measure of kWh. From here, it is therefore estimated a power of 200 W for the computer and 50 W for the monitor [145], and an average value of 0.006 kWh for the router [146].

  From the digital model, the next step is the additive manufacturing process. Since, however, 3D printing is a rather innovative technology, the SimaPro software does not present enough information to add this specific process in the databases. Therefore, in accordance with the literature, only the energy consumption of the process is considered, neglecting the instrumental part of the 3D printer [147, 148]. Electricity was included under "*Electricity, low voltage {IT} | electricity voltage transformation from medium to low voltage | Cut-off, S*" and a quantity of 0.66 kWh was considered, a value calculated based on the average consumption of a large printer. The value was reported on the basis of the information in the data sheet of the printer used for this thesis project [85].
- Cold plasma treatment at atmospheric pressure. Also, in this case there are the same materials used for this thesis work, i.e. the plasma consisting of the ionized gas argon, and TEOS (tetraethyl orthosilicate) as a precursor. The two products were entered under the headings "*Argon, liquid {RoW} | production | Cut-off, S*" and "*Tetraethyl orthosilicate {GLO} | production | Cut-off, S*". For both, moreover, the quantity necessary to carry out the cold plasma treatment on a cube of 1 cm^3 volume was estimated; therefore, for argon a quantity of 0.25 kg was reported, followed by a density of 1.784 kg/m^3, while for TEOS a quantity of 0.02 kg was reported, a density of 933 kg/m^3 and a lifetime of 5 years, in agreement with the time indicated for the PLA cube, precisely because the precursor

becomes part of the polymer matrix. In particular, for the precursor, its disposal has also been considered, both before, when the waste is produced, and after, when the end-of-life scenario of the cube is considered; TEOS, in fact, when deposited on the PLA, becomes part of the structure itself. The voice according to which its disposal was considered is " *Municipal solid waste {IT}* | *treatment of, incineration* | *Cut-off, S* ".

In addition, the plasma device is supported by an air compressor; therefore, the compressor input was also introduced, according to "*Air compressor, screw-type compressor, 4kW {RoW}*| *production* | *Cut-off, S*". The product was entered considering the usage time, of 30 minutes, and the lifetime, of 10 years. Of this, moreover, the electrical consumption was considered, which is about 250 W [149].

Each material reported as an input is entered into the system by multiplying the quantity by the functional unit and by the density of the same, all related to the useful life time for the time of use.

Next, in addition to the items concerning the materials proposed for the integration phase, the electricity of the entire system is reported, considering the energy contribution of the electronic equipment, whose value is equal to 1.226 kWh.

Then, also the transport of some of the materials used is considered, such as PLA filament (757 km, manufacturing company in Barletta - FabLab Venice) and the residue produced during the printing process, of which the transport from FabLab to the nearest incinerator (11 km, FabLab - Ecoprogetto Venezia S.r.l.), argon (5 km, Mestre - FabLab) and TEOS (10 km, STEA S.r.l., Venice - FabLab) is considered. The transport item is entered through "*Transport, freight, light commercial vehicle {Europe without Switzerland}* | *market for transport, freight, light commercial vehicle* | *Cut-off, S*", as it is assumed that the materials transported require medium-sized vehicles.

2.5.4.2 Case 2

The second case of integrative restoration, on the other hand, is based on a more traditional method, in which the use of the 3D printer coupled with cold plasma treatment is no longer proposed, but the realization of the final product by means of plaster, which is inserted into a mould based on silicone rubber (tab.14).

Table 12. Input and waste scenario of case 2: for each one product in SimaPro, quantity, density, transport, lifetime, electricity and allocation waste are indicated.

INPUT							
Phase	**Materials**	**Inventory**	**Quantity (g)**	**Density (kg/m^3)**	**Transport (km)**	**Lifetime Using time**	**Waste and allocation (g)**
Material for integration	Gypsum	*Gypsum, mineral {GLO} | market for | Cut-off, S*	1.3	1300	10	2 years	-
		Transport, freight, light commercial vehicle {Europe without Switzerland} | market for transport, freight, light commercial vehicle | Cut-off, S	-	-		-	-
	Water	*Water, ultrapure {RoW} | production | Cut-off, S*	$9.29*10^{-4}$	997	-	6 years 60 min	-
Material for cast	Silicon gum	*Synthetic rubber, {RoW} | production, Cut-off, S*	10	1100	11 10	3 days	10 (100 %)
		Municipal solid waste {IT} | treatment of, incineration | Cut-off, S	-	-		-	
		Transport, freight, light commercial vehicle {Europe without Switzerland} | market for transport, freight, light commercial vehicle | Cut-off, S	-	-		-	
WASTE SCENARIO							
End-of-life	Gypsum waste	*Municipal solid waste {IT} | treatment of, incineration | Cut-off, S*	1.3	-	11	-	100 %
		Transport, freight, light commercial vehicle {Europe without Switzerland} | market for transport, freight, light commercial vehicle | Cut-off, S		-		-	
	Silicon gum	*Municipal solid waste {IT} | treatment of, incineration | Cut-off, S*	10	-	11	-	100%
		Transport, freight, light commercial vehicle {Europe without Switzerland} | market for		-		-	

		transport, freight, light commercial vehicle | Cut-off, S					

In this case, therefore, the initial input is gypsum, inserted under the item "*Gypsum, mineral {GLO} | market for | Cut-off, S*", whose mass has been calculated considering a volume of 1 cm^3 and a density of 1300 kg/m^3; the final value obtained is 1300 mg.
In particular, for this specific case of integrative restoration the use of alabastrine gypsum is proposed, suitable to produce calcined gypsum artefacts, such as frames and rosettes, as it shows good characteristics of hardness, compactness and whiteness. Moreover, in order to obtain the final product, it is necessary to prepare the gypsum by adding the right amount of water; the mixing ratio is, therefore, equal to 140 g of gypsum + 100 g/ml of water [150]. On the basis of the doses indicated and knowing the mass of the gypsum, it is possible to find, through a proportion, the amount of water, equal to 0.929 ml. From here, using the entry "*Water, ultrapure {RoW} | production | Cut-off, S*", the value accompanied by the density (997 kg/m^3) was entered.
Then, for the realization of the mould the use the silicone rubber is preferable, which is entered in the software through the item "*Synthetic rubber, {RoW} | production, Cut-off, S*". The value entered, about 0.01 kg, was estimated on the basis of the amount of gypsum required for integration; in addition, the value is accompanied by the density of the material, equal to 1100 kg/m^3. In this case, the use of silicone rubber concerns only the formation of the cast to produce the cube and, therefore, following its use, the material, not covering other functionalities, is completely thrown away. The process is reported in the software under the category "waste treatment", by means of the entry " *Municipal solid waste {IT} | treatment of, incineration | Cut-off, S* ".
For both gypsum and silicone rubber, transport is also considered, inserted as in the previous case under the heading "*Transport, freight, light commercial vehicle {Europe without Switzerland} | market for transport, freight, light commercial vehicle | Cut-off, S*", and with a value of 10 km, since it is assumed that the purchase of the products takes place within the Mestre area.
Also in this case, the final output of the system is given by the chalk cube, characterized by a volume of 1 cm^3.

2.5.5 Life Cycle Impact Assessment (LCIA)

In the inventory phase, the environmental loads of the individual products considered in the two reinstatement cases were quantified. The effects associated with the environmental impacts are now quantified in the impact assessment phase, which is referred to as the Life Cycle Impact Assessment and is done using quantitative calculation tools.
Generally, any impact assessment method can be selected.
In this specific case, the ReCiPe 2016 Midpoint (H) methods were considered, through which indicators of life cycle impact categories can be calculated, and IPCC GWP 100a, which

characterizes different gaseous emissions according to their global warming potential, whose values are based on data published by the IPCC (Intergovernmental Panel on Climate Change).
Considering the specific case ReCiPe, the indicators are set on two levels: 18 midpoint indicators and 3 endpoint indicators. Each method contains factors according to three cultural perspectives: Individualistic (I), i.e. short-term, Hierarchical (H), i.e. a consensus model (default model), and Egalitarian (E), i.e. long-term. Unlike other approaches, ReCiPe does not include the potential impacts of future extractions in the impact assessment but assumes that these impacts were included in the inventory analysis.
In this case, the Midpoint, which considers the cause-effect relationship of an impact category, was considered and the hierarchical perspective (H) was followed.
The impact categories considered are:

- *Fine particulate matter formation*: to this category belong all those solid or liquid substances suspended in air, whose size varies from a few nanometers to 100 μm. The unit of measurement considered is the amount of $PM_{2.5}$ equivalent.
- *Marine eutrophication*: this is a characterization factor that takes into account the nutrients (N, P) of sewage effluents and fertilized agricultural land, which accelerate the growth of algae in marine environments thus contributing to marine eutrophication. Its unit of measurement is kg N eq.
- *Terrestrial acidification*: this category considers the impacts caused by acidification generated by emissions of acidifying gases into the atmosphere, which, going to deposit in water and soil, determine the increase in the concentration of hydrogen ions and therefore the increase of acidity. The main substances responsible for this impact are nitrogen oxides (NO_x), sulphur dioxides (SO_2) and ammonia (NH_3), which, however, contributes to this impact only after the soil nitrification process. In particular, in ReCiPe, sulfur dioxide is considered as the reference substance and a time horizon of 500 years is considered.

While in the case of the IPCC GWP method, the direct global warming potentials (GWP) are related to the impact of carbon dioxide and represent an index to estimate the relative contribution to global warming due to the emission of one kg of a particular greenhouse gas into the atmosphere compared to the emission of one kg of carbon dioxide. In addition, different time horizons (20a or 100a) can be considered through the method. A 100a horizon was considered for this analysis.
The two impact categories considered during the analysis are shown in Table 15, accompanied by the name of the group considered and the representative units of measurement.

Table 13. Impact categories considering during the analysis.

Method	Name of impact category group	Unit of measure
IPCC GWP 100a	❖	kg CO_2 eq
ReCiPe 2016 Midpoint (H)	Fine particulate matter formation	kg $PM_{2.5}$ eq
	Marine eutrophication	kg N eq
	Terrestrial acidification	kg SO_2 eq

Chapter 3

In this chapter, results of the analyses carried out are reported, with the aim to study the filament and to propose a comparison between cold plasma treated and non-treated samples. Moreover, the multi-analytical approach aimed at verifying possible change as a result of accelerated aging, subsequently evaluating both the mechanical properties of the samples (t+n-t) before and after aging, and the acid resistance of the printed cubes (t+n-t).

3.1 RESULTS: FILAMENT AND SAMPLES CHARACTERIZATION

In this section, it's reported the results for both pure PLA filament and printed dog bones (t + n-t) before aging, obtained from colorimetric analysis, ATR FT-IR and Raman spectroscopies, thermogravimetry (TGA), differential scanning calorimetry (DSC), and dynamometric tests.

3.1.1 Colorimetric analysis

The colorimetric analysis results for the printed samples (t + n-t) are shown in Table 16, where the average values, with the standard deviation, of the three colorimetric parameters L*, a*, and b* are presented. The three values will be used later to calculate the color difference (ΔE) of the samples before and after accelerated aging.

Table 14. Average and standard deviation of L, a* and b* parameters of the 5 treated and 5 untreated plasma samples.*

Sample	**L***	**SD**	**a***	**SD**	**b***	**SD**
n-t	76.07	1.43	-0.52	0.06	6.1	0.72
t	75.48	1.28	-0.58	0.12	5.76	0.47

From the data obtained it is possible to observe that the two sets of samples taken into analysis do not present great colorimetric differences, that is, no variations can be detected by the naked eye. The value of L*, which represents the brightness, assumes a fairly high value, as the PLA layers that are part of the sample tend to reflect.
On the other hand, the values of a* and b*, that define the chromaticity of the color, assume for both samples the same algebraic sign: the coordinate a* is negative and expresses the green component, whereas the coordinate b* is positive and expresses the yellow component. In particular, in the case of the treated sample all values are lower, could be due to the deposition of the TEOS film, which led to a minimal colorimetric variation.

Then the reflectance curves are reported, where in abscissa there are the wavelengths, indicated in nm, while in ordinate the percentage reflectance (fig.42).

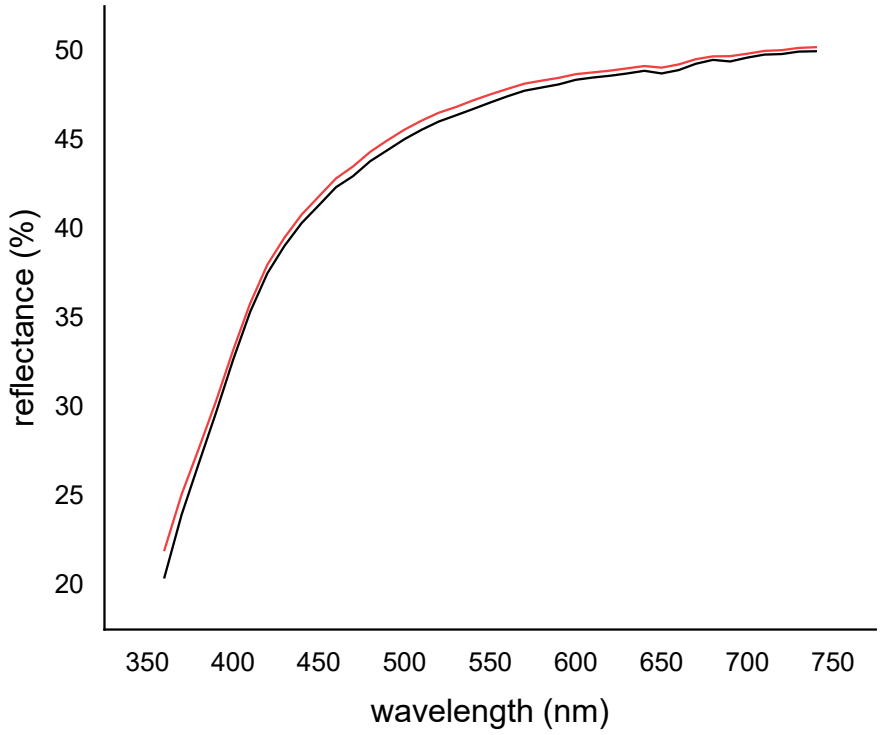

Figure 42. Reflectance curves of an untreated (black) and treated (red) plasma sample before accelerated aging, acquired with the colorimeter.

Analyzing the spectra, it is possible to see that the curves are particularly similar, as both show an initial increase followed by an approximately linear trend; it is assumed, therefore, the presence of a blue component, for the shoulder at about 450 nm (area that in the electromagnetic spectrum coincides with the blue/light blue).
Particular attention should also be paid to the scale of the ordinates, which appears slightly higher in the case of the plasma-treated sample (Fig.42).

3.1.2 Fourier transform infrared spectroscopy (FT-IR) in ATR mode

Figure 43 shows the FT-IR spectrum in ATR mode of the pure PLA filament, which is compared with the spectra obtained for two printed samples, one treated and one not treated by plasma (fig.43).

Thanks to the technique it is possible to trace the functional groups constituting the thermoplastic polymer, as well as assess any variations in IR signal due to the appearance or decrease of absorption intensity of particular species.

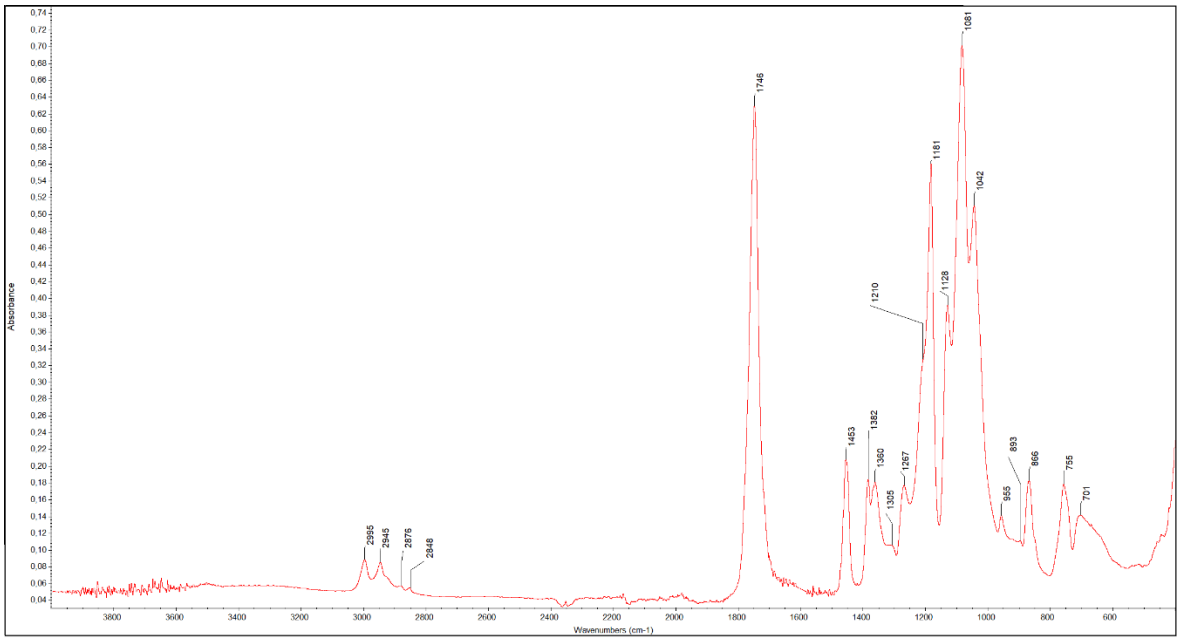

Figure 43. FT-IR spectrum in ATR mode of the PLA filament before accelerated aging.

The spectrum of the PLA filament shows three characteristic regions. The first region corresponds to the carbonyl peak, a particularly intense peak that is found at 1746 cm^{-1} and is associated with the stretching of the C=O double bond; typically, the main functional group of PLA (C=O) also appears in the 695÷760 cm^{-1} region, where in this case there are two peaks, one at 755 cm^{-1} and one at 701 cm^{-1}. It should be remembered, in fact, that PLA is derived from lactic acid and consists of polymer chains rich in carboxylic acids.

A second very interesting peak is given by the stretching vibration of the -C-O- bond of the -CH-O- group, present at 1181 cm^{-1}. The last region consists of three characteristic peaks (1128, 1081, and 1042 cm^{-1}) attributed to the C-O- stretching vibration in the -O-C=O group.

The stretching and bending motions of the CH and CH_3 groups, on the other hand, fall in the 3000-2800 cm^{-1} and 1454÷1360 cm^{-1} intervals.

There are, in addition, peaks at 866 cm^{-1} and 755 cm^{-1} that refer to the amorphous and crystalline phases of PLA.

Next, the peaks at 1305 cm^{-1} and 1267 cm^{-1} indicate the COC stretching present in the CH+COC group, while the peak at 1210 cm^{-1} indicates the COC stretching group. Finally, the peak at 955 cm^{-1} refers to CH_3 and CC rocking and the peak at 893 cm^{-1} to C-COO stretching [95-100].

Following this, Figure 44 shows the FTIR spectrum of the PLA filament after the annealing process; the analysis was performed on the residue obtained as a result of the TGA-DSC analysis.

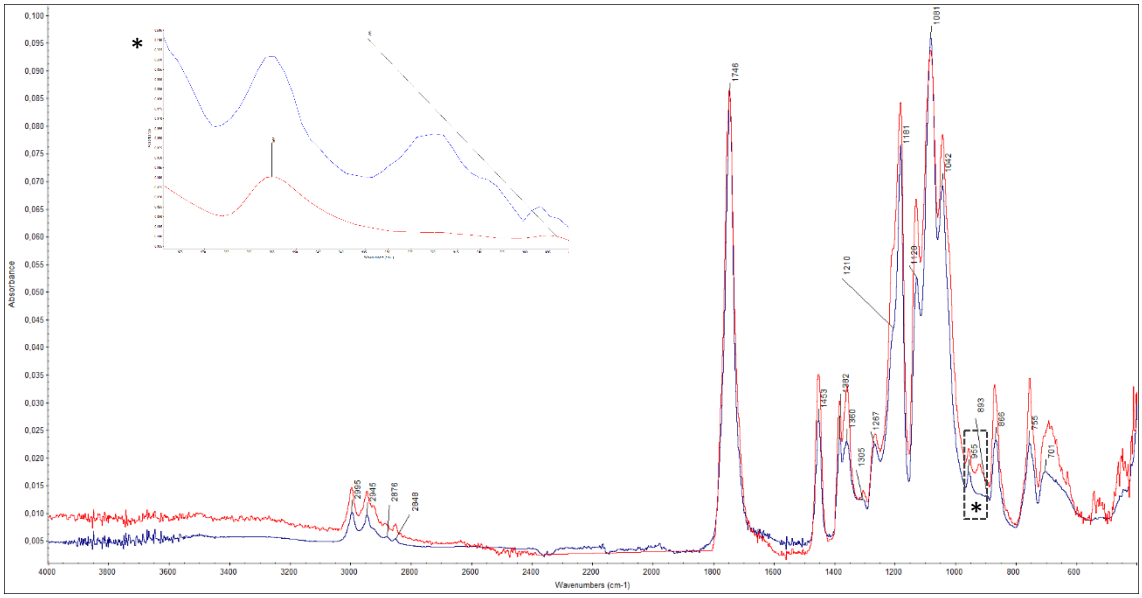

Figure 44. FT-IR spectrum in ATR mode of the PLA filament after annealing process (red), compared with spectrum of PLA filament (fig.43); an enlargement of the peak at 955 cm^{-1}, present in both spectra, and of the peak at 920 cm^{-1}, present in the annealed filament is reported.

Comparing the spectrum obtained after the annealing process with the spectrum of the filament before the process it is possible to observe a general increase of the peaks; probably part of the variation comes from a different baseline of the two spectra.

Starting from the region 3000÷2800 cm^{-1}, related to the stretching of methyl groups, it is possible to find a higher intensity for the peak at 2995 and 2848 cm^{-1}; moreover, a new peak is found at 2927 cm^{-1}.

The same behavior is observed in the 1500÷1250 cm^{-1} region (methyl CH group stretching, and COC stretching) and in the 1200÷700 cm^{-1} region (CH_3 stretching region, carboxyl and carbonyl group stretching).

In particular, in the spectrum related to the annihilated PLA there is an increase in the shoulder at 1210 cm^{-1} (due to alkyl-ketone chain vibration), followed by an increase in the intensity of the band at 1181 cm^{-1}, due to COC stretching, and the formation of a new peak at 920 cm^{-1}, indicating that the polymeric material, during the annealing process, has undergone a minimal crystallization; both peaks, in fact, represent the crystalline structure of PLA [151-155]. A confirmation of this can be provided by DSC analysis, in particular by comparing the crystallinity degrees before and after annealing (Fig.48).

Then the spectra of two samples (t + n-t) made by additive manufacturing FDM are compared to each other (Fig.45).

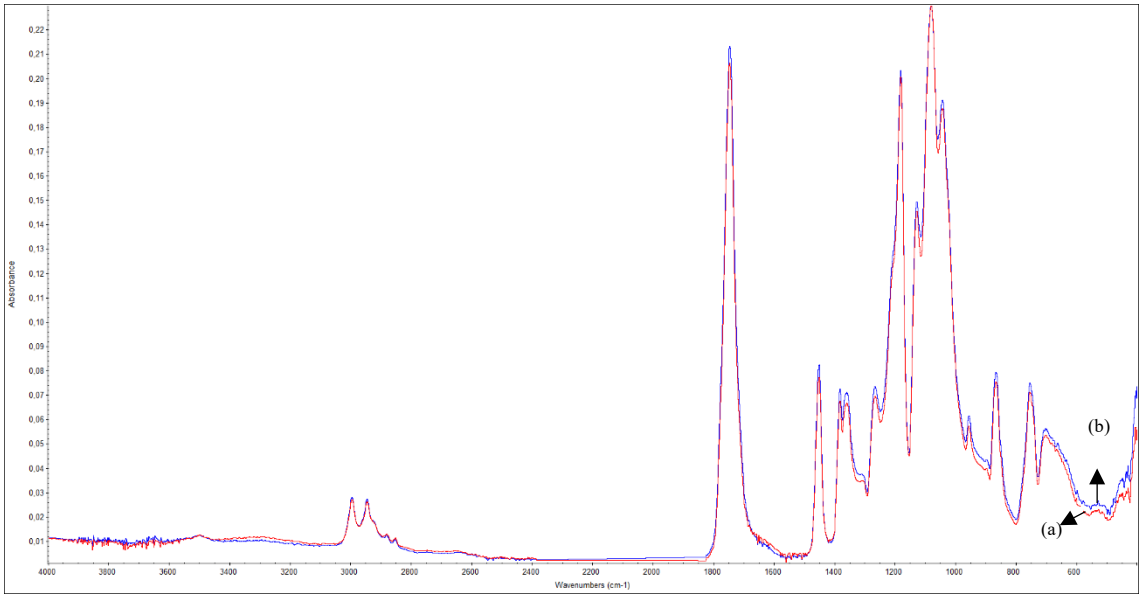

Figure 45. ATR-mode FTIR spectra of two overlapping samples: (a) sample t and (b) sample n-t.

Comparing, instead, the two samples it is possible to notice that the intensity of the peaks is approximately equal; therefore, no relevant differences or the presence of different peaks compared to the pure PLA filament (fig.43) can be noticed.

According to the information reported in the literature [63,156-158], argon-based plasma treatment should lead to a slight increase in the intensities of the peaks related to the CO and OC=O functional groups, followed by a minimal decrease in the peaks related to the methyl groups. The changes are mainly due to the surface activation of the plasma, which should promote the formation of carboxyl and carbonyl groups as well as surface hydroxyl groups.

Therefore, the changes that are reported in the literature could not be observed in this case. According to some studies [140], in fact, the incorporation of oxygen on PLA samples treated with argon plasma is much less pronounced than on samples treated with air plasma.

In addition, it is possible to hypothesize that the typical precursor (TEOS) bands are not visible [159].

3.1.3 Raman spectroscopy

Figure 46 shows the Raman spectrum of the pure PLA filament. Each peak is then associated with peaks found in the literature, and, for each, a brief description is given in Table 16.

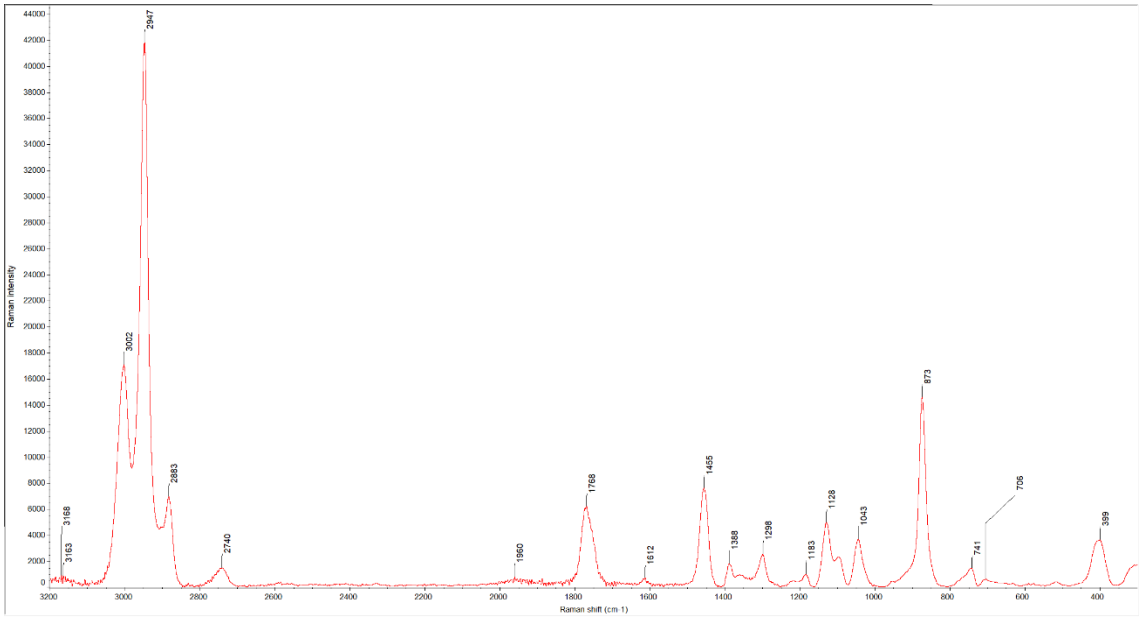

Figure 46. Raman spectrum of the PLA filament before accelerated aging.

In the Raman spectrum, there are both asymmetric stretching vibrations, at 3002 cm^{-1}, and symmetric stretching vibrations, at 2947 and 2883 cm^{-1}, of C-H in the $-CH_2$ and $-CH_3$ groups.
However, the main bands of the polymer can be observed in the region below 1800 cm^{-1}, where the C=O stretching groups are recognized. The peak representing them, in fact, is located at 1768 cm^{-1}, and consists of a particularly strong signal, while a weaker signal is given by the peak at 741 cm^{-1}.
Other peaks that characterize the PLA are at 1455 cm^{-1}, which indicates the asymmetric CH_3 groups, and at 1388 cm-1, which refers to the symmetric CH_3 group.
The next peaks refer to the COC group at 1298 cm^{-1}, the CH_3 rocking vibration at 1128 cm^{-1}, and the C-CH_3 stretching at 1043 cm^{-1}.
The C-COO stretching of the repetitive unit within the structure gives the very strong band at 873 cm^{-1}. Finally, below 800 cm^{-1} three bands are observed, corresponding to the deformations of the C=O, C-CO and C-O-C groups [112].
The Raman spectrum related to the pure PLA filament is followed by the spectra of two printed samples (1 t + 1 n-t), shown in Figure 47.

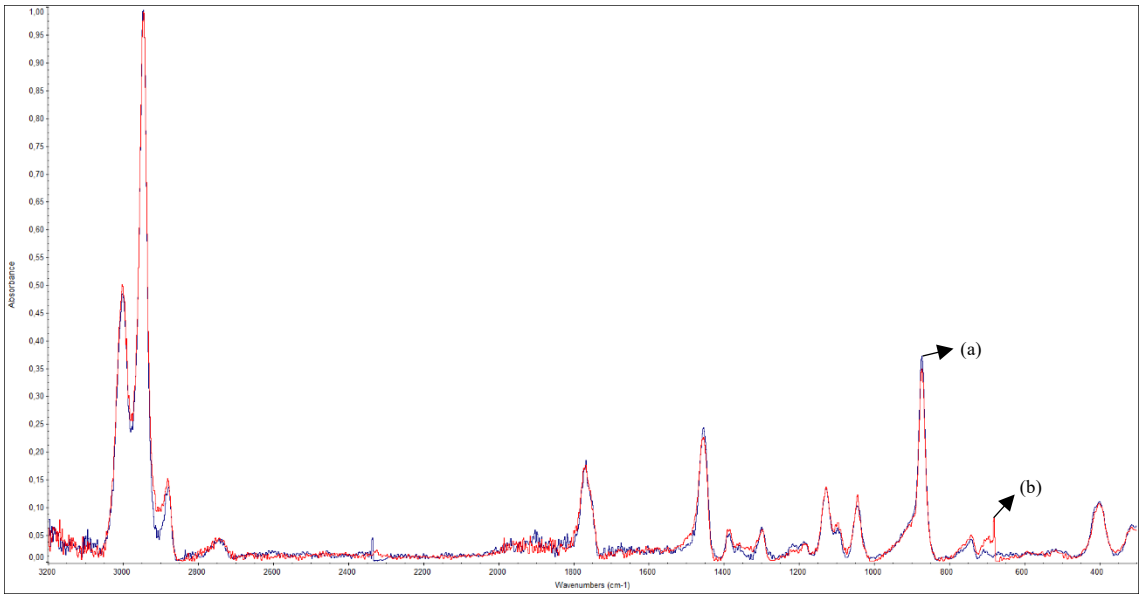

Figure 47. Raman spectra of two samples: (a) sample t and (b) sample n-t.

The spectra appear very similar and therefore show minimal changes in intensity. As in the case of the PLA filament, the comparison of the two spectra shows the characteristic peaks of the polymer, related to the stretching of the C=O group, the asymmetric deformation of the CH_3 group and the elongation of the C-COO group. Furthermore, no change in the peaks is observed.
Moreover, even in the case of Raman spectroscopy, the peaks related to the silicon present in the coating applied during plasma treatment are not found. According to the information in the literature, in fact, the presence of TEOS should be detected thanks to an intense peak at about 656 cm^{-1} which corresponds to the stretching vibrations of the Si-O bond [160-163].

3.1.4 Thermogravimetry (TGA) and Differential Scanning Calorimetry (DSC)

Figure 48 shows the results for the thermal stability test of the pure PLA filament, before and after annealing, through the thermogravimetric curve (TGA), which considers the weight percentage change versus temperature (°C), and the differential scanning calorimetry (DSC) curve, with which the heat flux (µV/mg) versus temperature (°C) is reported. The temperature

range was chosen both based on the parameters that were selected to print the polymer, where the temperature is 210 °C, and to verify the decomposition range of the material.
In addition, the values obtained during the analysis are shown in Table 17.

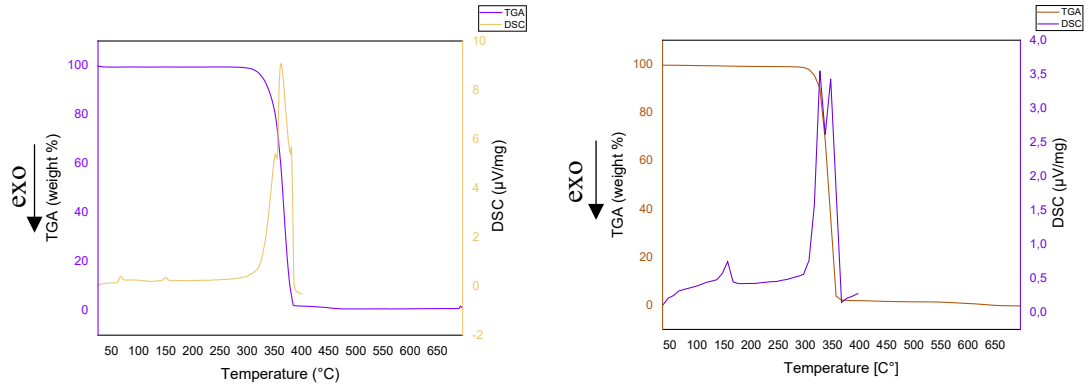

Figure 48. TGA-DSC curves of PLA filament before (left) and after (right) annealing process.

Table 15. Results obtained for PLA filament after annealing, during DSC analysis: glass transition temperature (T_g), melting temperature (T_m), enthalpy of melting (ΔH_m) and crystallinity degree (χ).

	DSC				TGA	
Sample	T_g (°C)	T_m (°C)	ΔH_m (J/g)	χ (%)	$T_{onset-I}$ (°C)	$T_{onset-f}$ (°C)
Before annealing	65.0	150.0	5.1	5.5	320.0	390.0
After annealing	34.5	150.0	19.3	20.7	300/310	360.0

Thermogravimetric analysis shows that the PLA, whose initial weight is 8.46 mg, exhibits initial thermal stability from about 25 to 300°C; in fact, the trend of the curve appears linear without any change in slope. Subsequently the polymer starts to undergo a significant weight loss starting from a temperature of about 320.0°C, which corresponds to $T_{onset-i}$. The degradation step continues up to 390.0°C, where there is a loss of 97% of the analyzed sample. Between the initial onset temperature and the final onset temperature there is the temperature of maximum degradation rate (T_{vmax}), equal to 362.0°C.
Finally, following the almost complete degradation of the polymeric material, from 400°C to 700°C no weight loss is observed.
Then the DSC curve (pink curve) shows both an exothermic and endothermic trend. The curve shows an initial inflection, corresponding to the T_g, equal to 65.0°C, and represents the moment when there is an increase in the specific heat of the polymer; while it is hypothesized that the exothermic peak present at 150.0°C may correspond to a low T_m thus making the coil material ideal for 3D printing, in particular for the FDM technique [97,164-166].

Subsequently, as mentioned above in the TG technique, three more exothermic peaks are present in the 300÷400°C temperature range, a central and particularly intense one corresponding to a T of 362.0°C, and two less intense lateral peaks presenting a value of 351.0°C and 381.0°C. The three peaks, therefore, refer to three phases of degradation of polylactic acid; in fact, as the temperature increases, the polymer undergoes a maximum degradation, through the phenomenon of pyrolysis, which initially involves volatile organic compounds and, subsequently, concerns high molecular weight compounds. In general, the thermal degradation of PLA is a complex phenomenon and can include different types of reactions: radical and non-radical, chain scission, depolymerization, intra- and inter-molecular transesterification, hydrolysis [166,167].

The TGA curve of the PLA filament after it has undergone annealing shows a similar trend to the TGA curve of PLA before annealing process. Therefore, a linear and slightly decreasing trend from 25 to about 290/300°C can be seen here as well. After that, the curve decreases rapidly and the temperature corresponding to the maximum degradation rate, T_{vmax}, is 328.6°C.

The initial onset temperature ($T_{onset-i}$) is around 300/310°C while the final onset temperature ($T_{onset-f}$) is around 360°C. Again, there is a 97% percent mass loss.

The results obtained from the TGA analysis are confirmed by the DSC curve.

First of all, it is possible to notice a decrease in the value of the glass transition temperature (T_g) where the inflection point corresponds to a value of 34.5°C; the value of the Tm, instead, turns out to be the same as the previous situation, i.e., equal to 150°C.

Moreover, in the temperature range where the inflection point of the TGA curve is present, there are two exothermic peaks that refer to two degradation kinetics of the polymeric material, the first one equal to 329°C and the second one is at about 350°C. Compared to the results obtained previously, in which there were three peaks related to the degradation of PLA, in this case it is possible to state that the polymer, in addition to present a slightly lower thermal resistance, shows a two-step degradation.

Generally, the results obtained during the DSC analysis are also confirmed by the literature, where it was verified that T_g tends to decrease, while T_m, as well as the degree of crystallinity, tend to increase. In particular, the decrease in T_g can be attributed to the chain cleavage process; moreover, the degree of crystallinity of PLA tends to increase gradually, until the chain undergoes cleavage (chemi-crystallization phenomenon) [168].

While the increase in T_m might suggest that the secondary crystallization related to the decrease in molar mass, is not due to the formation of new crystals, but rather to a process of crystallite thickening [169] or the formation of different families of crystallites [170]; these results are also confirmed by the FTIR spectrum of the annealed residue (fig.44).

Finally, the presence of the cold crystallization temperature is not found, precisely because it is assumed that the crystallization did not complete perfectly, due to the slow kinetics of the PLA [171].

Next, the TGA-DSC results of the n-t and t samples before aging in an inert atmosphere (N) are reported, (fig.49). Table 18 also shows the results obtained during DSC analysis.

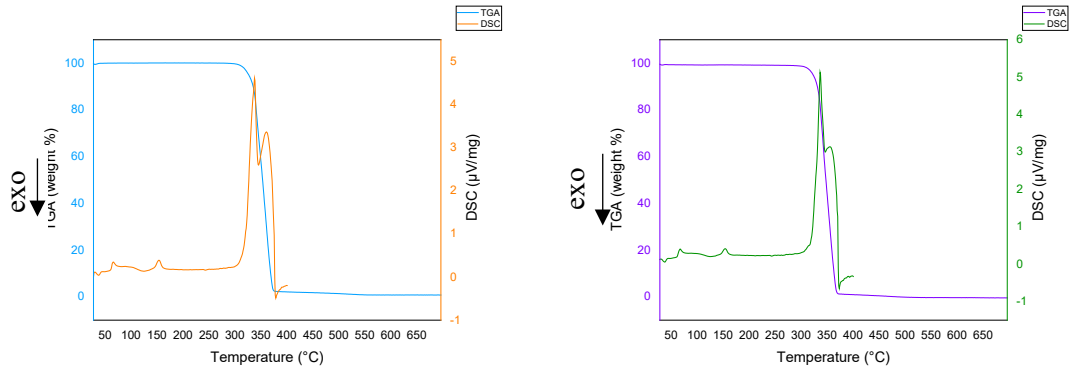

Figure 49. TGA-DSC curves of dog bones in an inert atmosphere: on the left results obtained for sample n-t, on the right results obtained for sample t.

Table 16. Results obtained for samples n-t and t, during DSC analysis: glass transition temperature (T_g), melting temperature (T_m), enthalpy of melting (ΔH_m) and crystallinity degree (χ).

	DSC				TGA	
Sample	T_g (°C)	T_m (°C)	ΔH_m (J/g)	χ (%)	$T_{onset-i}$ (°C)	$T_{onset-f}$ (°C)
n-t	61.0	154.0	13.8	14.8	334.0	370.0
t	61.6	154.1	11.9	12.8	328.0	360.0

Regarding the TGA curve of the n-t sample, the $T_{onset-i}$ is equal to 334.0°C whereas the end onset temperature is about 370.0°C. Making a direct comparison with the plasma treated sample, there is the $T_{onset-i}$ that is similar, i.e. equal to 328.0°C, whereas the end degradation temperature turns out to be at about 360.0°C. Therefore, compared to the PLA filament previously analyzed, both the beginning and the end degradation temperature show variations, although not significant. Certainly, during the FDM printing process, in which the filament was heated to a temperature of 210.0°C, a structural change occurred, during which the molecular chains were reorganized, giving the polymeric material different physical-chemical properties. Therefore, from the values obtained, it is possible to establish that on the one hand the printing process has led the material to resist 10°C more, before the same began to undergo a substantial loss of mass percentage; on the other hand, however, the degradation interval turns out to be shorter, because if before the temperature of the end of degradation was 390.0°C, now it is about 360/370°C, so the polymer shows a more rapid degradation process. At the end of the analysis there is a practically total loss of the polymeric material.

Also in this case, obviously, the flexure of the TGA curve is located in the region where there are two exothermic peaks, observed by DSC analysis, corresponding to the two degradation steps of the material and present at about 338.0°C and 361.0°C (sample n-t), and at 337.0°C and 373.0°C (sample t). Moreover, there is the T_g, corresponding to the first flexure of the curve, at about 61.0°C, and T_m at 154.0°C; the same values can be found also in the case of the treated sample.
In order to further analyze the behavior of the polymeric material after the printing process, a second thermal analysis is performed, considering a temperature range between 25 and 300°C. From the analysis it is observed the presence of cold crystallisation, at about 130.0°C, a phenomenon that was not previously observed; probably, the printing process did not allow the polymeric material to crystallize. Moreover, the absence of fillers within the structure, does not allow it to form nucleation centers thanks to which crystal growth is promoted [172].

Finally, the TGA-DSC curves of the n-t and t samples before aging in a mixed atmosphere (N_2/air) are reported (fig.50). Table 19 also reports the results obtained during DSC analysis.

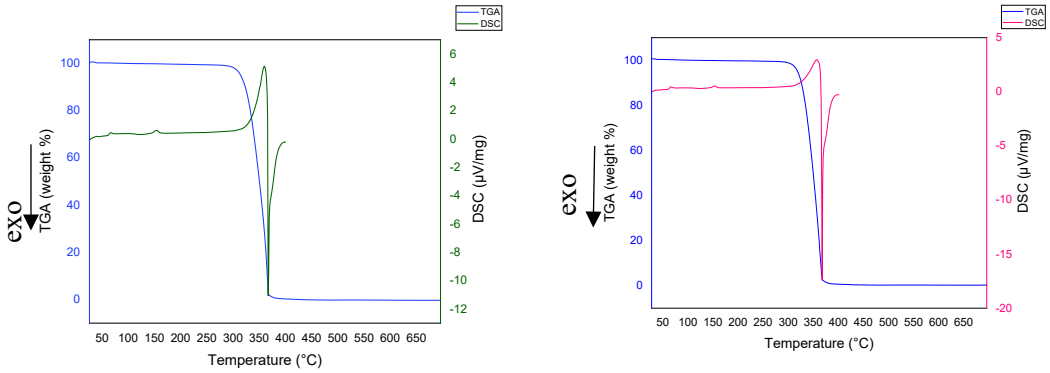

Figure 50. TGA-DSC curves of dog bones in mixed atmosphere (N_2/air): on the left results obtained for sample n-t, on the right results obtained for sample t.

Table 17. Results obtained for samples n-t and t, during DSC analysis: glass transition temperature (T_g), melting temperature (T_m), enthalpy of melting (ΔH_m) and crystallinity degree (χ).

	TGA				DSC	
Sample	T_g (°C)	T_m (°C)	ΔH_m (J/g)	χ (%)	$T_{onset-i}$ (°C)	$T_{onset-f}$ (°C)
n-t	62.0	154.0	9.1	9.8	330.0	≈ 370.0
t	61.5	153.6	8.1	8.7	332.0	≈ 370.0

Considering the TGA curve of both samples, it is possible to observe that, in the case of sample n-t the degradation start temperature is at about 252°C, where a slight loss in mass of the polymer

can be noticed, which continues especially at higher temperatures (≈330°C); while in sample t the $T_{onset-i}$ is equal to 332°C. Also in this case, an almost total loss of the polymeric material occurs. Turning, next, to the DSC curves, both the T_g and T_m appear similar in samples n-t and t; in order the T_g is equal to 62.0°C in the first case and 61.5°C in the second, while the T_m is 154.0°C in the first case and 153.6°C in the second.

Therefore, the differences that can be found between the PLA filament and the dog bones mainly derive from the printing process, whose extrusion temperature of 210°C led to a decrease of the T_g, although not significantly, and an increase in the T_m, whose variation could indicate a structural change in the material [97].

3.1.5 Dynamometric tests

The results obtained during dynamometric tests, both for n-t samples (tab.20, fig.51,52) and for t samples (tab.21, fig.53,54) are reported below. In particular, the tables show an average and a standard deviation of the data obtained during the test carried out on each sample; the parameters considered are the elastic modulus, the peak load, the tension at break and the deformation at break.
Then, the load vs extension curves are realized for each investigated specimen (fig.51, 53), finally reporting a picture of the specimens after the test (fig.52, 54).

Table 18. Dynamometric test data for the six untreated samples, before aging.

Parameters	**Values**	**SD**
Modulus	482.17 MPa	27.65
Peak Load	70.85 N	12.14
Peak Stress	5.90 MPa	1.01
Strain at break	1.64 %	0.26

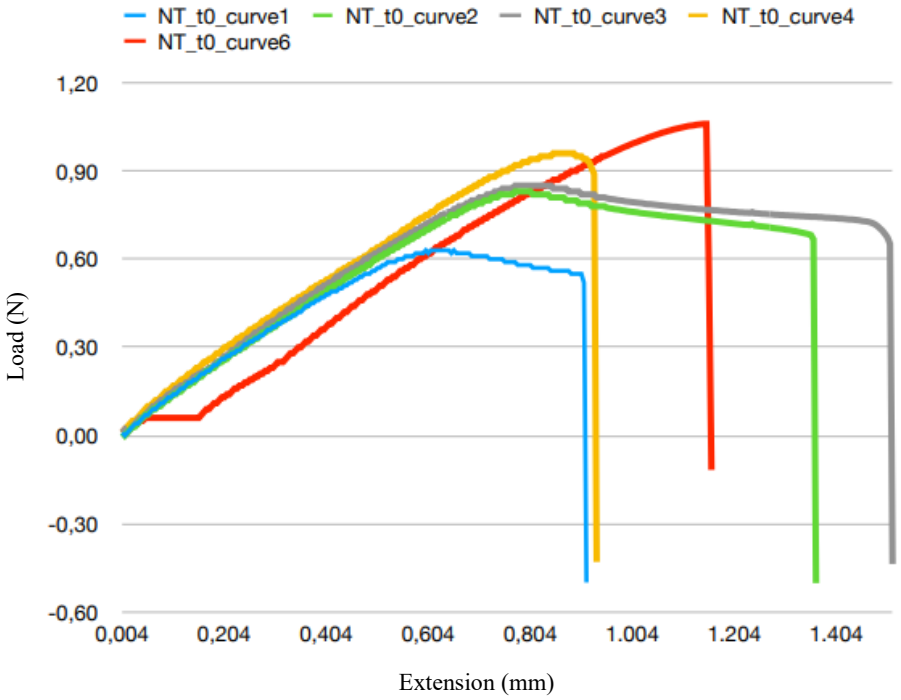

Figure 51. Load-extension diagram of six n-t samples, before aging.

Figure 52. The six untreated samples after dynamometric analysis.

Table 19. Dynamometric test data for the four treated samples, before aging.

Parameters	**Values**	**SD**
Modulus	466.52 MPa	20.38
Peak Load	66.43 N	4.57
Peak Stress	5.53 MPa	0.39
Strain at break	1.57 %	0.05

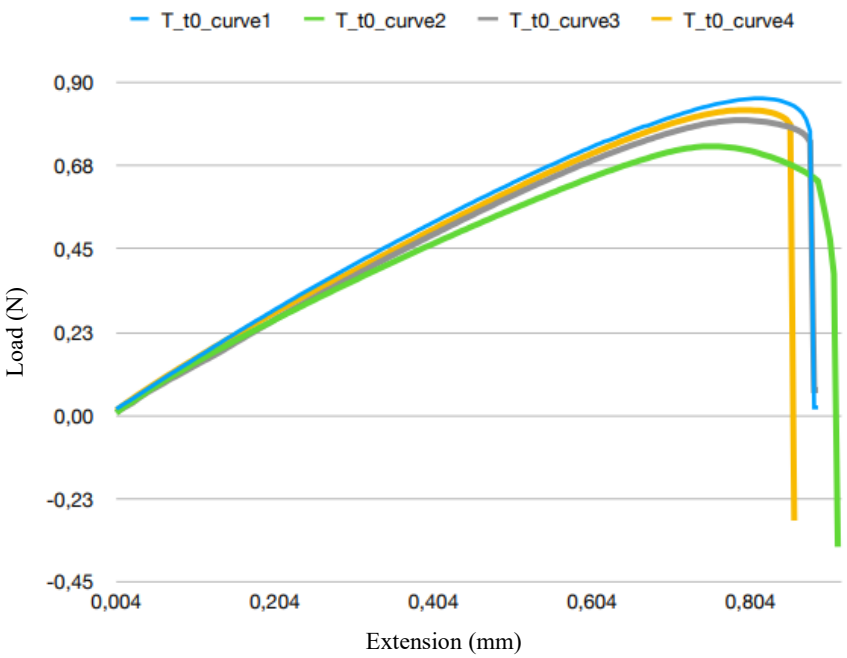

Figure 53. Load-extension diagram of four t samples, before aging.

Figure 54. The four treated samples after dynamometric analysis.

Comparing the results obtained, it is possible to state that the values of the untreated samples are higher than those of the treated samples.

In fact, according to the literature data, the plasma treatment should improve the mechanical properties, promoting the adhesion between the layers of the polymeric material [173]. In this case, therefore, it is assumed that the lower strength does not result so much from the low effectiveness of the deposited precursor, but rather from its excessive deposition on the samples during the printing process; this, therefore, led to the formation of vitrified surfaces in the polymer. The vitrification therefore made the materials more brittle and less tensile resistant.

In addition, an assessment can be made about the ductility and brittleness of the material by considering where the specimen broke during testing. Generally, a material shows ductile behaviour when the fracture occurs diagonally to the stress direction, while it shows brittle behaviour when the fracture is perpendicular to the stress direction, as the crystals are not well cohesive [174]. So, untreated specimens show ductile behaviour precisely because they tend to fracture more toward the center than at either end; while treated specimens show brittle behaviour because they tend to fracture near either end.

3.2 RESULTS OF ACCELERATED AGING

In this paragraph, the results obtained from the samples (t + n-t) after 2000 hours of accelerated aging are reported. The proposed analyses are the same as those discussed in the previous paragraph; thus there are:

- Colorimetric analysis, where the initial values are compared with the data obtained after 500, 1000, 1500 and 2000h of accelerated aging;
- ATR FT-IR, where the initial spectra are compared with the data obtained after 80h of accelerated ageing in a climatic chamber, and after 1500 and 2000h of ageing carried out outside the chamber;
- Raman spectroscopy, where the initial data are compared with the values obtained after 80h (aging in climatic chamber), and after 500, 1000, 1500 and 2000h of aging carried out outside the chamber;
- TGA-DSC, where the curves of the samples (t + n-t) before and after 2000h of artificial aging are reported.
- Dynamometric tests, through which a comparison is made between the 10 samples (5 t + 5 n-t) not aged and the 20 samples (5 n-t UV, 5 n-t RH, 5 t UV and 5 t RH) after they have undergone 2000h of aging.

3.2.1 Colorimetric analysis

The colorimetric data obtained during the analysis were processed in order to compare both the colorimetric variation, via the index ΔE, and the yellowing index, Y, of all samples, both plasma-treated and non-plasma-treated, before, during and after ageing, with a check every 500 hours. Tables 22 and 23 show, therefore, the values calculated for n-t and t samples at 0, 500, 1000, 1500, and 2000 hours of accelerated aging under incandescent light bulb.

In particular, the indices ΔE and Y are shown in the graphs in Figures 56 and 57 (n-t samples) and 59 and 60 (t samples), while the reflectance spectra of the n-t and t samples are shown in Figures 55 and 58.

Table 20. Colorimetric data of non-plasma-treated samples at 0, 500, 1000, 1500 and 2000h of accelerated aging; in order there are the three colorimetric parameters (L, a*, b*), colorimetric variation (ΔE) and yellowing index (Y). The SD of the three parameters, calculated for samples before aging and after 2000h, are also reported; SD of parameters after 2000h are extended to samples after 500, 1000 and 1500h.*

n-t_UV	L*	SD	a*	SD	b*	SD	ΔE	Y
Before	76.07	1.43	-0.52	0.06	6.1	0.72	-	46.77
After 500h	75.29	0.98	-0.15	0.08	4.64	0.13	2.17	48.74
After 1000h	75.27	0.98	-0.25	0.08	3.82	0.13	2.86	48.70
After 1500h	77.28	0.98	-0.16	0.08	3.50	0.13	4.35	52.00
After 2000h	75.50	0.98	-0.14	0.08	3.51	0.13	3.25	49.10

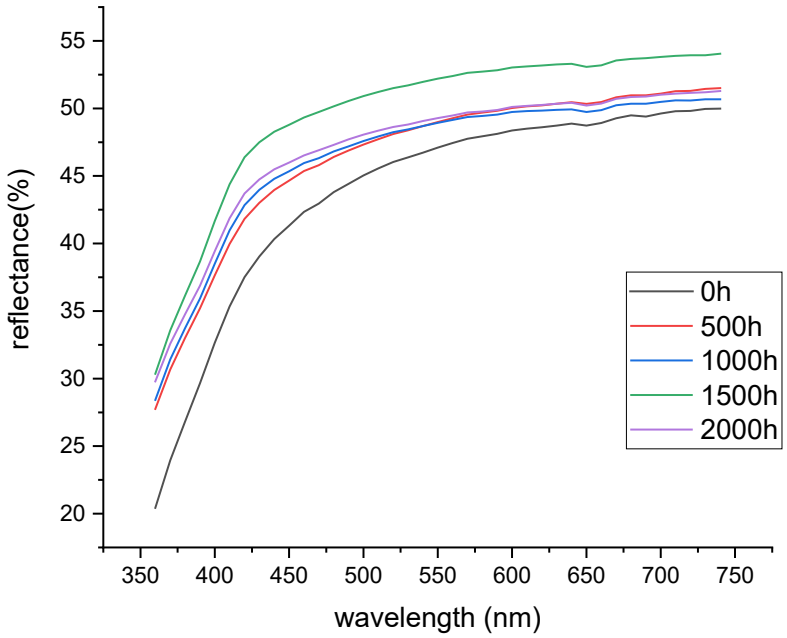

Figure 55. Reflectance spectra of non-plasma-treated samples at 0, 500, 1000, 1500, and 2000 hours of UV-accelerated aging; the wavelengths (nm) are shown in the abscissa, and the percent reflectance (%) is shown in the ordinate.

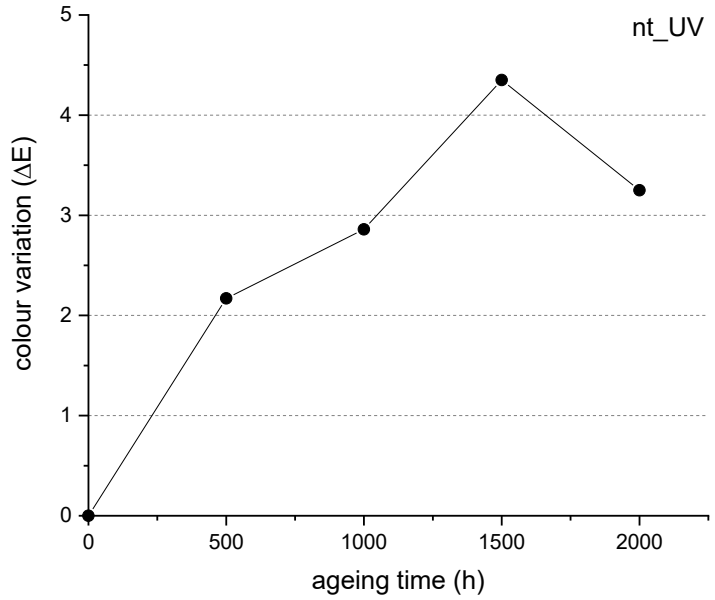

Figure 56. Color change (ΔE) of non-plasma-treated samples at 0, 500, 1000, 1500, and 2000 hours of UV-accelerated aging; time (h) is shown in the abscissa, and color change (ΔE) is shown in the ordinate.

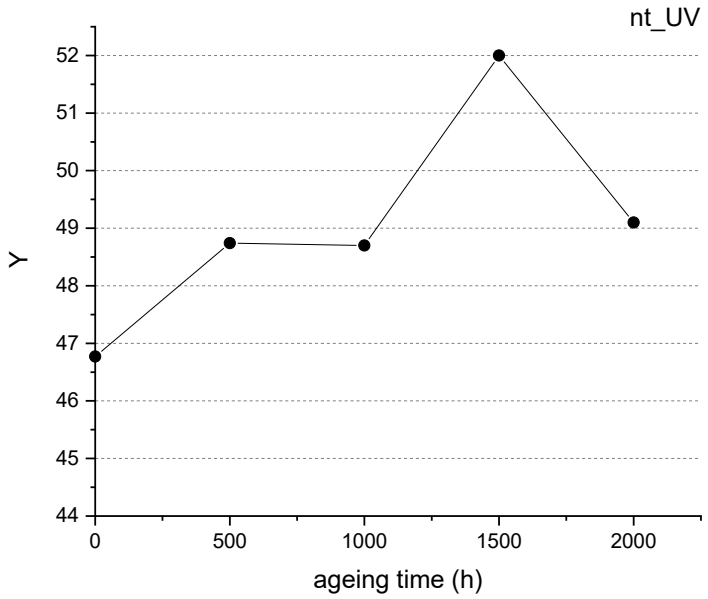

Figure 57. Yellowing index (Y) of non-plasma-treated samples at 0, 500, 1000, 1500, and 2000 hours of UV-accelerated aging; time (h) is shown in the abscissa, and color change (ΔE) is shown in the ordinate.

Table 21. Colorimetric data of plasma-treated samples at 0, 500, 1000, 1500 and 2000h of accelerated aging; in order there are the three colorimetric parameters (L, a*, b*), colorimetric variation (ΔE) and yellowing index (Y). The SD of the three parameters, calculated for the samples before aging and after 2000h, are also reported; the SDs of the*

samples before aging are extended to the samples after 500,1000, and 1500h of aging. SD of parameters after 2000h are extended to samples after 500, 1000 and 1500h.

t_UV	L*	SD	a*	SD	b*	SD	ΔE	Y
Before	75.88	1.28	-0.51	0.12	6.05	0.47	-	49.70
After 500h	75.65	2.63	-0.16	0.07	3.81	0.54	2.39	50.95
After 1000h	73.96	2.63	-0.19	0.07	4.14	0.54	2.73	46.65
After 1500h	72.53	2.63	-0.09	0.07	3.77	0.54	4.07	44.45
After 2000h	76.61	2.63	-0.13	0.07	3.21	0.54	2.95	51.00

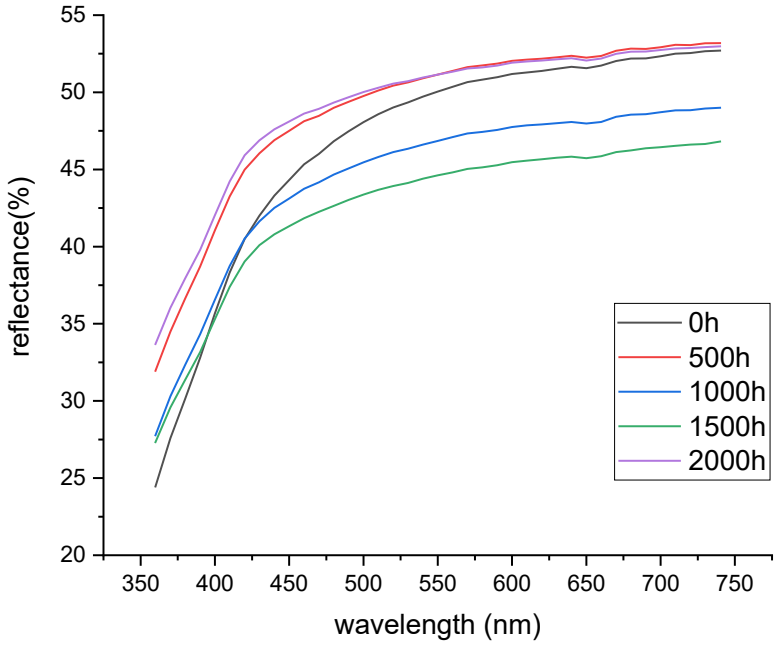

Figure 58. Reflectance spectra of plasma-treated samples at 0, 500, 1000, 1500, and 2000 hours of UV-accelerated aging; the wavelengths (nm) are shown in the abscissa, and the percent reflectance (%) is shown in the ordinate.

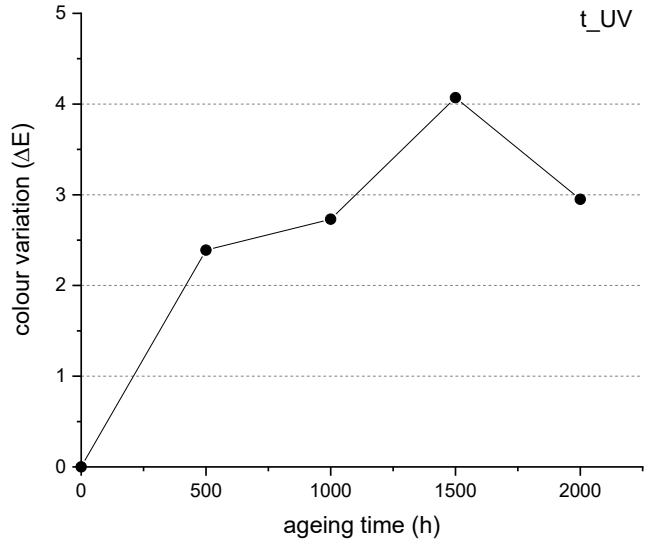

Figure 59. Color change (ΔE) of plasma-treated samples at 0, 500, 1000, 1500, and 2000 hours of UV-accelerated aging; time (h) is shown in the abscissa, and color change (ΔE) is shown in the ordinate.

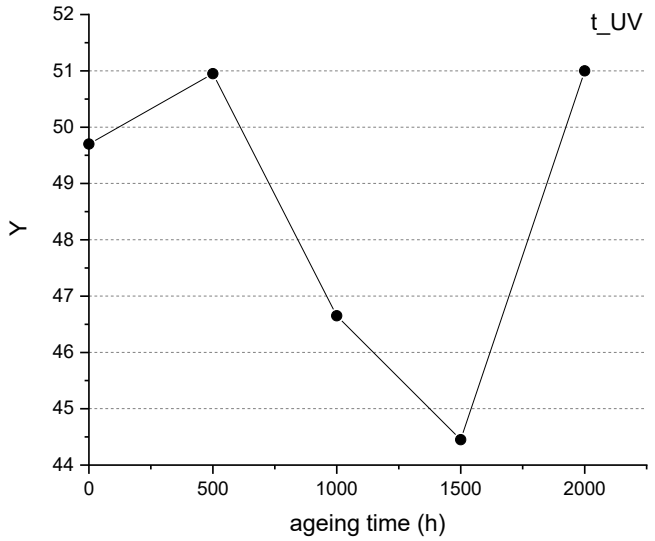

Figure 60. Yellowing index (Y) of plasma-treated samples at 0, 500, 1000, 1500, and 2000 hours of UV-accelerated aging; time (h) is shown in the abscissa, and color change (ΔE) is shown in the ordinate.

The reflectance spectra of samples n-t and t, shown in figures 55 and 58, show a similar trend; the only difference, in fact, appears in the percentage reflectance values, where in the case of untreated samples, from 0 to 1500 hours there is a general increase in the curve, while from 1500 to 2000 hours there is a slight decrease (2.76%). This is also verified in the graphs relating to the index ΔE and the parameter Y (fig.56,57), where there is a slight decrease in the values; in the specific case of ΔE, the variation is due to the parameters L* and b*, which from 1500 to 2000

hours decreased slightly (tab.22). The fluctuating value of the parameter ΔE derives from the values of the three colorimetric parameters, where it is possible to observe that, during aging, L* tends to increase and then decrease in the last step, a* from 0 to 500 hours increases and then remains constant over time, while b* decreases as aging proceeds.

On the contrary, in the case of the treated samples, the reflectance curves show first a general increase. The same trend is also visible in the case of the yellowing index, Y (fig.60), whereas the parameter ΔE shows an increase up to 1500 hours and a decrease from 1500 to 2000 hours. Considering the three colorimetric parameters (tab.23) there is an increase in the L* parameter, while a* and b* decrease. Overall, also in this case, the three colorimetric parameters tend to vary with aging: L* shows a decrease up to 1500 hours, and then increases in the last step, a* increases up to 1500, after which it decreases even if slightly, while b* shows a decrease, an increase and a second decrease.

Thus, comparing untreated and treated samples, the ΔE parameter shows a similar trend, and for the former it is slightly higher, while the Y index in n-t samples tends to increase during aging, and then decreases, while in t samples it decreases approximately, and then shows a rapid increase from 1500 to 2000 hours; in the latter case, in fact, the value appears slightly higher than in n-t samples.

Next, the graphs of n-t and t samples before and after accelerated aging carried out in a desiccator (RH≈70%) are reported, processed according to the data given in tables 24 and 25.

Figures 61 and 64 show the reflectance spectra of the n-t and t samples, while Figures 62 and 63, 65 and 66 show, in order, the colorimetric change indices ΔE and the Y parameter of the n-t and t samples.

Table 22. Colorimetric data of non-plasma-treated samples at 0, 500, 1000, 1500 and 2000h of accelerated aging; in order there are the three colorimetric parameters (L, a*, b*), colorimetric variation (ΔE) and yellowing index (Y). SD of parameters after 2000h are extended to samples after 500, 1000 and 1500h.*

n-t_RH	L*	SD	a*	SD	b*	SD	ΔE	Y
Before	76.07	1.43	-0.52	0.06	6.1	6.1	-	46.77
After 500h	73.75	3.31	-0.32	0.12	4.48	0.80	1.94	46.32
After 1000h	73.34	3.31	-0.37	0.12	4.7	0.80	1.84	45.68
After 1500h	72.9	3.31	-0.36	0.12	4.67	0.80	2.54	49.73
After 2000h	76.27	3.31	-0.40	0.12	4.43	0.80	2.98	50.49

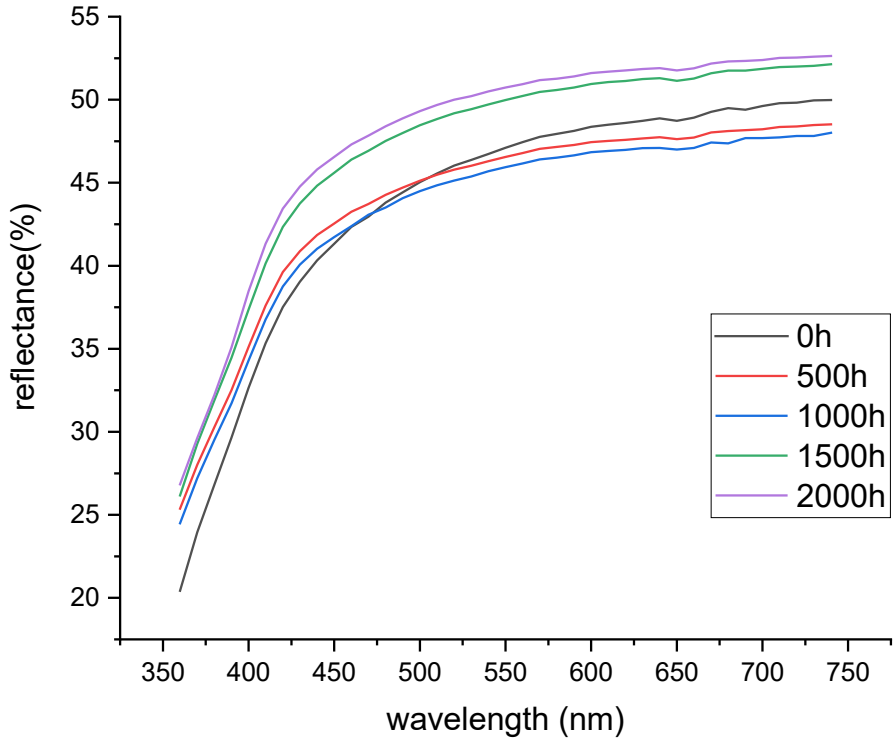

Figure 61. Reflectance spectra of non-plasma-treated samples at 0, 500, 1000, 1500, and 2000 hours of RH-accelerated aging; the wavelengths (nm) are shown in the abscissa, and the percent reflectance (%) is shown in the ordinate.

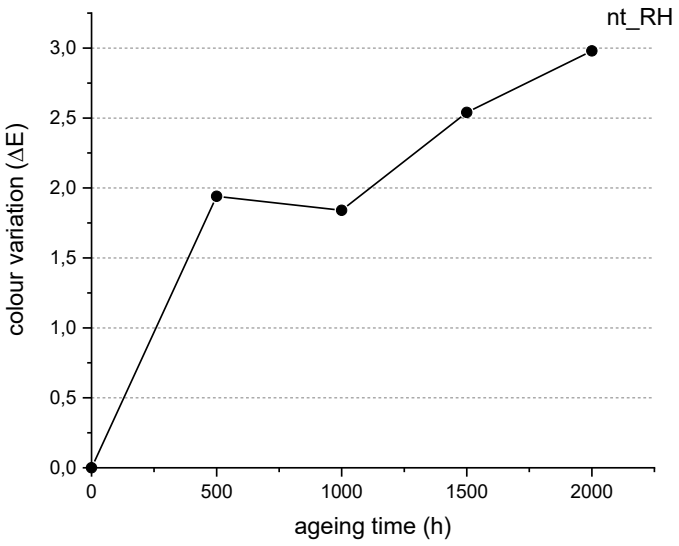

Figure 62. Color change (ΔE) of non-plasma-treated samples at 0, 500, 1000, 1500, and 2000 hours of RH-accelerated aging; time (h) is shown in the abscissa, and color change (ΔE) is shown in the ordinate.

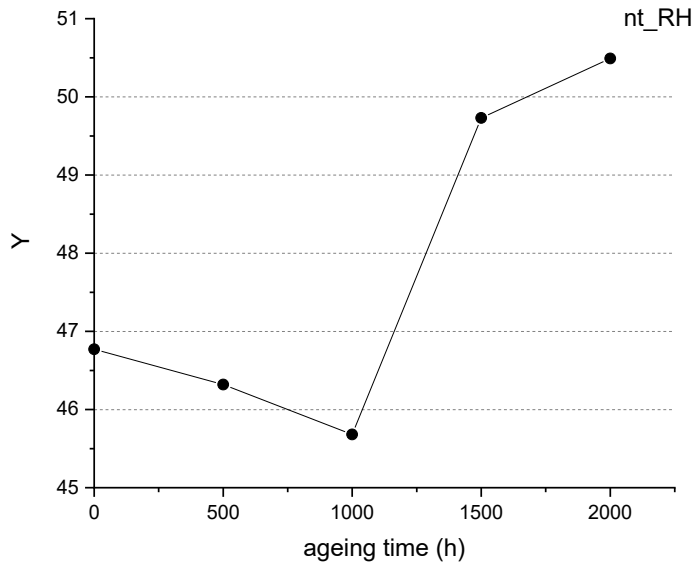

Figure 63. Yellowing index (Y) of non-plasma-treated samples at 0, 500, 1000, 1500, and 2000 hours of RH-accelerated aging; time (h) is shown in the abscissa, and color change (ΔE) is shown in the ordinate.

Table 23. Colorimetric data of plasma-treated samples at 0, 500, 1000, 1500 and 2000h of accelerated aging; in order there are the three colorimetric parameters (L, a*, b*), colorimetric variation (ΔE) and yellowing index (Y). SD of parameters after 2000h are extended to samples after 500, 1000 and 1500h.*

t_RH	L*	SD	a*	SD	b*	SD	ΔE	Y
Before	74.04	1.28	-0.4	0.12	6.4	0.47	-	46.77
After 500h	73.75	1.42	-0.32	0.12	4.48	0.30	1.94	46.32
After 1000h	73.34	1.42	-0.37	0.12	4.7	0.30	1.84	45.68
After 1500h	72.9	1.42	-0.36	0.12	4.67	0.30	2.54	49.73
After 2000h	76.27	1.42	-0.40	0.12	4.43	0.30	2.98	50.49

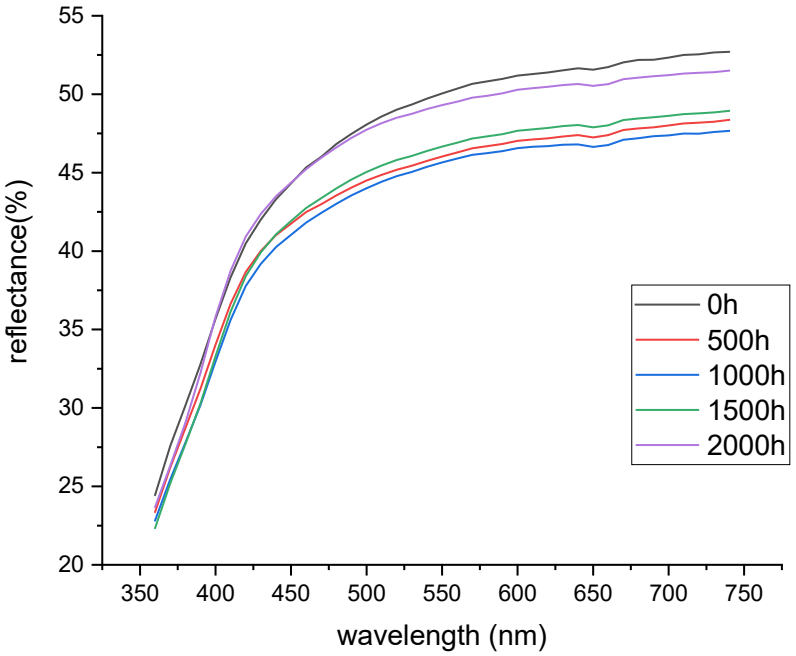

Figure 64. Reflectance spectra of plasma-treated samples at 0, 500, 1000, 1500, and 2000 hours of RH-accelerated aging; the wavelengths (nm) are shown in the abscissa, and the percent reflectance (%) is shown in the ordinate.

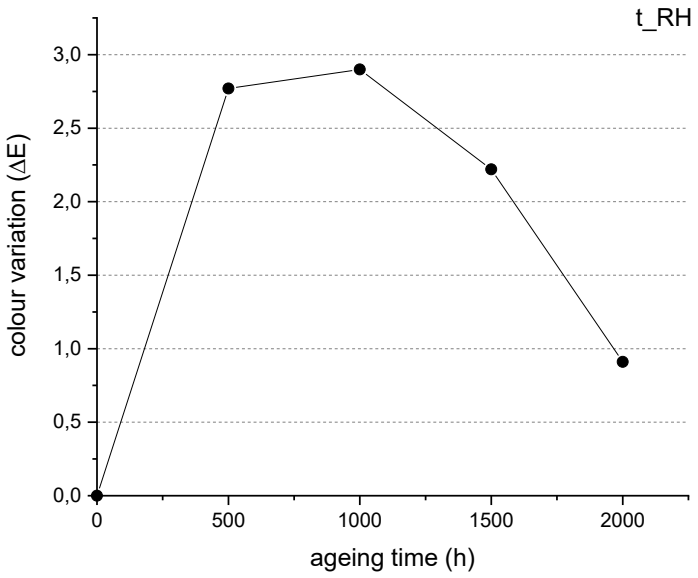

Figure 65. Color change (ΔE) of plasma-treated samples at 0, 500, 1000, 1500, and 2000 hours of RH-accelerated aging; time (h) is shown in the abscissa, and color change (ΔE) is shown in the ordinate.

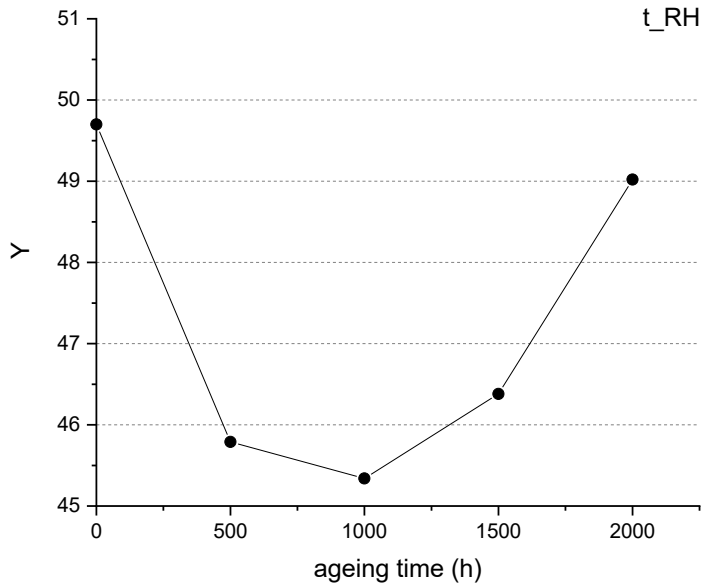

Figure 66. Yellowing index (Y) of plasma-treated samples at 0, 500, 1000, 1500, and 2000 hours of RH-accelerated aging; time (h) is shown in the abscissa, and color change (ΔE) is shown in the ordinate.

In the case of the reflectance spectra (fig.61,64), a rather fluctuating trend can be seen, especially in the case of treated samples, where the curves first undergo a decrease, from 0 to 1000 hours, then an increase, from 1000 to 1500 hours, and then a second decrease from 1500 to 2000 hours. The curves of the untreated samples, on the other hand, show a decrease from 0 to 1000 hours and then an increase from 1000 to 2000 hours.

Considering the colorimetric change, ΔE, in the case of the n-t samples a gradual increase from 0 to 2000 hours is observed, while in the case of the treated samples there is an initial increase from 0 to 1000 hours, followed by a decrease up to 2000 hours total. Going to compare the three parameters L*, a* and b*, it is possible to see that in both cases, the parameter L* tends to increase from 1500 to 2000 hours (tab.24,25).

Finally, comparing the Y parameter for both untreated and treated samples, the values first decrease, then increase from 1000 to 2000 hours.

Comparing, on the other hand, the values of Y with the values of b*, it is observe that the yellowing index tends to increase with aging; on the contrary, b* tends to decrease.

Therefore, from the results obtained it is possible to state that the colorimetric variations are mainly due to the L* parameter, which indicates the surface brightness of the material. In addition, the colorimetric variations, indicated according to the parameter ΔE, do not present high values; in fact, during the collection and analysis of data, no change in the aesthetic level was found through the observation with the naked eye. Furthermore, from the results obtained, it is observed

that RH aging resulted in fewer surface aesthetic changes, compared to UV aging, an effect probably due to the plasma treatment.

3.2.2 Fourier transform infrared spectroscopy (FT-IR) in ATR mode

Figures 67-70 show the ATR FT-IR spectra for the untreated and treated samples after undergoing accelerated aging. In particular, a direct comparison is shown between the unaged sample (0h) and the aged sample both in the climatic chamber, i.e. after 80 hours, and outside the same, i.e. after 1500 and 2000h.

The objective of the analysis is to study any chemical changes due both to a treatment in a dryer, which involves a hydrolytic degradation, and to a treatment under an incandescent light bulb, which promotes photo-oxidation of PLA. Before delving into the interpretation of the peaks, we point out that the specimens, after RH-aging, curved slightly; whereas after UV-aging the specimens showed no relevant change.

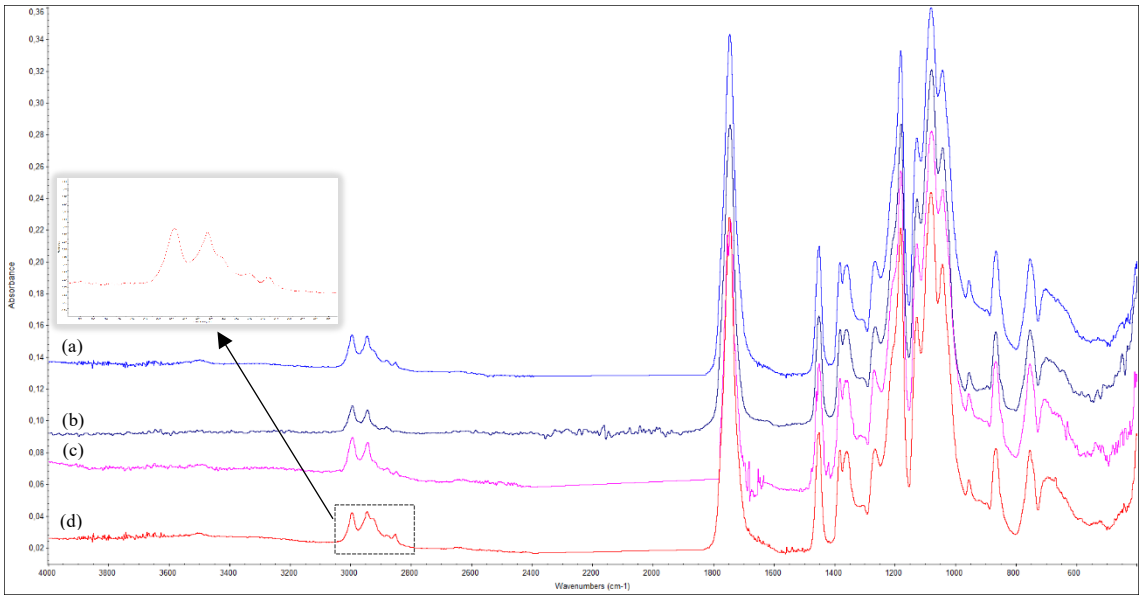

Figure 67. FT-IR spectrum in ATR mode of an untreated plasma sample. From top to bottom there are: the spectrum before ageing (a), the spectrum after 80h of ageing in the chamber (b) the spectrum after 1500h (c) and the spectrum after 2000h of ageing outside the chamber (d), performed under incandescent lamp. An enlargement of the 3000-2800 cm^{-1} spectral range of a second measurement is reported.

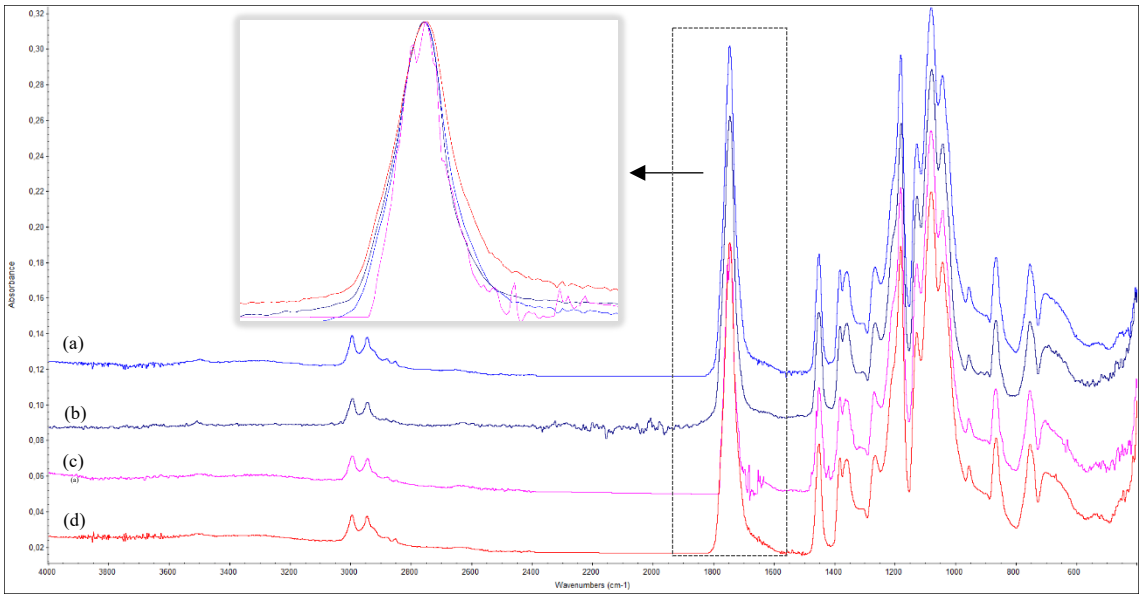

Figure 68. FT-IR spectrum in ATR mode of a treated plasma sample. From top to bottom there are: the spectrum before ageing (a), the spectrum after 80h of ageing in the chamber (b) the spectrum after 1500h (c) and the spectrum after 2000h of ageing outside the chamber (d), performed under incandescent lamp. An enlargement of the overlap of all carbonyl peaks at 1746 cm^{-1} is reported.

Comparing the ATR FTIR spectra of the n-t samples (fig.67) and the t samples (fig.68), no particular changes are observed before and after 80, 1500, and 2000 hours of aging under an incandescent bulb. Accelerated aging, in fact, did not lead to the broad band at 3400 cm^{-1}. In addition, in order to determine the extent of PLA degradation, the carbonyl index (CI) was measured (tab.26), relating the carbonyl peak at approximately 1750 cm^{-1} to the methyl peak present at approximately 3000 cm^{-1}. For both the n-t and t samples, however, the value of the dimensionless parameter remained almost unchanged, i.e., around 29, although in the case of the treated samples, a small increase in the amplitude of the peak from 0 to 2000 h was noted.

Table 24. Carbonyl index of untreated and treated sample.

Sample	**CI**	**Sample**	**CI**
nt_0h	29.10	*t_0h*	28.38
nt_80h	29.35	*t_80h*	28.64
nt_1500h	28.57	*t_1500h*	29.03
nt_2000h	30.85	*t_2000h*	30.01

Next, Figures 69 and 70 show the spectra for the n-t and t specimens, before and after accelerated aging under RH≈70% conditions.

According to the literature, however, the intensity of the C=O peak at about 1750 cm^{-1} should decrease with aging, due to COO cleavage. In addition, due to the same degradation process, the

peaks at 1454, 1384, 1359, 1180-1041, and 871 cm^{-1} should also decrease. In particular, the change in the peak at 871 cm^{-1} could result from a change in the mass fraction of crystallinity, as the band is attributed to the amorphous phase of the polymeric material [104].

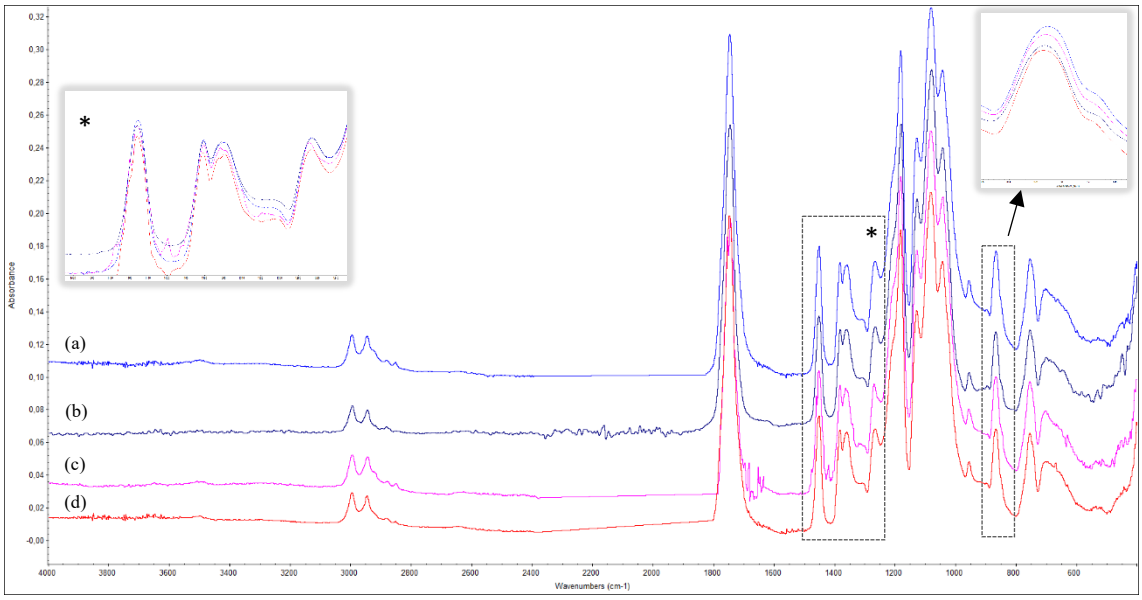

Figure 69. FT-IR spectrum in ATR mode of an untreated plasma sample. From top to bottom there are: the spectrum before ageing (a), the spectrum after 80h of ageing in the chamber (b) the spectrum after 1500h (c) and the spectrum after 2000h of ageing outside the chamber (d), performed in a desiccator at RH≈70%. Also, on the left is the enlargement of the peaks in the 1500-1200 cm^{-1} region, and on the right is the enlargement of the peaks in the 900-800 cm^{-1} region.

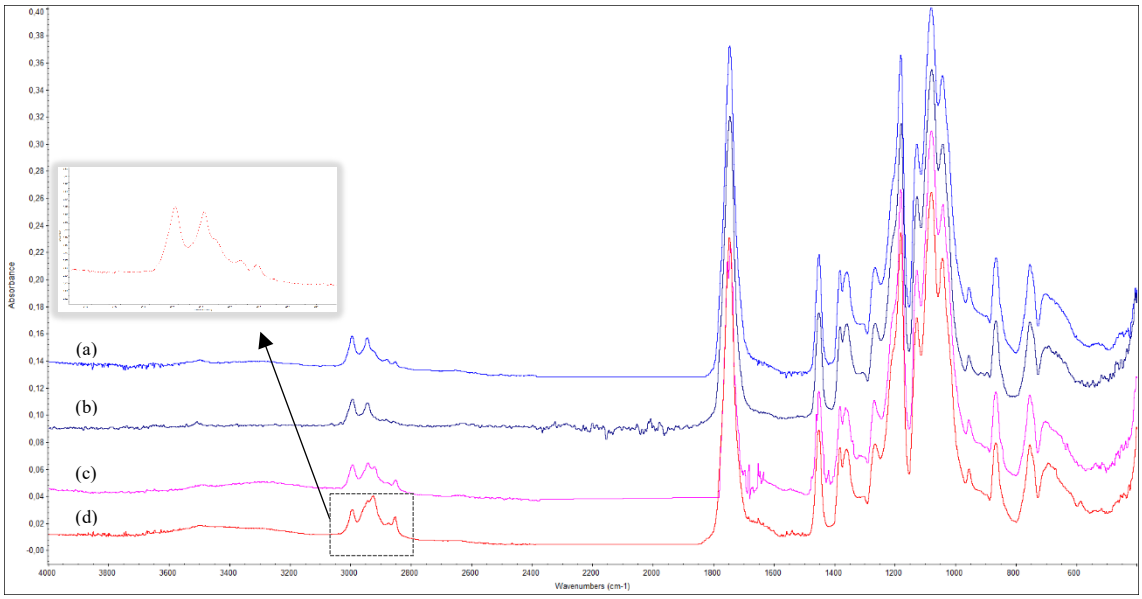

Figure 70. FT-IR spectrum in ATR mode of a treated plasma sample. From top to bottom there are: the spectrum before ageing (a), the spectrum after 80h of ageing in the chamber (b) the spectrum after 1500h (c) and the spectrum after 2000h of ageing outside the chamber (d), performed in a desiccator at RH≈70%. An enlargement of the 3000-2800 cm^{-1} region is reported.

Comparing the ATR FTIR spectra of the n-t samples (fig.69) with the t samples (fig.70), no new peaks were observed before after 80, 1500 and 2000 hours of aging in the desiccator. Also in this case, measuring the carbonyl index did not show an important variation; moreover, the band width remains almost unchanged. Thus, the average value for both cases is about 29 (tab.27), as in the previous case.

In particular, in the case of the n-t samples there was a small decrease, going from 0 to 2000 hours of the peaks present in the region 1455-1250 cm^{-1}, as well as in the case of the peak at about 871 cm^{-1}, where it is possible to observe, in the magnification shown, also a decrease in amplitude. The decrease was observed by superimposing the various spectra and enlarging the area of interest; but, in order to confirm what was observed, the areas of the peaks present at about 1454, 1384, 1359, and 871 cm^{-1} were measured and related to the areas of the methyl peaks present at about 3000 cm^{-1}. Going from 0 to 2000 hours, there are: for the peak at 1454 cm^{-1}, the value goes from 5.5 to 3.23, for the peak at 1384 cm^{-1} it goes from 6.68 to 4.23, for the peak at 1359 cm^{-1} it goes from 1.64 to 1.26, and for the peak at 871 cm^{-1} it goes from 3.57 to 2.35 (tab.28).

Table 25. Variation of carbonyl index for different peaks: 1454, 1384, 1359 and 871 cm^{-1}.

	CI (1454 cm^{-1})	**CI (1384 cm^{-1})**	**CI (1359 cm^{-1})**	**CI (871 cm^{-1})**
nt_0h	5.50	6.68	1.64	3.57
nt_2000h	3.23	4.23	1.26	2.35

The observed decrease is, therefore, due to the cleavage of the COO bond; therefore, it is possible to state that the degradation mechanism is mainly based on the hydrolysis of the ester bond, an effect that tends to increase by increasing the relative humidity conditions and thus leads to the breakage of the long macromolecular chain.

On the contrary, in the case of t samples, no variations were observed in the intensity of the peaks, which show the same height and amplitude in time. For this reason, it could be assumed that the cold plasma treatment gave the polymeric material greater resistance in conditions of high relative humidity.

Also here, in the specific case of the treated sample, after 2000 hours of aging, an enlargement of the peaks present between 3000-2800 cm^{-1} are reported, as the first measurement showed a higher absorption around 2900 cm^{-1}.

Table 26. Carbonyl index of untreated and treated sample.

Sample	**CI**	**Sample**	**CI**
nt_0h	30.10	*t_0h*	28.38
nt_80h	30.35	*t_80h*	29.03

nt_1500h	28.59	*t_1500h*	28.76
nt_2000h	28.25	*t_2000h*	29.86

Finally, especially in the case of treated samples, a slight increase in the peak at about 1700÷1650 cm^{-1} is noted, related to the unsaturated vinyl groups, which tend to intensify with aging [107].

3.2.3 Raman spectroscopy

Figures 71-74 show the Raman spectra relative to the untreated and treated samples after undergoing accelerated aging. In particular, a direct comparison between the unaged sample (0h) and the aged sample both in the climatic chamber are showed, i.e. after 75 hours, and outside it, i.e. after 500, 1000, 1500 and 2000h.

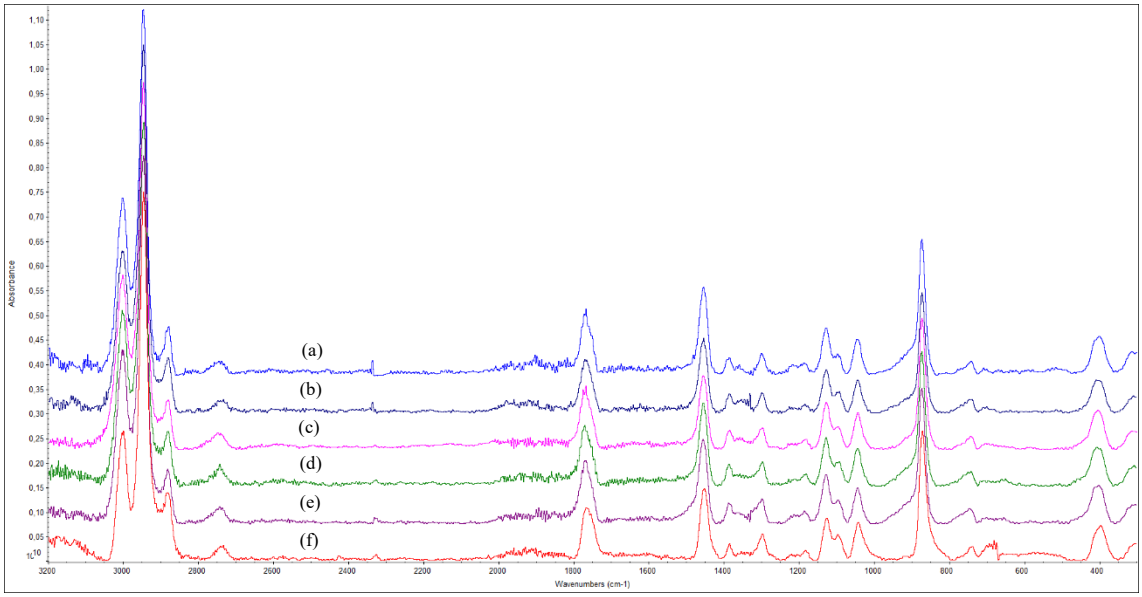

Figure 71. Raman spectra of an untreated plasma sample. From top to bottom there are: the spectrum before ageing (a), the spectrum after 75h of ageing in the chamber (b) the spectrum after 500h (c), the spectrum after 1000h (c), the spectrum after 1500h (d), the spectrum after 1500h (e) and the spectrum after 2000h of ageing outside the chamber (f), performed under incandescent lamp.

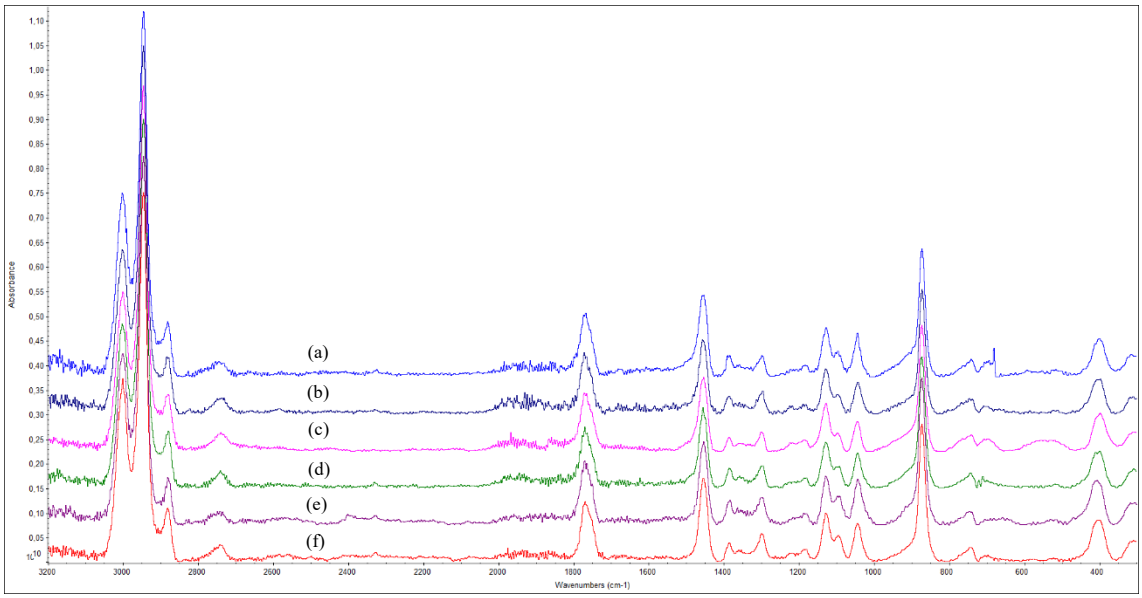

Figure 72. Raman spectra of a treated plasma sample. From top to bottom there are: the spectrum before ageing (a), the spectrum after 75h of ageing in the chamber (b) the spectrum after 500h (c), the spectrum after 1000h (c), the spectrum after 1500h (d), the spectrum after 1500h (e) and the spectrum after 2000h of ageing outside the chamber (f), performed under incandescent lamp.

Considering the Raman spectra of the n-t and t samples (fig.71,72) before and after 75, 500, 1000, 1500 and 2000 hours of aging under an incandescent bulb, no relevant differences or new peak formations are noted.

In the case of the spectra of the non-plasma-treated samples, there is an increase in the peak at 2740 cm^{-1} and the shoulder present at about 1092 cm-1, which in order refer to the methyl groups and the C-O-C group of the polymeric material.

At the same time, the peaks related to the stretching of the CH_3 group, present at 3000, 2883 and at 1455 cm^{-1}, as well as the peaks at 1768 and at 741 cm^{-1}, which represent the C=O group, tend to decrease as aging increases, in agreement with what is reported in the literature [175].

Also, in the case of the spectra of the treated samples there is an increase in the peak at 2740 cm^{-1}, the shoulder at about 1092 cm^{-1}, and in this case also the peak at about 400 cm^{-1}, which refers to the C-CO group.

On the contrary, the only decrease is found for the peak at 706 cm^{-1}, which indicates the carbonyl group C=O; therefore, also in this case there is a correspondence with the results present in the literature.

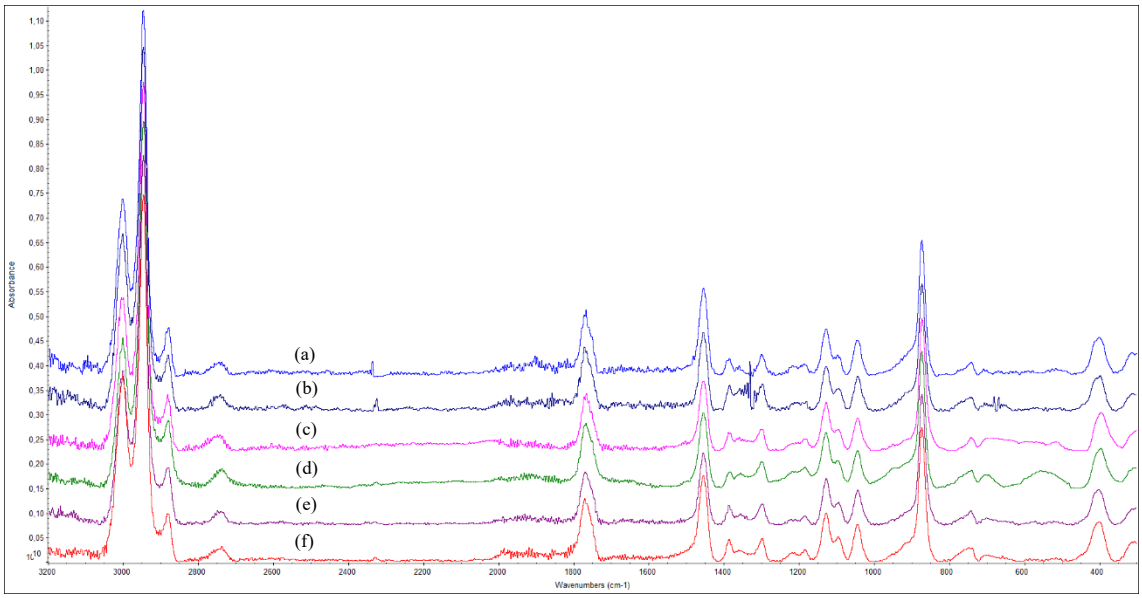

Figure 73. Raman spectra of an untreated plasma sample. From top to bottom there are: the spectrum before ageing (a), the spectrum after 75h of ageing in the chamber (b) the spectrum after 500h (c), the spectrum after 1000h (c), the spectrum after 1500h (d), the spectrum after 1500h (e) and the spectrum after 2000h of ageing outside the chamber (f), performed in a desiccator at RH≈70%.

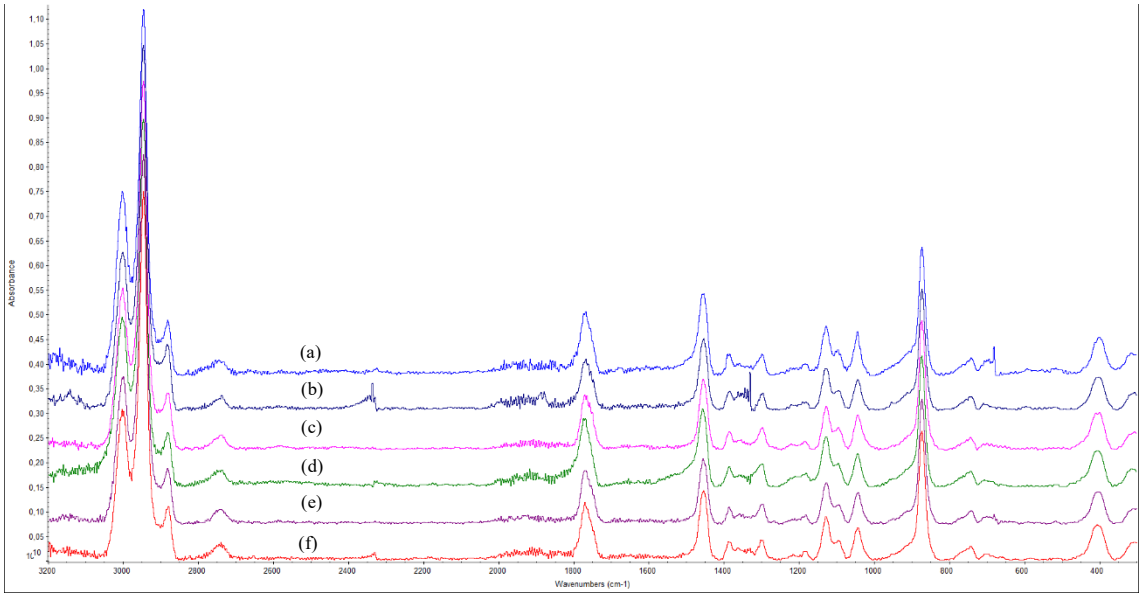

Figure 74. Raman spectra of a treated plasma sample. From top to bottom there are: the spectrum before ageing (a), the spectrum after 75h of ageing in the chamber (b) the spectrum after 500h (c), the spectrum after 1000h (c), the spectrum after 1500h (d), the spectrum after 1500h (e) and the spectrum after 2000h of ageing outside the chamber (f), performed in a desiccator at RH≈70%.

Subsequently, comparing the Raman spectra for the n-t and t samples (fig.73,74) before and after 75, 500, 1000, 1500 and 2000 hours of aging in the desiccator, no relevant differences or the formation of new peaks are observed.

In the case of n-t samples, a decrease in the peak at about 2880 cm^{-1}, related to symmetric CH_3 stretching, is observed, while the peaks at 3000 (CH_3 stretching), 1768 (C=O stretching) and at 400 cm^{-1} (C-CO) increase.
Considering, instead, the t samples a decrease of the peaks at 3000, 1768, 1455 (CH_3 symmetric stretching) and at about 1050 (C-CH_3) cm^{-1} is noticed; in this case the results obtained are in agreement with those of literature [175].

Compared to FTIR spectroscopy, which allows to investigate the functional groups of the polymer and any degradation by-products resulting from aging, Raman spectroscopy does not allow to highlight these aspects. According to the results, in fact, even if some variations in the height and amplitude of the peaks have been evidenced, it is not possible to state that there have been chemical changes in the polymeric material, as it was done, instead, by FTIR spectroscopy. Similar results were obtained by L. Cai et.al [176].

3.2.4 Thermogravimetry (TGA) and Differential Scanning Calorimetry (DSC)

The values obtained from the n-t and t samples, before and after 2000h of RH and UV aging, in order to have a direct comparison of the values obtained, are reported (tab.29). In the case of the DSC analysis, the glass transition and melting temperatures, the enthalpy of fusion and the degree of crystallinity are considered. For the TGA analysis, on the other hand, the temperature of the beginning and end of degradation is reported.

Table 27. Results obtained for n-t and t samples, before and after RH and UV aging, during TGA-DSC analysis: glass transition temperature (T_g), melting temperature (T_m), enthalpy of melting (ΔH_m) and crystallinity degree (χ).

	DSC				**TGA**	
Sample	T_g (°C)	T_m (°C)	ΔH_m (J/g)	χ (%)	$T_{onset-I}$ (°C)	$T_{onset-f}$ (°C)
n-t	62.0	154.0	9.13	9.8	252.0	≈ 365
t	61.5	153.6	8.1	8.7	332.0	≈ 370
n-t_RH	61.2	154.3	18.3	19.6	338.9	≈ 380
t_RH	62.5	153.9	8.6	9.3	341.7	≈ 380
n-t_UV	62.4	153.7	7.6	8.2	344.3	≈ 380
t_UV	64.8	154.8	6.7	7.2	347.0	≈ 380

Starting from the n-t and t and RH aged samples, TGA analysis shows $T_{onset-i}$ and $T_{onset-f}$ to be similar; then comparing them with the samples before aging, a significant difference is observed

compared to the untreated sample, probably due to a number of chemical changes that occurred during aging.

Turning then to DSC, both T_g and T_m do not show relevant differences, even compared to the samples before aging According to a study conducted by A. Copinet et.al [177], the value of T_g should decrease precisely because PLA, under high RH conditions, tends to absorb water, which determines the hydrolysis of ester bonds, breaking the long macromolecular chains; moreover, water molecules lead to an increased mobility of polymer chains.

In addition, according to another analysis, carried out by H. Tsuji et.al [178], theoretically the T_m values should also decrease, due to the structural change of the surface of the crystalline regions, as a result of hydrolytic degradation; however, during the study, no change was found after accelerated aging.

The only variation that was found concerns the degree of crystallinity of the untreated sample (fig.75); in fact, from before to after aging, the value seems to double, probably due to the removal of the amorphous chains during the degradation phase [179], and therefore, to the increase of the surface area of the crystalline residues [178]; this variation seems to be confirmed by the data obtained in the analysis of the n-t RH sample (Fig.69), where a decrease in the peak at 871 cm-1 was found, which indicates a change in the mass fraction of crystallinity. In fact, it is possible to hypothesize that hydrolysis occurs mainly in the amorphous regions rather than in the crystalline ones, being easily accessible. Therefore, the remaining polymer chains, presenting greater mobility, can reorganize and thus increase the degree of crystallinity [180].

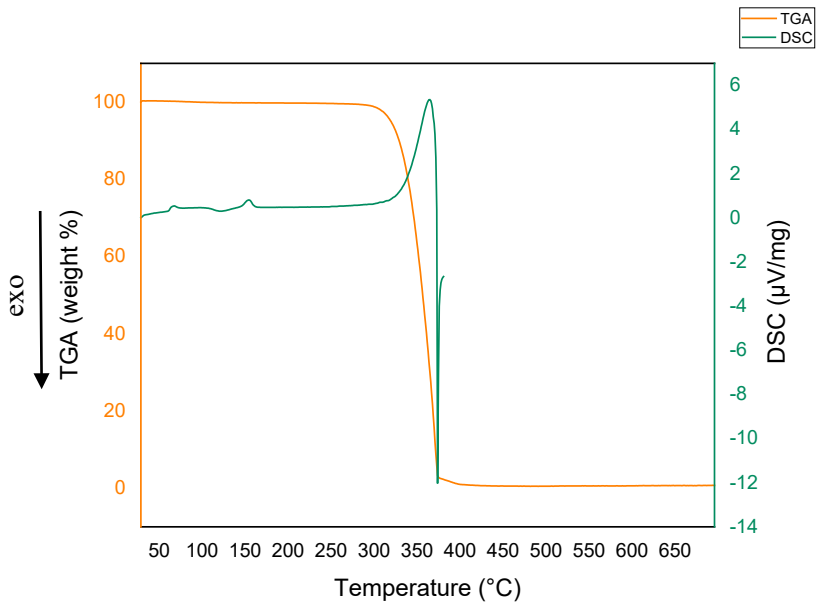

Figure 75. TGA-DSC curves of the n-t sample, obtained after RH aging.

Next, for the n-t and t and UV-aged samples, it is possible to find the same differences observed for the RH-aged samples, compared to the samples before aging, in the case of the TGA analysis. In particular, the temperature at which the degradation of the treated specimen begins appears higher than for the other samples.

Considering, on the other hand, the DSC analysis, no relevant differences are found regarding T_g and T_m.

According to the results obtained reported in the literature [181], the T_g tends not to vary with time. This behavior can be attributed to the photodegradation process of PLA, which causes both polymer chain scission and recrystallization. The two phenomena confer opposite effects on the T_g, because if on one hand the chain scission, leading to an increase in molecular mobility, tends to reduce the temperature, on the other hand the recrystallization increases the value as a consequence of the reduction in the mobility of macromolecules. Obviously, the increase in crystallinity and the simultaneous molecular decomposition makes the polymer more brittle.

3.2.5 Dynamometric tests

The results of the dynamometric tests reported below refer to the n-t and t samples after 2000 hours of UV and RH aging.

Therefore, as in the case of the specimens before aging, the average values of the parameters obtained at each tensile test (tab.30-33), the load vs extension curves (fig.76,78,80,82) and the specimens immediately after the tests (fig.77,81,83,85) are reported.

Table 28. Dynamometric test data for the five untreated samples, after UV-aging.

Parameters	**Values**	**SD**
Modulus	507.166 MPa	30.3
Peak Load	61.857 N	5.19
Peak Stress	5.18 MPa	0.43
Strain at break	1.562 %	0.20

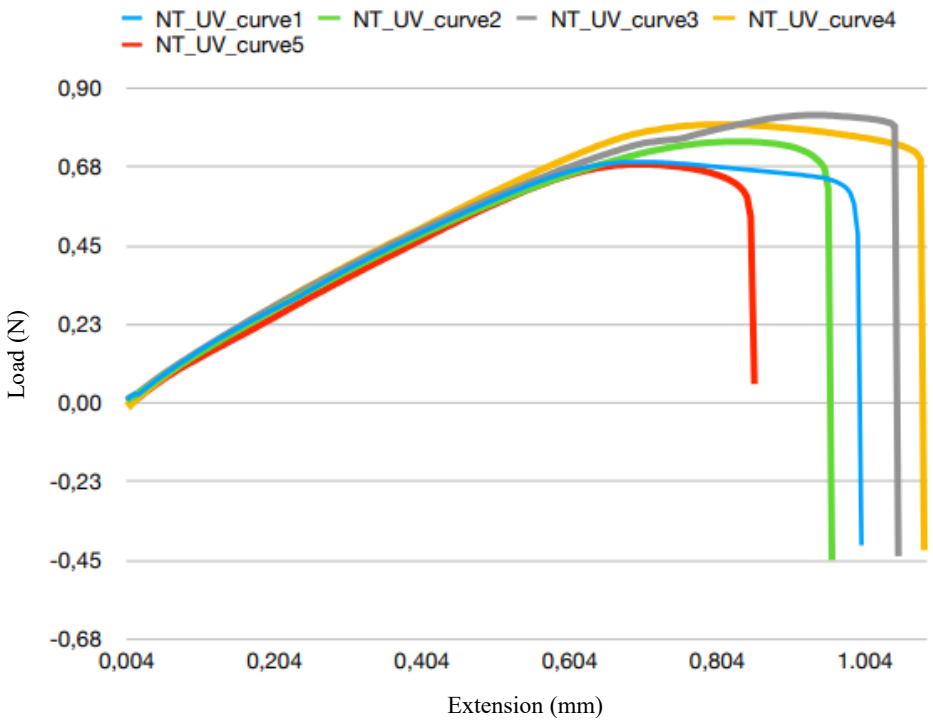

Figure 76. Load-extension diagram of five n-t samples, after UV-aging.

Figure 77. The five untreated samples after dynamometric analysis.

Table 29. Dynamometric test data for the five treated samples, after UV-aging.

Parameters	**Values**	**SD**
Modulus	513.71 MPa	43.47
Peak Load	59.32 N	12.69
Peak Stress	4.94 MPa	1.03
Strain at break	1.33 %	0.25

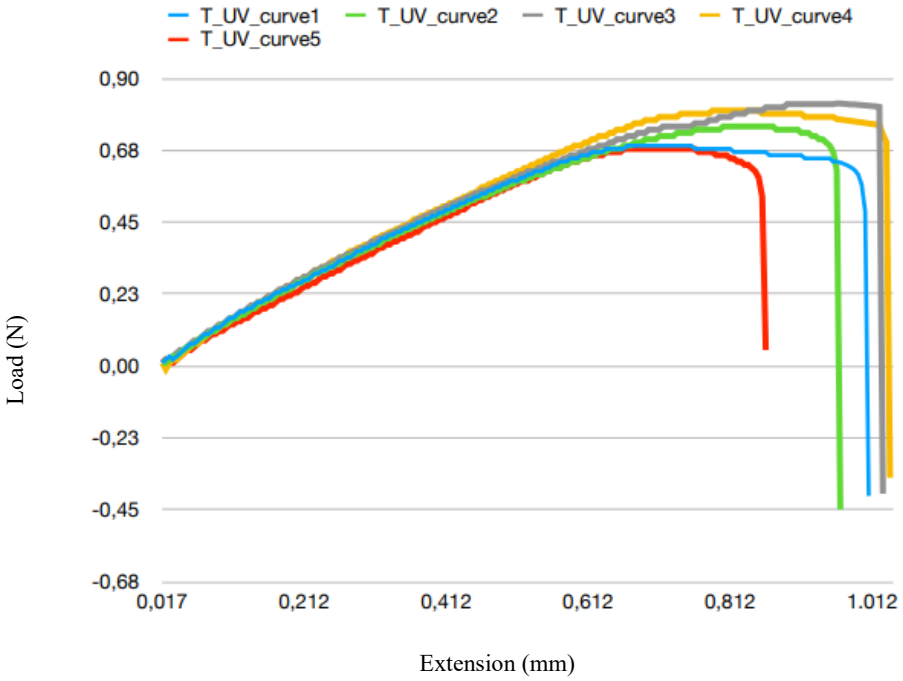

Figure 78. Load-extension diagram of five t samples, after UV-aging.

Figure 79. The five treated samples after dynamometric analysis.

Comparing the results of the two types of samples (n-t and t), there is a higher value of the modulus of elasticity in the treated samples, whereas the other values, i.e. peak load, tension at break and strain at break, are higher for the untreated sample.

Compared with the specimens before aging, the results obtained after UV aging show a higher modulus of elasticity, while the other parameters are lower. Therefore, it is possible to state that the samples after UV-aging show lower tensile strength, being more brittle and less elastic.

This is reflected in the literature [176], where it was observed that exposure to photo-oxidation gives PLA lower mechanical strength, as it causes both an increase in the amount of chain terminations and a reduction in the crystallinity of the material, thus reducing the strength of the material.

It has, moreover, been verified that for long times of exposure to UV radiation, the reduction in molecular weight becomes more pronounced and the elastic modulus begins to decrease. In fact, the tensile strength and deformation resistance to the breaking point gradually decrease as the exposure time increases. While UV radiation initially results in structural and molecular reorganization, it subsequently causes a number of chemical changes as it breaks down weak chemical bonds and molecular chains, forming shorter chains and thus making the plastic material more brittle [181-186].

Finally, the breakage appears more ductile in untreated samples, and more brittle in treated samples (fig.77,79). Considering, instead, the rupture line in the specimens, it is possible to find the same characteristics as in the specimens before aging: t specimens show a rupture closer to the shrinkage point of the specimen.

Table 30. Dynamometric test data for the five untreated samples, after RH-aging.

Parameters	**Values**	**SD**
Modulus	425.51 MPa	36.53
Peak Load	60.26 N	23.19
Peak Stress	5.02 MPa	1.94
Strain at break	1.87 %	0.53

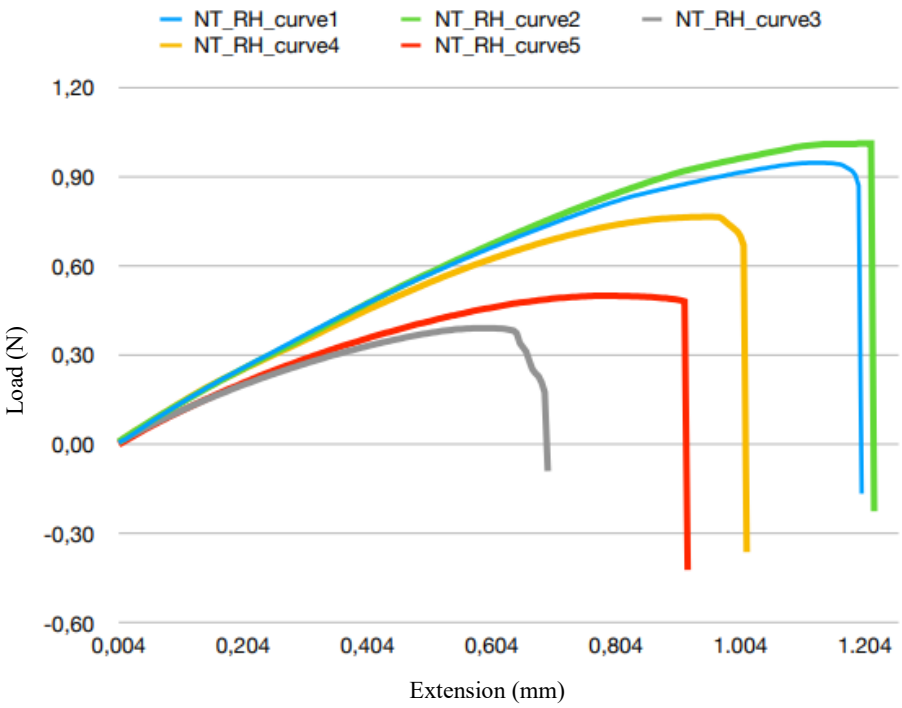

Figure 80. Load-extension diagram of five n-t samples, after RH-aging.

Figure 81. The five untreated samples after dynamometric analysis.

Table 31. Dynamometric test data for the five treated samples, after RH-aging.

Parameter	**Values**	**SD**
Modulus	456.93 MPa	57.92
Peak Load	74.81 N	8.14
Peak Stress	6.24 MPa	0.68
Strain at break	2.21 %	0.15

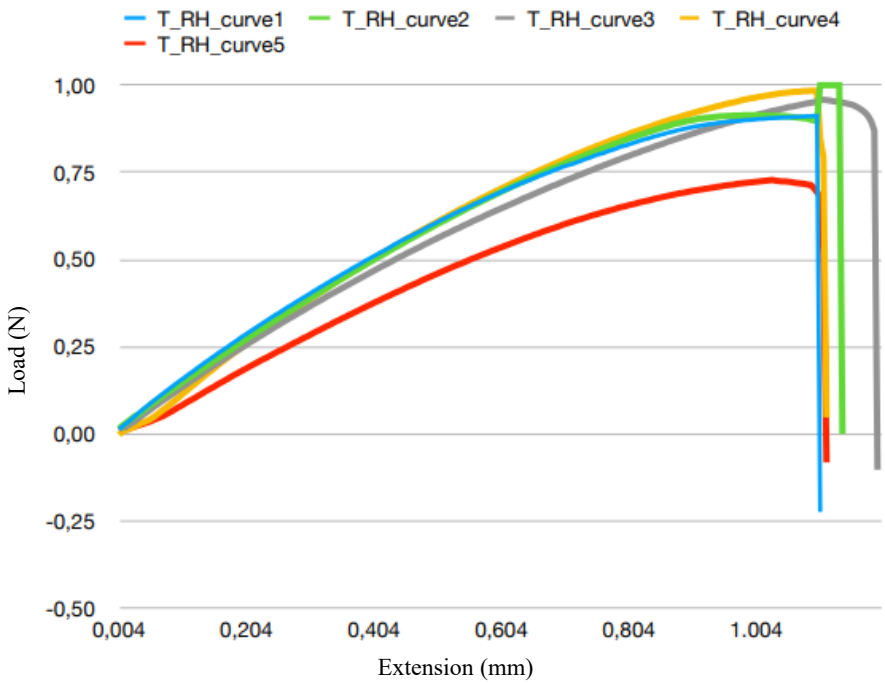

Figure 82. Load-extension diagram of five n-t samples, after RH-aging.

Figure 83. The five treated samples after dynamometric analysis.

Finally, considering the results of the n-t and t specimens after RH aging, it is possible to observe that the parameters for the treated specimens are slightly higher than for the untreated specimens; therefore, in this case it can be stated that the treatment led to a higher strength of the RH≈70% aged specimens.

On the other hand, comparing the specimens before and after aging, it can be seen that the elastic modulus values tend to decrease, while the other parameters in the case of the treated specimens increase after aging; the parameters of the untreated specimens, however, are slightly lower than the specimens before aging, apart from the deformation at break which, on the contrary, is higher.

In fact, according to some studies reported in the literature [104], PLA, following RH aging, presents a higher tensile strength due to the plasticizing effect conferred by moisture. This higher resistance is found in the case of the deformation at break of the samples, whose values are higher than those of the other samples.
In fact, according to other results reported in the literature [182], the mechanical properties of almost all additive PLA-based samples decreased following combined UV/RH aging, apart from pure PLA which showed no significant changes in tensile modulus during aging. It was hypothesized that the impact strength was due precisely to a plasticization effect, as well as a change in the polymer structure [183-186], as was verified by DSC analysis.
Finally, in this case the untreated samples show a brittle fracture, while the treated ones show a ductile fracture (fig.81,83). Compared to the previous cases and considering the rupture line, it is observed that the point is not close to the shrinkage zone but is more central to the specimen.

3.3 FILAMENT STRENGTH EVALUATION

In order to evaluate the resistance of polylactic acid to acids, the two cubes are first placed in nitric acid (HNO_3) and then in acetic acid (CH_3COOH). In particular, in the case of acetic acid, the spectra obtained by the FTIR spectroscopic technique in ATR mode of both the untreated cube and the plasma-treated cube are reported.

3.3.1 Acid attack resistance tests

Initially it was decided to place both the filament (≈2 cm) and the two cubes inside tubes containing nitric acid. The materials were left for about 3 months in immersion; Figure 84 shows the results obtained.

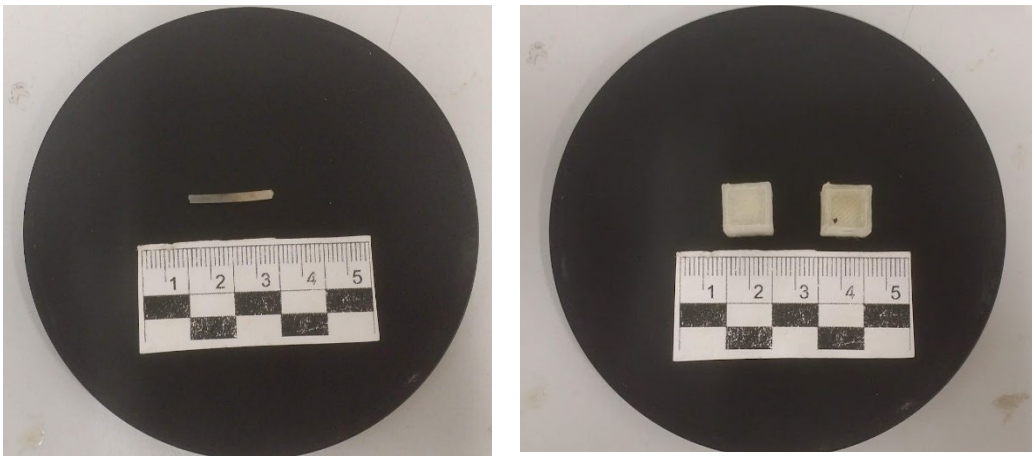

Figure 84. Nitric acid resistance test results: on the left the PLA filament, on the right the two cubes (n-t and t) after about 2160 hours of immersion in acid.

As previously hypothesized, nitric acid did not cause any effect on the polymeric material, just because, unlike the latter, it is an inorganic material and therefore incompatible with it. Therefore, from the results obtained it is possible to state that the acid did not cause any swelling or softening of the PLA, as well as the formation of cracks or micro-fractures was not observed. The only variation is found in the aesthetic point of view, where the color seems to have turned to yellow; the yellowing could be due to the formation of yellow chromophore species.

It is not possible to say the same thing in the case of the results obtained following immersion in acetic acid of the two cubes (fig.85).

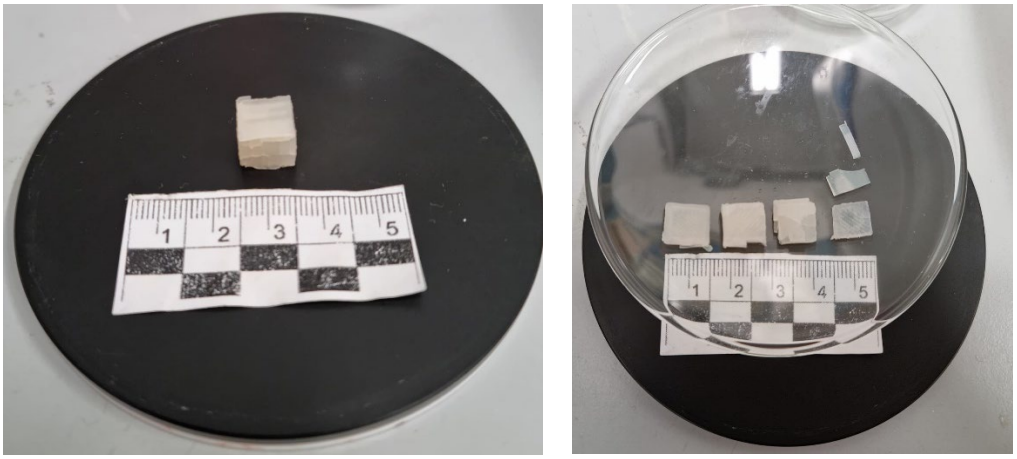

Figure 85. Acetic acid resistance test results: left cube n-t, right cube t, after 840 hours of acid immersion.

The effects that were obtained are in agreement with what was previously hypothesized, as polylactic acid and acetic acid, being organic in nature, are chemically similar.

In general, organic agents can interact with the molecular chains of thermoplastics, causing both signs of swelling and dissolution in the material, and a series of microfractures within the entire structure, leading, finally, to the failure of the components, as in the case reported.

In particular, in the plasma treated cube there is a complete separation of the different layers deposited during the FDM printing process. The breakage does not depend so much on the inefficiency of the TEOS as on the printing and deposition parameters of the same adopted during the realization of the cubes. Probably the inadequate application time of the precursor caused the layers to vitrify, giving the polymeric material more sensitivity and less resistance to organic acids.

With the aim of verifying any changes at the chemical-structural level, samples are analyzed by ATR FTIR spectroscopy (fig.86,87).

According to some studies [187,188], during the acid hydrolysis of PLA, the cleavage process starts from the ends of the polymer chain and leads to the formation of low molecular weight degradation products, such as lactic acid and lactate; lactic acid is then cleaved forming lactic acid oligomers, which are mostly insoluble. It has also been observed that the OH terminal group of the lactic acid oligomer plays a key role in the degradation of the polymeric material, as it causes the cleavage of the first ester bond. Finally, the degradation of the polymer in an acidic environment is expected to result in a low production of free carboxyl groups.

Therefore, according to what has been reported, analyzing the ATR FTIR spectra should show a decrease in the peaks present at 893 and 866 cm^{-1}, related to the ester group, COO, and an increase in the peaks representing the carbonyl group C=O (1746, 755 and 701 cm^{-1}), present in lactic acid and lactate.

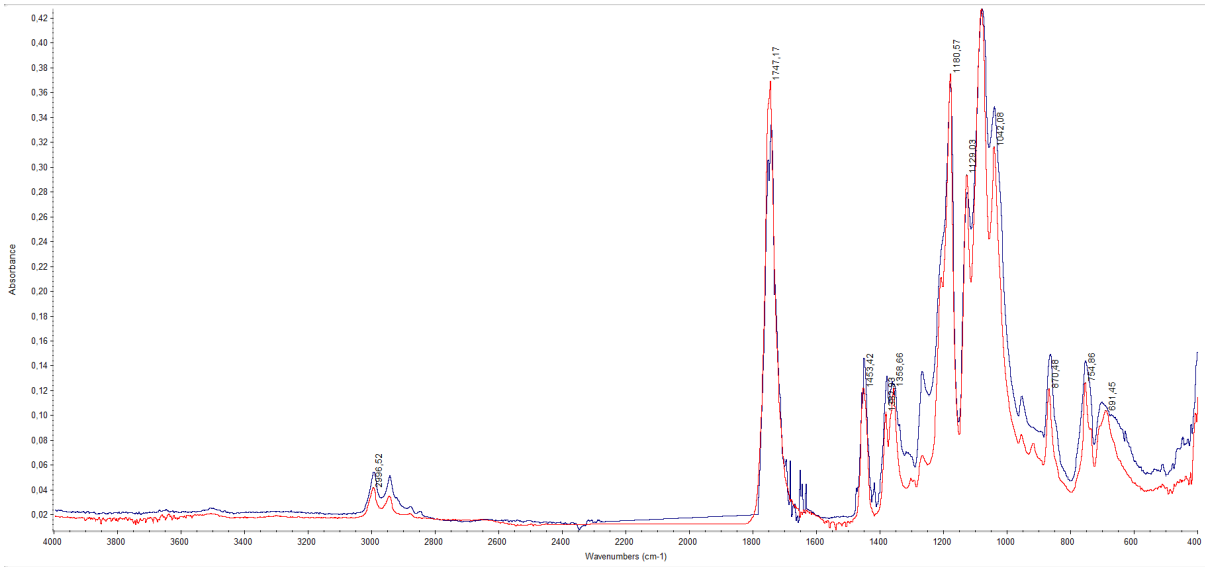

Figure 86. FT-IR spectra in ATR mode: comparison between the sample n-t printed before aging (blue curve) and the cube n-t after immersion in acetic acid (red curve).

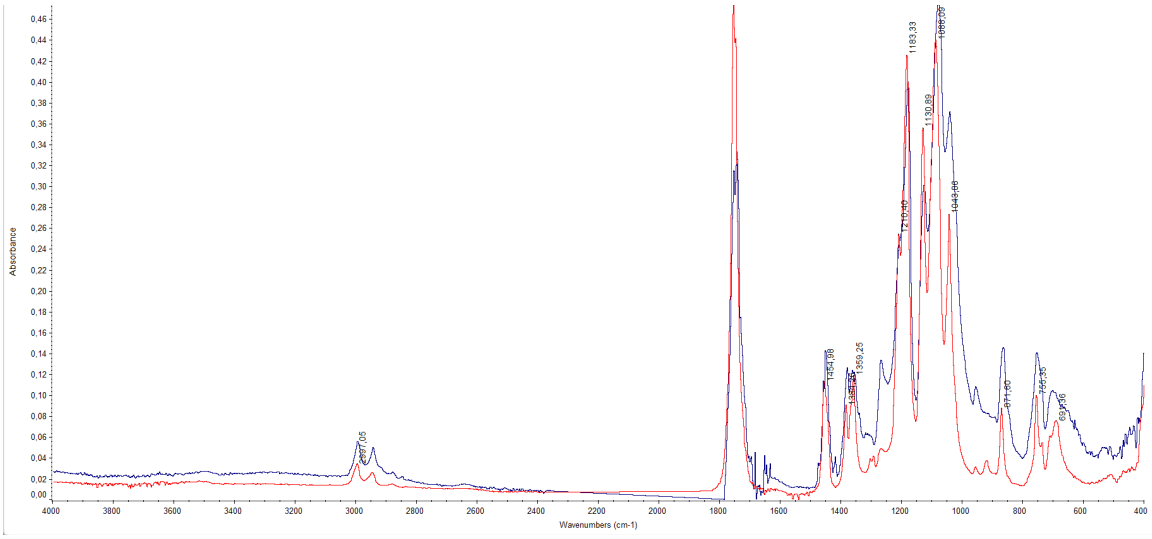

Figure 87. FT-IR spectra in ATR mode: comparison between the sample t printed before aging (blue curve) and the cube t after immersion in acetic acid (red curve)

Observing the ATR FTIR spectra of the n-t and t cubes (fig.86,87), the polylactic acid-related peaks, already described above, can be seen. In addition to this, minor differences were found in the amplitude and intensity of some peaks, compared to the peaks obtained for the samples printed before aging.

For example, in the case of the n-t cube, the shoulder present at about 1209 cm^{-1}, related to the stretching of the COC group, appears more pronounced, while the peaks at 870 (C-COO stretching) and 754 (CO bending) cm^{-1} show a smaller amplitude. From the comparison, the formation of peaks at 919 and 691 cm^{-1}, and a shoulder at about 740 cm^{-1} was also observed.

Subsequently, the same peaks are also observed in the case of the treated cube, some of which appear more pronounced: at 919, shoulder at about 740 and at 712 cm^{-1}, and the peak at 1209 cm^{-1}.

Therefore, in both cases a decrease in the ester group, at about 870 cm^{-1}, and an increase in the peak at about 1746 cm^{-1}, relative to the carbonyl group, are observed. The changes are in agreement with what has been stated previously that immersion in acid caused cleavage of ester bonds and formation of lactic acid and lactate. The decrease in the peak to about 870 cm^{-1} could also result from the formation of CO_2, following a reaction between the carbonyl group and acetic acid [189].

The test carried out in acetic acid represents an extreme test to evaluate the resistance of the polymer; under normal conditions, if the use of the material in the field of Cultural Heritage to make copies of artifacts or integrative restorations is proposed, it will never encounter an aggressive and invasive environment as the one recreated for this study.

3.4 LIFE CYCLE INTERPRETATION

This section presents the results of the LCIA phase, obtained for the ReCiPe 2016 Midpoint (H) and IPCC GWP 100a impact categories.
First, the results for the two proposed integrative restoration scenarios are shown, considering the entire life cycle, thus both the assembly phase and the end-of-life cycle of the materials. Then, for both cases considered, the percentage differences are measured, referring to all categories present in the two investigation methodologies.
Finally, 4 of the 18 impact categories are compared, in the case of ReCiPe 2016 Midpoint (H), and the only impact category present in IPCC GWP 100a, in order to identify the processes and flows that most influence the final result.

3.4.1 ReCiPe 2016 Midpoint (H)

Below, Table 34 shows the overall results for the impacts of the individual impact categories found in ReCiPe 2016 Midpoint (H), for both cases: the first, about the innovative restoration method, and the second about the traditional one. Also, there are the variance, in percentage, of different values present in all impact categories.

Table 32. Case 1: Global results of impact categories, obtained with ReCiPe Midpoint (H).

Impact category	**Unit**	**Innovative case of restoration**		**Traditional case of restoration**		**Variance %**	
		LCA_3D printing assembly	PLA end-of-life	LCA_assembly	Waste materials	Assembly	End-of-life
Global warming	kg CO2 eq	21.4	5.91	3.95E3	4.35E3	- 39%	141%
Stratospheric ozone depletion	kg CFC11 eq	1.26E-5	3.56E-6	0.00229	3.2E-5	27%	- 99%
Ionizing radiation	kBq Co-60 eq	1.85	0.272	216	2.05	14%	- 93%
Ozone formation, Human health	kg NOx eq	0.0446	0.026	9.53	0.617	49%	- 83%
Fine particulate matter formation	kg PM2.5 eq	0.0363	0.00887	7.24	0.128	22%	- 91%
Ozone formation, Terrestrial ecosystems	kg NOx eq	0.0472	0.0268	10.4	0.619	48%	- 85%

Terrestrial acidification	kg SO2 eq	0.0763	0.02	15	0.366	23%	- 89%
Freshwater eutrophication	kg P eq	0.0112	0.00126	1.18	0.0117	10%	- 90%
Marine eutrophication	kg N eq	0.00123	8.49E-5	0.0754	0.000735	6%	- 85%
Terrestrial ecotoxicity	kg 1,4-DCB	40.7	31.3	7.13E3	2.1E3	37%	- 48%
Freshwater ecotoxicity	kg 1,4-DCB	0.551	0.391	91.8	1.41E3	- 90%	126%
Marine ecotoxicity	kg 1,4-DCB	0.771	0.551	130	2.01E3	- 90%	125%
Human carcinogenic toxicity	kg 1,4-DCB	0.777	0.272	125	3.94	15%	- 88%
Human non-carcinogenic toxicity	kg 1,4-DCB	15.5	11.9	2.76E3	5.54E4	- 92%	119%
Land use	m2a crop eq	0.759	0.163	104	1.12	20%	- 94%
Mineral resource scarcity	kg Cu eq	0.042	0.0209	14.6	0.32	47%	- 94%
Fossil resource scarcity	kg oil eq	8.16	1.95	2.39E3	14.5	23%	- 97%
Water consumption	m3	1.89	0.0222	58.4	5.46	- 7%	637%

Comparing the results obtained in the different impact categories, it is possible to state that the first case proposed, related to the use of PLA for integration process, is advantageous. In fact, it can be seen that almost all the values of the categories are lower than in the second case, where it's proposed the use of traditional material, that is gypsum.

The percentage differences of the two cases are then presented in Figure 88.

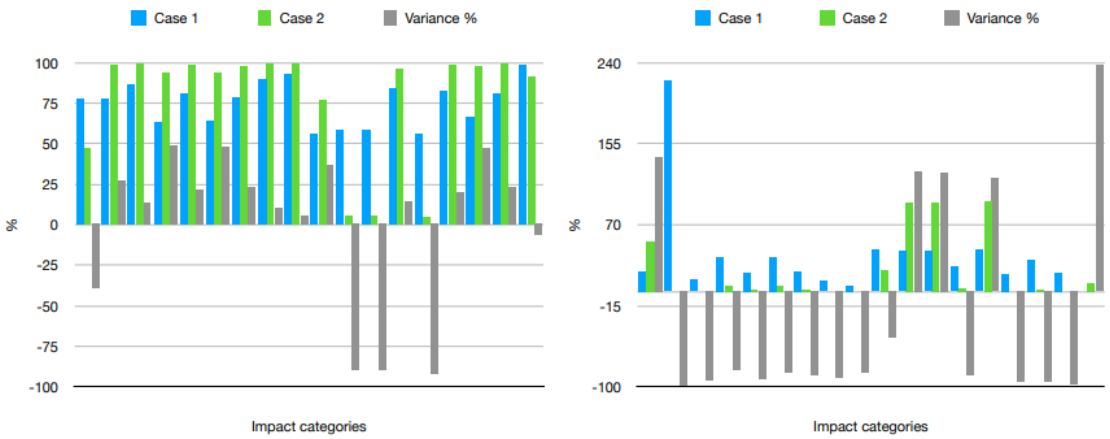

Figure 88. Comparison of the percentage values of the impact categories of the two cases (case 1: blue, case 2: green) with variance (gray). On the left are values related to material assembly, on the right are values related to end-of-life cycle. The two graphs are from a personal reproduction.

From the two graphs (fig.88), it is possible to observe the relative contributions of each step in the process. In the graph on the left, the categories that present a greater difference are "*Ozone formation, Human health*" and "*Ozone formation, Terrestrial ecosystems*". While in the graph on the right, the category that shows a significant difference is "*Water consumption*". It should be remembered that the values are related to individual cases and not to each other; the comparison, in fact, makes it possible to verify how the impact categories differ, with values generally appearing greater in case 1.

From a comparison of all 18 categories, then there is the estimation of the impacts of the various inputs, considering 4 impact categories: fine particulate matter formation, which considers $PM_{2.5}$ particulate matter formation (yr/kg of PM2.5 equivalent); human non-carcinogenic toxicity, which characterizes human toxicity by taking into account environmental persistence (fate), accumulation in the human food chain (exposure), and toxicity (effect) of a chemical (yr/kg of 1,4-dichlorobenzene or 1,4-DCB); ozone formation human health, which accounts for destruction of the stratospheric ozone layer by entropogenic emissions (yr/kg of CFC-11); terrestrial ecotoxicity, which accounts for human toxicity from dichlorobenzene (yr/kg of 1,4-DCB), (fig.89-96).

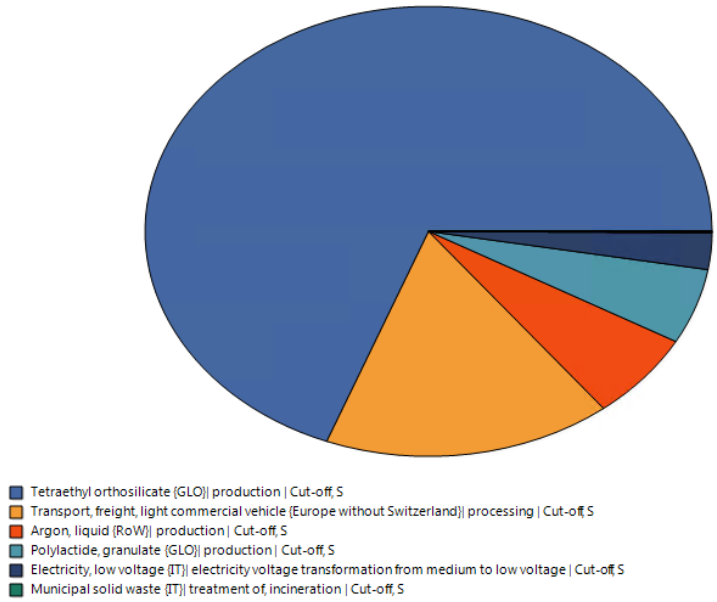

Figure 89. Fine particulate matter formation of case 1 (innovative restoration).

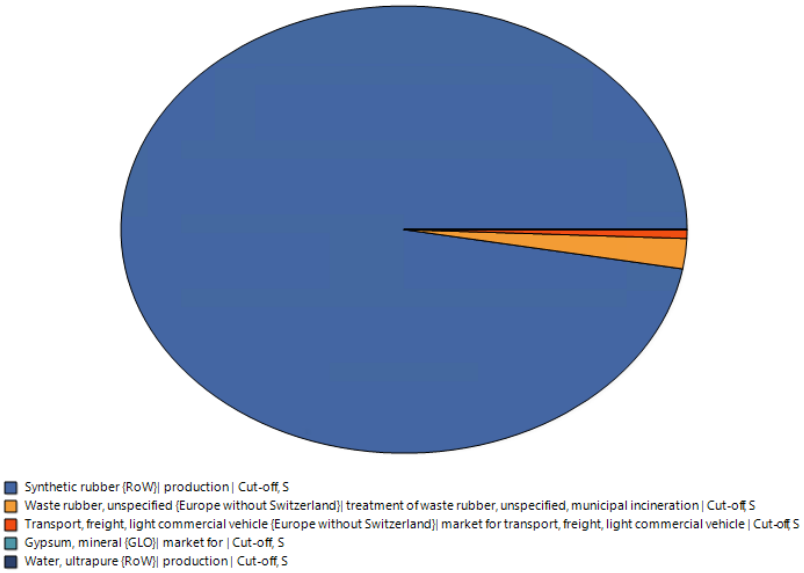

Figure 90. Fine particulate matter formation of case 2 (traditional restoration).

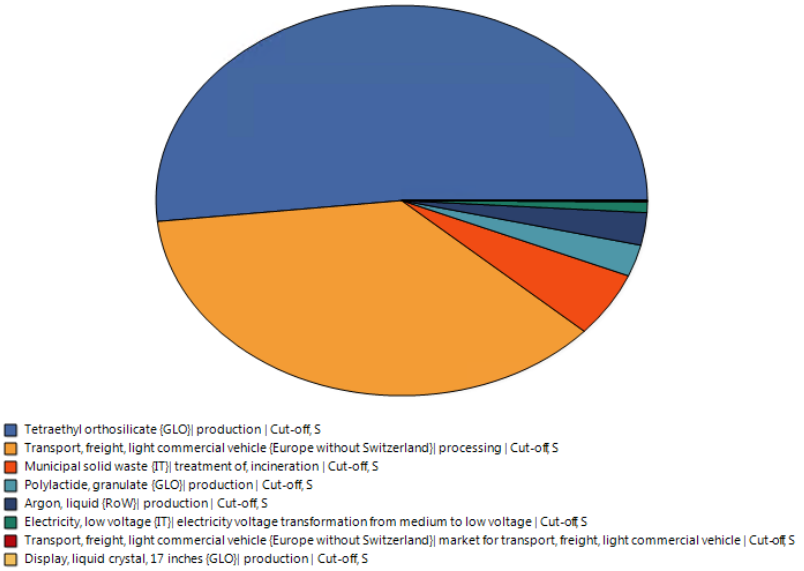

Figure 91. Human non-carcinogenic toxicity for case 1 (innovative restoration).

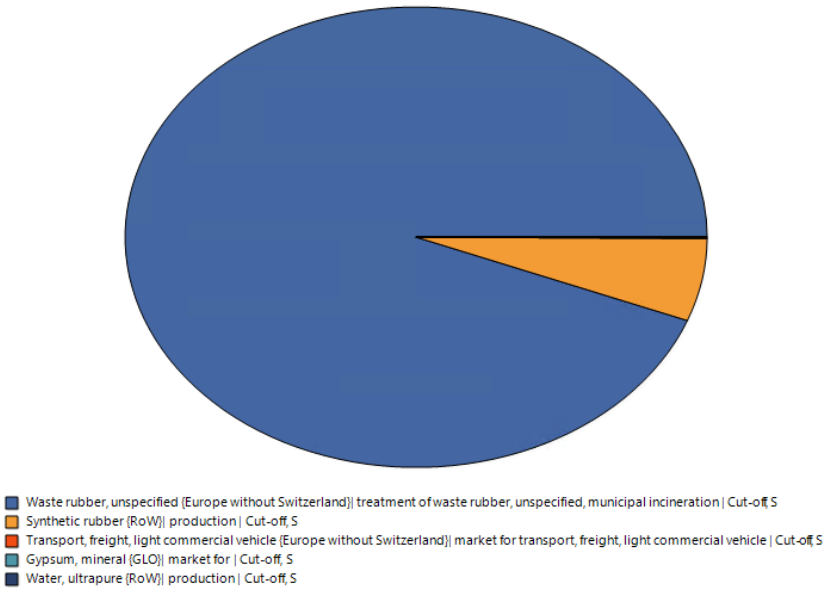

Figure 92. Human non-carcinogenic toxicity of case 2 (traditional restoration).

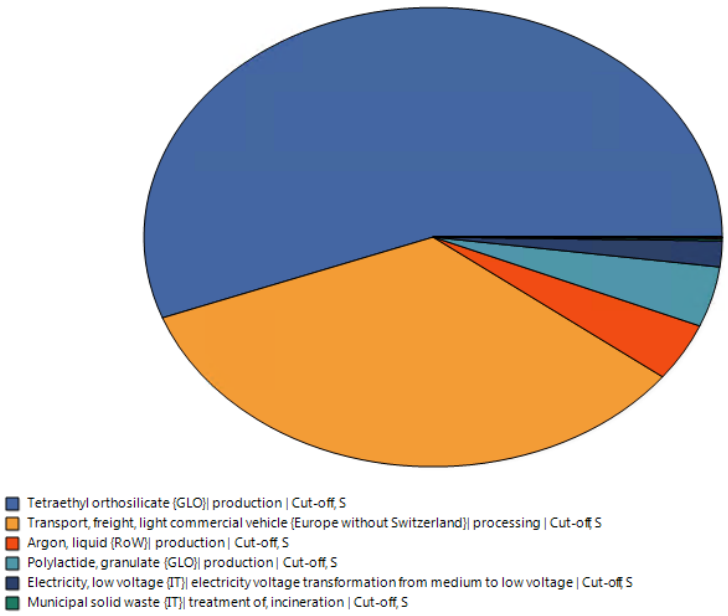

Figure 93. Ozone formation human health of case 1 (innovative restoration).

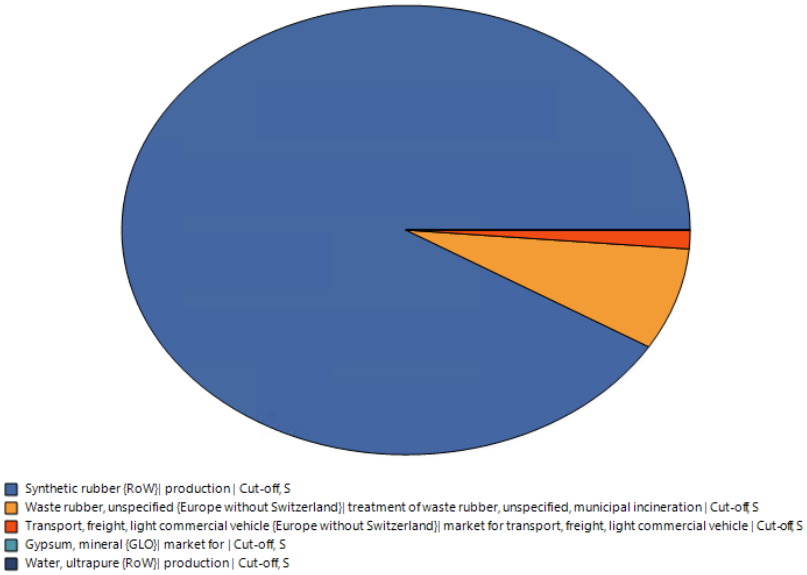

Figure 94. Ozone formation human health of case 2 (traditional restoration).

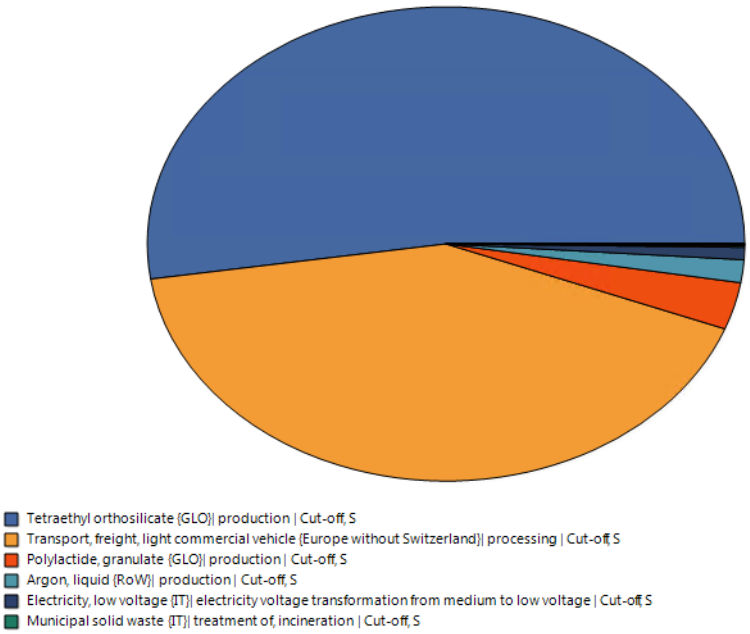

Figure 95. Terrestrial ecotoxicity of case 1 (innovative restoration).

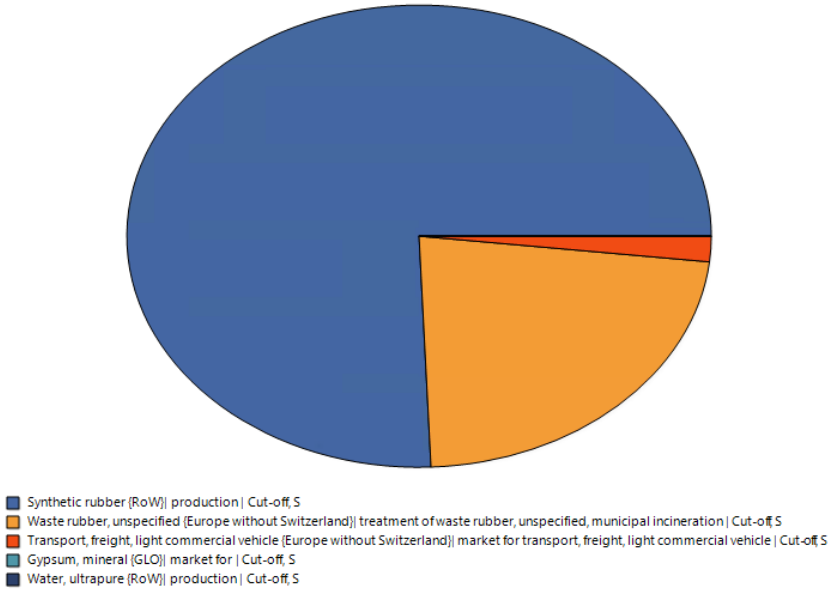

Figure 96. Terrestrial ecotoxicity of case 2 (traditional restoration).

In almost all categories it is possible to notice that, in the first case, the major impact comes from TEOS, followed immediately by transport, while in the second case the most relevant impact comes from silicone rubber; only in the category "*human non-carcinogenic toxicity*" the most relevant impact comes from the disposal process of silicone rubber, followed by the rubber itself.

3.4.2 IPCC GWP 100a

Tables 35 and 36 show the results relative to the IPCC GWP 100a methodology. For each case considered, the values obtained in terms of carbon dioxide emissions are reported.

Table 33. Case 1: Global results of impact categories, obtained with IPCC GWP 100a.

Impact category	Unit	LCA_3D printing assembly	PLA end-of-life
IPCC GWP 100a	kg CO2 eq	21	5.87

Table 34. Case 2: Global results of impact categories, obtained with IPCC GWP 100a.

Impact category	Unit	LCA_assembly	Waste materials
IPCC GWP 100a	kg CO2 eq	3.87E3	4.35E3

As in the case of the ReCiPe Midpoint (H) methodology, it is possible to state that the first case proposed is advantageous with respect to the second. In fact, the value relating to the assembly process of the materials in the second case is two orders of magnitude higher than in the first case;

while, considering the end-of-life process of the materials, there is a difference of three orders of magnitude between the first and second cases.

Below, it's reported the two cases with the relative percentage difference, referring to the values reported in Tables 35 and 36 (fig.97).

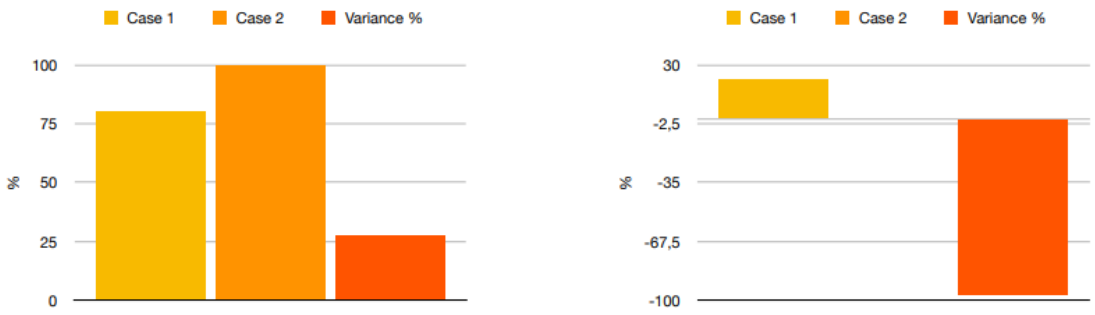

Figure 97. Comparison of the percentage values of the impact categories of the two cases (case 1: yellow, case 2: orange) with variance (dark orange). On the left are values related to material assembly, on the right are values related to end-of-life cycle. The two graphs are from a personal reproduction.

Thanks to the two graphs shown in figure 89, it is possible to affirm what was said previously. In the second case, moreover, there is a negative difference, since the data considered are related to the process of assembling the case itself; therefore, even here the same thing that was said for the tables in figure 88 is valid.

Referring, therefore, to the values present in tables 37 and 38, it is argued that the first case presents an impact that is considerably less than the second case reported.

Finally, Table 39 shows the most significant impacts of the inputs inserted in the system, considering Global Warming, which is expressed in kg of CO_2 equivalent (kg CO2 eq.), i.e. all emissions of climate-altering gases are converted into carbon dioxide through impact factors.

Table 35. Impact of inputs in IPCC GWP 100a impact category; the top two graphs come from the SimaPro software, while the bottom two come from a personal reproduction.

Case 1	**Case 2**

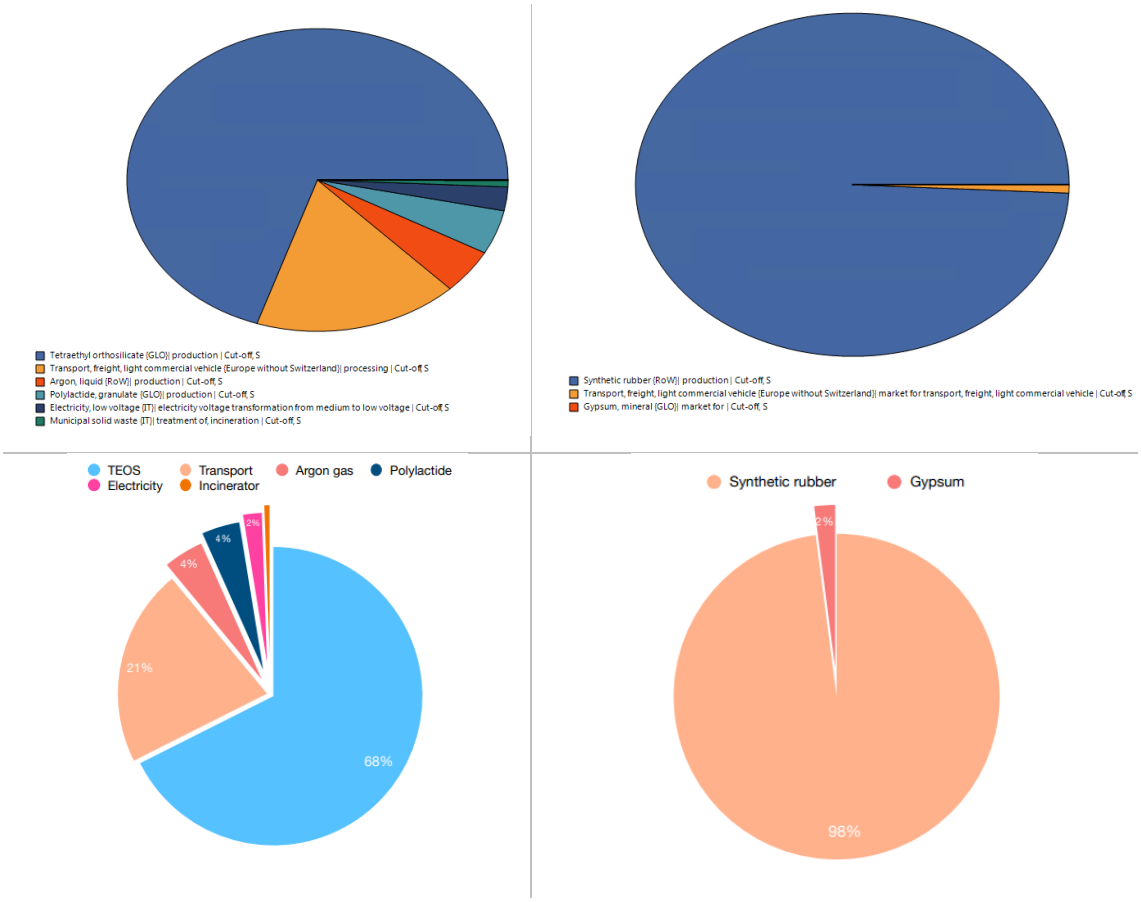

Analysis of the relative contributions of the phases into which the life cycle is divided shows that, for both processes, the phases with the greatest impact are TEOS (case 1) and silicone rubber (case 2).

From a more detailed observation, it is possible to find that in the first case the tetraethyl orthosilicate precursor shows the most relevant impact (about 67%), and is followed by transport (21%), which concerns both the path from the place of production/purchase to the FabLab, i.e. the place where the cube is made, and the path introduced to bring some of the applied materials to the place of disposal. Minor impacts also derive from argon plasma, PLA, energy used and the incinerator (about 4 and 2%).

In the second case, on the other hand, the product that shows a major impact is silicone rubber, used for the mould (about 98%), followed by transportation and gypsum (about 2%).

Therefore, from the results obtained through the two methodologies ReCiPe and IPCC GWP, it is possible to state that the first case, related to innovative methodology of restoration, of the proposed integrative restoration shows a lower impact than the second case. In the second case, in fact, the most relevant impact is given by the silicone rubber and its disposal process. On the contrary, in the first case the polymeric material proposed to realize the integration, i.e. polylactic acid, shows a minimal impact, thanks to its compostable and biodegradable nature.

Silicone rubber, in general, is widely used in the field of Cultural Heritage and restoration especially for the realization of casts and moulds, since, being a highly elastic material, it is able to reproduce objects by capturing every detail, thus realizing a variety of copies. Depending on the function for which it is intended, it is possible to find on the market those to be cast for metal castings, those mouldable with rapid hardening, those elastic and brushable. For this reason, therefore, another type of material is not proposed.

Probably the cause of the high impact could derive from the input inserted (synthetic rubber), which, although chemically similar to the proposed material, might not represent it to the right extent in terms of environmental impact.

In the first case study, on the other hand, the greatest impact derives from TEOS, the coating that is deposited between the layers of polymeric material during the printing process, with the aim of improving its chemical and mechanical properties. In order to reduce the impact, it could be proposed to alternate the switching on and off of the device during the printing process, in order to halve its impact on the environment.

Conclusion

For this study, the behaviour of a pure PLA filament, a material widely used in 3D printing is analyzed. In recent years, in fact, digital fabrication has achieved considerable success in many areas, thanks to its ease of use by the user, its versatility in the face of different economic needs, and the possibility of using an increasingly wide range of materials.

Digital fabrication, recently, has invested especially in the field of Cultural Heritage, where, thanks to 3D printing and scanning, it is possible to digitally preserve works of art, performing simulations of aging and deterioration, as well as assisting the various restoration operations, proposing multimedia museum exhibitions and providing paths for the visually impaired and blind. Thanks to these features, we want to propose the use of FDM technology to reproduce missing parts of artifacts and place them as an integration on the artifact. Obviously, depending on the case study considered, it is possible to select the most convenient rapid prototyping methodology, as well as the material that best suits the needs and conditions in which it is stored.

Through this thesis project, therefore, the study and analysis of the chemical and mechanical properties of PLA-based specimens, made by the FDM additive printing process coupled with a plasma flashlight is proposed. In fact, it's compared the different behaviour of untreated and cold plasma treated samples at atmospheric pressure, a technique that offers the possibility to increase the adhesiveness and surface wettability of the material. Moreover, during the treatment, a protective coating, siloxane-based (TEOS), was deposited in order to obtain a material resistant in outdoor environment, i.e. against wear and atmospheric agents. This evaluation was made possible thanks to the simulation of hypothetical external degradative conditions, divided into two types: UV radiation and relative humidity (RH≈70%).

The study was made possible thanks to the use of colorimetric analysis, FT-IR spectra in ATR mode, Raman spectra, TGA-DSC thermograms and dynamometric tests, used both before and after artificial aging.

A first characterization was obtained through ATR-FTIR and Raman spectroscopies, which confirmed the nature of the material used, i.e. polylactic acid.

Then, also the TGA-DSC technique allowed to trace the typical temperatures of the polymer, which were then compared with the temperatures obtained following an annealing process carried out on the pure PLA filament. The objective was to evaluate if, from an analytical point of view, structural differences were found when the material is heated at a lower temperature than Tm. From a direct comparison of the results, it was found that the T_g of the annihilated filament tended to decrease, probably due to a chain scission process, while the T_m, as well as the degree of crystallinity, χ, tended to increase, possibly due to a process of crystallite thickening, or due to

the formation of different crystallite families. The results are, moreover, confirmed by ATR-FTIR analysis of the annihilated residue.

Subsequently, untreated and cold plasma treated specimens were compared. Both IR and Raman spectroscopy, besides showing the typical PLA peaks, did not show any relevant difference. On the contrary, thanks to the dynamometric tests it was possible to observe that the non-plasma treated specimens showed a higher tensile strength than the treated ones. This unexpected result might not be due to the ineffectiveness of the deposited precursor, but rather to its excessive deposition on the specimen surfaces during the printing process, which probably led to the formation of vitrified surfaces in the polymer.

The samples were also subjected to colorimetric measurements both before and after accelerated aging, with the goal of obtaining objective feedback regarding possible color variations.

It was observed that UV aging resulted in greater aesthetic changes at the surface level, compared to RH aging.

However, the results obtained from the measurements did not reveal any particular color changes; in fact, no aesthetic changes were detected with the naked eye.

ATR-FTIR analyses of the untreated and treated UV-aged samples showed no alterations in the composition of the polymer matrix, whose peaks were the same as the spectral analyses performed previously for the filament. On the contrary, the samples subjected to RH aging showed changes, albeit minimal; it was, in fact, possible to find a decrease in the COO bond, whose cleavage refers to the degradation mechanism of hydrolysis of the ester bond, a phenomenon that tends to increase with increasing RH. On the other hand, the cleavage, and therefore the reduction of the peak related to the COO group, was not observed for the untreated samples, which seem to show greater resistance under conditions of high relative humidity.

Compared to IR spectroscopy, Raman did not allow us to investigate the polymer functional groups and any degradation by-products resulting from aging. Therefore, it was not possible to state that there were chemical changes in the polymeric material.

Passing, subsequently, to TGA-DSC, in the case of the untreated and aged sample in relative humidity, an increase in the degree of crystallinity was found, probably due to a change in the mass fraction of the crystalline fraction, as the amorphous polymer chains result to be more easily accessible during the hydrolysis process; this, therefore, might have led to a structural reorganization. Turning then to the untreated and treated UV-aged samples, it was hypothesized that the photooxidation process, from which the polymer chain cleavage and recrystallization occurs, causes an increase in the crystalline fraction and the simultaneous molecular decomposition, making the polymeric material more brittle.

The causes of UV aging were also found in the results related to dynamometric tests, where it was verified that for long UV exposure times, the reduction in molecular weight becomes more pronounced and the elastic modulus begins to decrease. In this sense, both tensile strength and

deformation strength gradually decrease. Hence, it is assumed that if UV radiation initially causes structural and molecular reorganization, it later causes molecular chains to break, making the material more brittle. In terms of the results obtained for RH aged samples, however, it was observed that the increased tensile strength may result from a possible plasticizing effect conferred by moisture. The greater strength, moreover, could also derive from plasma treatment, a result that was also confirmed by colorimetric measurements. Moreover, in all cases, the treated specimens showed a brittle behaviour while the untreated ones showed a more ductile behaviour; on the contrary, only in the case of the RH aged specimens, an inverse behaviour was found, i.e. the treated specimens appeared more ductile.

Finally, the adhesiveness of treated and untreated polymeric material in both nitric and acetic acid was evaluated. In the specific case of acetic acid, similar in nature to the polymer as it is organic, it led to signs of swelling and dissolution of the material, especially in the material consisting of the protective coating. The ATR-FTIR analysis carried out on the samples after immersion in acid allowed to verify the formation of low molecular weight degradation products, such as lactic acid and lactate.

Also, in this case it is assumed that the low resistance of the sample does not derive so much from the ineffectiveness of the treatment, but rather from an excessive deposition of siloxanic material between the layers. Previous research, in fact, has shown that the presence of siloxane-based coatings, deposited by cold plasma, gave satisfactory results when the sample was placed in formic acid and acetone.

Finally, the material chosen for this research shows a low environmental impact, as it is biodegradable, compostable and "sustainable", it is emphasized. Therefore, through the LCA methodology we wanted to compare two hypothetical cases of integrative restoration, one based on the use of PLA (innovative technique), the other based on the use of plaster for the integration and silicone rubber for the cast (traditional method).

The results obtained confirmed the sustainable nature of the polymer, whose impact is minimal compared to silicone rubber. It has been assumed that most of it is attributable to the input inserted, which, although chemically similar, is assumed not to represent it to the right extent, in terms of environmental impact. In this sense, is not proposed the use of a different material, precisely because rubber is widely used in the field of Cultural Heritage to make casts and moulds.

It is hoped that subsequent studies will be carried out, in particular to provide a more in-depth analysis of both mechanical and acid resistance by depositing the siloxane-based coating on the polymer layers of the printed material in the right amount.

Bibliography

[1] 3D Printing & Additive Manufacturing - A Complete Overview (hubs.com)

[2] ISO/ASTM 52900:20158(en), *Additive manufacturing – General principles – Terminology*, https://www.iso.org/obp/ui#iso:std:iso-astm:52900:ed-1:v1:en

[3] Charles W. Hull, *Apparatus for production of three-dimensional objects by stereolithography*, 11 March 1986.

[4] Stampa tridimensionale, https://www.treccani.it/enciclopedia/stampa-tridimensionale_(Enciclopedia-Italiana)/

[5] H. Agrawaal, J.E. Thompson, *Additive manufacturing (3D printing) for analytical chemistry*, Talanta Open, vol. 3, August 2021, https://doi.org/10.1016/j.talo.2021.100036

[6] https://formlabs.com/it/industries/education/

[7] Fab lab Venezia, https://www.fablabvenezia.org/

[8] L. Bravi, F. Murmura, G. Santos, *Manufacturing labs: where new digital technologies help improve life quality*, International Journal for Quality Research, vol. 4, 2018, pp. 957-974

[9] Manifattura additiva vs sottrattiva, https://stampa3d.valorebf.it/manifattura-additiva-vs-sottrattiva/

[10] Tecnologia&Design, Produzione con macchine CNC, http://www.tecnologiaedesign.it/web/servizi/produzione/macchine-cnc/

[11] L'elettroerosione EDM a filo e tuffo: tecnologia di precisione, https://vehiclecue.it/elettroerosione-filo-tuffo-edm/19388/

[12] Lavorazione con fascio laser, https://it.wikipedia.org/wiki/Lavorazione_con_fascio_laser

[13] Taglio ad acqua come funziona e dove si usa, http://www.betelli.it/taglio-ad-acqua-funziona-si-usa/

[14] Y. Hongyi, J.C. Lim, Y. Liu, X. Qi, Y.L. Yap, V. Dikshit, W.Y. Yeong, J. Wei, *Performance evaluation of ProJet multi-material jetting 3D printer*, Virtual and Physical Prototyping, September 2016, https://doi.org/10.1080/17452759.2016.1242915

[15] N. Afshar-Mohajer, C-Y Wu, T. Ladun, D.A. Rajon, Y. Huang, *Characterization of particulate matters and total VOC emissions from a binder jetting 3D printer*, Building and Environment, vol. 93, November 2015, pp. 293-301, https://doi.org/10.1016/j.buildenv.2015.07.013

[16] T. Sivarupan, N. Balasubramani, P. Saxena, D. Nagarajan, M. El Mansori, K. Salonitis, M. Jolly, M. S. Dargusch, *A review on the progress and challenges of binder jet 3D printing of sand moulds for advanced casting*, Additive Manufacturing, vol. 40, 2021, pp. 1-17

[17] A. Ramya, S.L. Vanapalli, *3D printing technologies in various applications*, International Journal of Mechanical Engineering and Technology (IJMET), vol. 7, May-June 2016, pp. 396-409

[18] Stampa 3D additive e sottrattiva, https://3d4growth.com/stampa-3d-additiva-sottrattiva

[19] Stratasys, https://www.stratasys.com/it

[20] 3D Printing: Different Techniques, Processes and Technologies, 3D Printing Manufacturing Methods Techniques, Processes, Technologies (advice-manufacturing.com)

[21] 3D Printing from scratch, Types of 3D printers or 3D printing technologies overview, Types of 3D printers or 3D printing technologies overview | 3D Printing from scratch

[22] F. Pignatelli, *L'evoluzione della stampa 3D e le sue applicazioni in campo museale*, SCIRES-IT, SCIentific RESearch and Information Technology, vol. 3, 2013, pp. 143-158
[23] Stratasys, Storia della stampa 3D, https://www.stratasys.com/it/explore/article/3d-printing-history
[24] STAMPA3Dstore.com, Guida completa alle tecnologie di Stampa 3D, https://www.stampa3dstore.com/guida-completa-alle-tecnologie-di-stampa-3d-da-seltek/
[25] A. B. Varotsis, *Introduction to FDM 3D printing*, HUBS. A protolabs company, https://www.hubs.com/knowledge-base/introduction-fdm-3d-printing/#work
[26] adreco plastics, *ABS plastic properties*, https://adrecoplastics.co.uk/abs-plastic-properties/
[27] creative mechanisms, *Everything you need to know about ABS plastic*, https://www.creativemechanisms.com/blog/everything-you-need-to-know-about-abs-plastic
[28] All3DP, *What is PLA and what is it made of?*, https://all3dp.com/2/is-pla-biodegradable-what-you-really-need-to-know/
[29] S. Riaz, N. Fatima, A. Rasheed, M. Riaz, F. Anwar, Y. Khatoon, *Metabolic engineered biocatalyst: a solution for PLA based problems,* International Journal of Biomaterials, 2018, pp. 1-10
[30] M. Alexandri, R. Schneider, K. Mehlmann, J. Venus, *Recent advances in D-lactic acid production from renewable resources: case studies on agro-industrial waste streams*
[31] Freelabster, Qual è la differenza tra ABS e PLA?, https://www.freelabster.com/it/blog/qual-e-la-differenza-tra-abs-e-pla/
[32] L. E. Depero, F. Signorini, A. Zacco, *Materiali polimerici per la stampa 3D con tecnologia FDM*, in Tecnologie, 2016
[33] *Studio di alcuni filamenti per la stampa 3D nel restauro di sculture lignee: Un esempio applicativo di integrazione di parti mancanti*, Tesi di Laurea Magistrale, pp. 29-35
[34] M. M. Hanon, L. Zsidai, *Comprehending the role of process parameters and filament color on the structure and tribological performance of 3D printed PLA*, Journal of Materials Research and Technology, 2021, pp. 1-25, https://doi.org/10.1016/j.jmrt.2021.08.061
[35] A. Frache, G. Camino, *Degradazione, stabilizzazione e ritardo alla fiamma di polimeri*, 2012, Collana AIM testi, Roma, Capitolo 1 – Le problematiche della degradazione dei polimeri, https://books.google.it/books?hl=it&lr=&id=8WNgiHQXjWsC&oi=fnd&pg=PP9&dq=degradazione+chimica+polimeri&ots=ZtrTIOndzs&sig=34-XCAvjY7TyfdYnI35D3gXD9x4&redir_esc=y#v=onepage&q=degradazione%20chimica%20polimeri&f=false
[36] G. Rajeshkumar, S. A. Seshadri, G. L. Devnani, M. R. Sanjay, S. Siengchin, J. P. Maran, N. A. Al-Dhabi, P. Karuppiah, V. A. Mariadhas, N. Sivarajasekar, A. R. Anuf, *Environmental friendly, renewable and sustainable poly lactic acid (PLA) based natural fiber reinforced composites – A comprehensive review*, Journal of Cleaner Production, vol. 310, 2021, pp. 1-26
[37] V. G. Surange, P. V. Gharat, *3D printing process using Fused Deposition Modelling (FDM)*, International Research Journal of Engineering and Technology, vol. 3, 2016, pp. 1403-1406
[38] IO1 – Metodologia per la definizione di esercizi di stampa 3D adatti all'istruzione trasversale, *Guida tecnica per la stampa 3D*, O1A1-IT.pdf

[39] R. Scopigno, P. Cignoni, N. Pietroni, M. Callieri, M. Dellepiane, *Digital Fabrication Techniques for Cultural Heritage: A Survey*, Visual Computing Lab, CNR-ISTI, 2015, pp. 1-17
[40] C. Balletti, M. Ballarin, F. Guerra, *3D printing: State of the art and future perspectives*, Journal of Cultural Heritage, vol. 26, 2017, pp. 172-182, https://doi.org/10.1016/j.culher.2017.02.010
[41] G. Tucci, V. Bonora, *From real to "real". A review of geomatic and rapid prototyping techniques for solid modelling in cultural heritage field*, International Archives of the Photogrammetry, Remote Sensing and Spatial Information Sciences, vol. XXXVIII-5/W16, 2011, pp. 575-582
[42] A. Reichinger, S. Maierhofer, W. Purgathofer, *High-quality tactile paintings*, Journal on Computing and Cultural Heritage, vol. 4, 2011, pp. 1-5, https://doi.org/10.1145/2037820.2037822
[43] Tactile Museum ANTEROS, cavazza.it
[44] Scheda Tecnica, *Unocad, tecnologie per l'arte in sicurezza*, Tecnologie per i Beni Culturali, http://mediageo.it/ojs/index.php/archeomatica/article/viewFile/785/717
[45] Smithsonian 3D digitization, 3d.si.edu
[46] MakerBot Thingiverse, thingiverse.com
[47] Apollonio F. I., Basilissi V., Callieri M., Dellepiane M., Gaiani M., Ponchio F., Rizzo F., Rubino A. R., Scopigno R., Sobra' G., *A 3d-centered information system for the documentation of a complex restoration intervention,* Journal of Cultural Heritage, 29, 2018, pp. 89-99
[48] Maptitude, Geographic Information System, https://www.caliper.com/maptitude/gis_software/default.htm
[49] T. Lòpez-Martìnez, A. Garcìa-Bueno, V. J. Medina-Flòrez, *New methodology for the assessment of cleaning treatments. Applications of photogrammetry for restoration*, Journal of Cultural Heritage, vol. 30, 2018, pp. 117-123, https://doi.org/10.1016/j.culher.2017.09.019
[50] M. Higueras, A. I. Calero, F. J. Collado-Montero, *Digital 3D modeling using photogrammetry and 3D printing applied to the restoration of a Hispano-Roman architectural ornament*, Digital Applications in Archaeology and Cultural Heritage, vol. 20, 2021, pp. 1-11, https://doi.org/10.1016/j.daach.2021.e00179
[51] PSFC Plasma Science and Fusion Center Massachusetts Institute of Technology, *What is Plasma?*, https://www.psfc.mit.edu/vision/what_is_plasma
[52] C. Tendero, C. Tixier, P. Tristant, J. Desmaison, P. Leprince, *Atmospheric pressure plasmas: A review*, Spectrochimica Acta Part B: Atomic Spectroscopy, vol. 61, 2006, pp. 2-30, https://doi.org/10.1016/j.sab.2005.10.003
[53] M. Scapinello, *Studio di processi al plasma freddo a pressione atmosferica per il trattamento delle fibre tessili,* Università degli studi di Padova, 2012
[54] C. Dalla Pria, *Ottimizzazione del trattamento su materiali industriali tramite jet al plasma freddo a pressione atmosferica*, Università degli studi di Padova, 2018-19
[55] L. Bardos, H. Baránková, *Cold atmospheric plasma: Sources, processes, and applications*, vol. 518, 2010, pp. 6705-6713, https://doi.org/10.1016/j.tsf.2010.07.044
[56] F. Fanelli, F. Fracassi, *Atmospheric pressure non-equilibrium plasma jet technology: general features, specificities and applications in surface processing of materials*, Surface & Coatings Technology, 2017, pp. 174-175, http://dx.doi.org/10.1016/j.surfcoat.2017.05.027

[57] The restoration of the “Capsella Vaticana”, https://www.youtube.com/watch?v=r5JClO-9MQM
[58] La Capsella Vaticana. Una tecnica innovativa per un restauro all’avanguardia, Diagnostica&Restauro, https://www.museivaticani.va/content/dam/museivaticani/pdf/eventi_novita/iniziative/giovedi_musei/2021/67_restauro_capsella.pdf
[59] N. Sprang, D. Theirich, J. Engemann, *Plasma and ion beam surface treatment of polyethylene*, Surface and Coatings Technology, vol. 74-75, 1995, pp. 689-695, https://doi.org/10.1016/0257-8972(95)08340-5
[60] J. B. Lynch, P. D. Spence, D. E. Baker, T. A. Postlethwaite, *Atmospheric pressure plasma treatment of polyethylene via a pulse dielectric barrier discharge: Comparison using various gas compositions versus corona discharge in air*, Journal of Applied Polymer Science, vol. 71, 1999, pp. 319-331, https://doi.org/10.1002/(SICI)1097-4628(19990110)71:2<319::AID-APP16>3.0.CO;2-T
[61] O. Kwon, S. Tang, S. Myung, N. Lu, H. Choi, *Surface characteristics of polypropylene film treated by an atmospheric pressure plasma*, Surface & Coatings Technology, vol. 192, 2005, pp. 1-10, doi:10.1016/j.surfcoat.2004.09.018
[62] R. Wolf, A. C. Sparavigna, *Role of Plasma Surface Treatments on Wetting and Adhesion*, Engineering, vol. 2, 2010, pp. 397-402, doi:10.4236/eng.2010.26052
[63] J. Podsiadly, E. Dörsam, *Effects of argon low temperature plasma on PLA film surface and aging behaviors*, Vacuum, vol. 145, 2017, pp. 278-284, https://doi.org/10.1016/j.vacuum.2017.09.001
[64] A. Vilaplana, V. Fombuena, D. García, M. D. Samper, L. Nàcher, *Surface modification of polylactic acid (PLA) by air atmospheric plasma treatment*, European Polymer Journal, vol. 58, 2014, pp. 23-33, https://doi.org/10.1016/j.eurpolymj.2014.06.002
[65] N. Inagaki, K. Narushima, Y. Tsutsui, Y. Ohyama, *Surface modification and degradation of poly(lactic acid) films by Ar-plasma*, Journal of Adhesion Science and Technology, vol. 16, 2002, pp. 1041-1054, https://doi.org/10.1163/156856102760146156
[66] V. Agudo, M. Oliva, A. M. Moreno, M. L. Martìn, *Effect of plasma treatment on the surface properties of polylactic acid films*, Polymer Testing, vol. 96, 2021, pp. 1-8, https://doi.org/10.1016/j.polymertesting.2021.107097
[67] M. Wang, P. Favi, X. Cheng, N. H. Golshan, K. S. Ziemer, M. Keidar, T. J. Webster, *Cold atmospheric plasma (CAP) surface nanomodified 3D printed polylactic acid (PLA) scaffolds for bone regeneration*, Acta Biomaterialia, vol. 46, 2016, pp. 256-265, https://doi.org/10.1016/j.actbio.2016.09.030
[68] O. Laput, I. Vasenina, M. C. Salvadori, K. Savkin, D. Zuza, I. Kurzina, *Low-temperature plasma treatment of polylactic acid and PLA/HA composite material*, Journal of Materials Science, vol. 54, 2019, pp. 11726-11738, https://doi.org/10.1007/s10853-019-03693-4
Biblio per LCA
[69] Degree thesis of M. Carai, *Deposizione e caratterizzazione di ricoprimenti di silice su acciaio inox ottenuti con plasma atmosferico*, Università degli Studi di Padova, 2011/2012

[70] F. Nicolazo, A. Goullet, A. Granier, C. Vallée, G. Turban, B. Grolleau, *Study of oxygen/TEOS plasmas and thin SiO_x films obtained in an helicon diffusion reactor*, Surface and Coatings Technology, vol. 98, 1998, pp. 1578-1583
[71] Personal communication
[72] I. Muro-Fragua, A. Sainz-Garcìa, P. F. Gòmez, M. Lòpez, R. Mùgica-Vidal, E. Sainz-Garcìa, P. Toledano, Y. Sàenz, M. Lòpez, M. Gonzàlez-Raurich, M. Prieto, A. Alvarez-Ordònez, A. Gonzàlez-Marcos, F. Alba-Elìa, *Atmospheric pressure cold plasma anti-biofilm coatings for 3D printed food tools*, Innovative Food Science & Emerging Technologies, vol. 64, 2020, pp. 1-12
[73] Master's thesis of L. Giansante, *Utilizzo della torcia al plasma per la valorizzazione energetica di RSU nel sistema integrato di smaltimento*, Politecnico di Torino, 2020
[74] A. Ciroth, C. Di Noi, T. Lohse, M. Srocka, *OpenLCA 1.10. Comprehensive User Manual*, GreenDelta, 2020
[75] H. Pilz, B. Brandt, R. Fehringer, *L'impatto delle materie plastiche sul consumo energetico e sulle emissioni di gas serra lungo il loro ciclo di vita in Europa*, denkstatt, 2010
[76] Degree thesis of F. De Filippis and G. Faella, *Analisi LCA (Life Cycle Assessment) del processo produttivo radome condotto presso l'azienda MBDA Italia S.p.A.,* Università Degli Studi Di Napoli Federico II, 2015/2016
[77] P. Masoni, E. Scimia, *Life Cycle Assessment: sviluppo di indicatori specifici per l'Italia per la fase di valutazione d'impatto*, ENEA, Roma, 1999
[78] Degree thesis of V.A. Candian, *Utilizzo della metodologia LCA per la valutazione di interventi di efficientamento energetico e calcolo della carbon footprint su una piscina pubblica*, Università Ca' Foscari, Venezia, 2018/2019
[79] R. Hischier, B. Weidema, *Implementation of Life Cycle Impact Assessment Methods*, ecoinvent centre, St. Gallen, 2010
[80] TDS, Polymer DataSheet, PDF, https://www.eumakers.com/pla-filament-color-transparent.html
[81] ISO 527-2, *Plastics – Determination of tensile properties*, second edition 2012-02-15
[82] Joyful Printing, *Materiali biodegradabili*, 2020, http://it.joyful-printing.org/info/biodegradable-materials-49726442.html
[83] STP Viewer – ABViewer 14, https://3d-viewers.com/it/step-viewer.html
[84] FabLab Venezia, *Stampa e scansione 3D*, https://www.fablabvenezia.org/macchine/
[85] Delta Wasp 3MT, https://www.3dwasp.com/stampante-3d-grande-delta-wasp-3mt/
[86] A. Patelli, E. Verga, L. Nodari, S. M. Petrillo, A. Delva, P. Ugo, P. Scopece, *A customised atmospheric pressure plasma jet for conservation requirements*, Materials Science and Engineering, vol. 384, 2017
[87] Nadir, Plasma & Polymers, *Plasma Stylus Noble, Technical specifications*, https://www.nadir-tech.it/it/tecnologie/plasma-2/prodotti-plasma/stylus-plasma-noble/plasma-stylus-noble-specifiche-tecniche/
[88] A. Frova, *Luce colore visione. Perché si vede ciò che si vede*, 2015, BUR scienza, Milano, Italia
[89] Tesi di E. Pedrotti, *Interazione tra luce e materia: colorimetria e fotodegrado in ambito illumitecnico*, Ingegneria elettrotecnica, Università degli Studi di Padova

[90] Konica Minolta, Spettrofotometri portatili CM-26dG / CM-26d / CM-25d, https://www5.konicaminolta.eu/it/strumenti-di-misura/prodotti/misura-di-colore/spettrofotometri-portatili/cm-26dg-series/introduzione.html
[91] A. Gorassini, *Spettrofotometria infrarossa in riflettanza totale attenuata (FTIR-ATR)*, http://www.ipac.regione.fvg.it/userfiles/file/gorassini.pdf
[92] D. A. Skoog, D. M. West, F. J. Holler, S. R. Crouch, *Fondamenti di Chimica Analitica di Skoog e West*, 2015, EdiSES, Napoli, Italia, pp. 714-715
[93] A. Ausili, M. Sànchez, J. C. Gòmez-Fernàndez, *Attenuated total reflectance infrared spectroscopy: A powerful method for the simultaneous study of structure and spatial orientation of lipids and membrane proteins*, Biomedical Spectroscopy and Imaging, vol. 4, 2015, pp. 159-170, DOI 10.3233/BSI-150104
[94] FT-IR/ATR, https://biomateriali.files.wordpress.com/2012/12/ftir.pdf
[95] K. Yuniarto, Y. A. Purwanto, S. Purwanto, B. A Welt, H. K. Purwadaria, T. C. Sunarti, *Infrared and Raman studies on Polylactide Acid and Polyethylene Glycol-400 Blend*, Atti della conferenza AIP, vol. 1725, 2016, https://doi.org/10.1063/1.4945555
[96] E. E. Popa, M. Rapa, O. Popa, G. Mustatea, V. I. Popa, A. C. Mitelut, M. E. Popa, *Polylactic Acid/Cellulose Fibres Based Composites for Food Packaging Applications,* Materiale Plastice, vol.54, pp. 673-677, 2017, DOI: 10.37358/MP.17.4.4923
[97] M. A. Cuiffo, J. Snyder, A. M. Elliott, N. Romero, S. Kannan, G. P. Halada, *Impact of the Fused Deposition (FDM) Printing Process on Polylactic Acid (PLA) Chemistry and Structure,* Applied Sciences, vol. 7, 2017, doi:10.3390/app7060579
[98] V. Vascotto, Tesi di Laurea in Ingegneria Processi Industriali e Materiali, *Preparazione e caratterizzazione di sistemi compositi in polimeri biodegradabili e idrossiapatite per la realizzazione di scaffold,* 2011-2012
[99] N. Wang, X. Zhang, X. Ma, J. Fang, *Influence of carbon black on the properties of plasticized poly(lactic acid) composites*, Polymer Degradation and Stability, vol. 93, 2008, pp. 1044-1052, https://doi.org/10.1016/j.polymdegradstab.2008.03.023
[100] B. W. Chieng, N. A. Ibrahim, W. M. Z. W. Yunus, M. Z. Hussein, *Poly(lactic acid)/Poly(ethylene glycol) Polymer Nanocomposites: Effects of Graphene Nanoplatelets*, Polymers, vol. 6, 2014, pp. 93-104, doi:10.3390/polim6010093
[101] G. De, D. Kundu, B. Karmakar, D. Ganguli, *FTIR studies of gel to glass conversion in TEOS-fumed silica-derived gels*, Journal of Non-Crystalline Solids, vol. 155, 1992, pp. 253-258
[102] M. Gardette, S. Thèrias, J. L. Murariu, P. Dubois, *Photooxidation of polylactide/calcium sulphate composites*, Polymer Degradation and Stability, vol. 96, 2011, pp. 616-623
[103] S. Bocchini, K. Fukushima, A. Di Biasio, A. Fina, A. Frache, F. Geobaldo, *Polylactic Acid and Polylactic Acid-Based Nanocomposite Photooxidation*, Biomacromolecules, vol. 11, 2010, pp. 2919-2926
[104] M. E. Gonzàlez-Lòpez, A. S. Martìn del Campo, J. R. Robledo-Ortìz, M. Arellano, A. A. Pèrez-Fonseca, *Accelerated weathering of poly(lactic acid) and its biocomposites: A review*, Polymer Degradation and Stability, vol. 179, 2020

[105] D. Rasselet, A. Ruellan, A. Guinault, G. Miquelart-Garnier, C. Sollogoub, B. Fayolle, *Oxidative degradation of polylactide (PLA) and its effects on physical and mechanical properties*, European Polymer Journal, 2013, pp. 1-8
[106] A. Araùjo, G. L. Botelho, M. Silva, A. Machado, *UV stability of Poly(Lactic Acid) Nanocomposites*, Journal of Materials Science and Engineering, vol. 2, 2013, pp. 75-83
[107] A. Copinet, C. Bertrand, S. Govindin, V. Coma, Y. Couturier, *Effects of ultraviolet light (315 nm), temperature and relative humidity on the degradation of polylactic acid plastic films*, Chemosphere 55, 2004, pp. 763-773
[108] L. A. K. Staveley, *The Characterization of Chemical Purity: Organic Compounds*, London Butterworths, New York, 1971, pp. 149-153, books.google.com
[109] Spettroscopia Raman, https://people.unica.it/flaminiacesaremarincola/files/2011/12/Lez6-ChimFisBiol-Raman.pdf
[110] La spettroscopia Raman, in Research for Cultural Heritage, http://www.researcheritage.com/2017/05/La-Spettroscopia-Raman.html
[111] P. Vandenabeele, *Raman spectroscopy*, Analytical and Bioanalytical Chemistry, 2010
[112] K. Vano-Herrera, A. Misiun, C. Vogt, *Preparation and characterization of poly(lactic acid)/poly(methyl methacrylate) blend tablets for application in quantitative analysis by micro Raman spectroscopy*, Journal of Raman Spectroscopy, vol. 46, 2015, pp. 273-279
[113] G. Kister, G. Cassanas, M. Vert, *Effects of Morphology, Conformation and Configuration on the IR and Raman Spectra of Various Poly(lactic acid)s,* Polymers, vol. 39, 1998, pp. 267-273, https://doi.org/10.1016/S0032-3861(97)00229-2
[114] M. Gnyba, M. Szczerska, M. Keranen, J. Suhonen, *Sol-Gel materials investigation by means of Raman Spectroscopy*, XVII IMEKO World Congress, 2003, pp. 237-240
[115] Tesi di Laurea Magistrale in Ingegneria dei Materiali di F. Casamento, *Studio di blend polimerici a base di PLA: effetto di compatibilizzanti naturali*, Politecnico di Torino, 2019
[116] L. Zhang, Z. Lin, Q. Zhou, S. Ma, Y. Liang, Z. Zhang, *PEEK modified PLA shape memory blends: towards enhanced mechanical and deformation properties*, Frontiers of Materials Science, 2020, pp. 177-187, https://doi.org/10.1007/s11706-020-0502-z
[117] P. Stagnaro, G. Luciano, R. Utzeri, *La calorimetria differenziale a scansione e l'analisi termogravimetrica nella caratterizzazione termica dei materiali polimerici*, https://moodle2.units.it/pluginfile.php/283832/mod_resource/content/1/Appunti-%20DSC-TGA.pdf
[118] J. Pires, A. J. Cruz, *Techniques of Thermal Analysis applied to the Study of Cultural Heritage*, 2007, Journal of Thermal Analysis and Calorimetry, vol. 87, pp. 411-415
[119] P. K. Gallagher, *Handbook of Thermal Analysis and Calorimetry. Vol. 1. Principles and practice*, 1998, Elsevier, Amsterdam, http://pyrotechnics.net.ru/library/thermo/Handbook_of_Thermal_Analysis_and_Calorimetry_Volume_1.pdf
[120] S. Yang, Z. Wu, W. Yang, M. Yang, *Thermal and mechanical properties of chemical crosslinked polylactide (PLA)*, Polymer Testing, vol. 27, 2008, pp. 957-963, https://doi.org/10.1016/j.polymertesting.2008.08.009

[121] PEDIAA, Difference between elastic and plastic deformation, 2018, https://pediaa.com/difference-between-elastic-and-plastic-deformation/
[122] G. Petrucci, *Proprietà dei materiali e prove meccaniche*, Università degli studi di Palermo, http://www1.unipa.it/giovanni.petrucci/Disp/Materiali.pdf
[123] Tesi di Laurea in Ingegneria aerospaziale di G. F. Gentile, *Prove sperimentali su componenti polimerici realizzati mediante stampa 3D*, Facoltà di Ingegneria Civile e Industriale, Sapienza, Università di Roma
[124] J. R. C. Dizon, *Mechanical Characterization of 3D-Printed Polymers*, in "Additive Manufacturing", vol. 20, 2018, pp. 44-67
[125] MTS Insight® Electromechanical Testing Systems. Affordable and easy-to-use platforms for performing virtually any static test, https://www.upc.edu/sct/documents_equipament/d_69_id-423.pdf
[126] R. L. Feller, *Accelerated Aging. Photochemical and Thermal Aspects*, The Getty Conservation Institute, 1995
[127] ASTM G 154, *Standard Practice for Operating Fluorescent Light Apparatus for UV Exposure of Nonmetallic Materials*, https://www.wewontech.com/190114007.pdf
[128] EN 1297, *Flexible sheets for waterproofing - Bitumen, plastic and rubber sheets for roof waterproofing - Method of artificial ageing by long term exposure to the combination of UV radiation, elevated temperature and water*
[129] ASTM D 4799: 2008, *Standard Practice for Accelerated Weathering Test Conditions and Procedures for Bituminous Materials (Fluorescent UV, Water Spray, and Condensation Method)*, https://www.wewontech.com/testing-standards/190125038.pdf
[130] ISO 11341: 2004, *Paints and varnishes – Artificial weathering and exposure to artificial radiation - Exposure to filtered xenon-arc radiation*, https://www.sis.se/api/document/preview/905111/
[131] UNI EN 14509: 2006, *Self-supporting double skin metal faced insulating panels - Factory made products – Specifications*
[132] ASTM G 155: 2005, *Standard Practice for Operating Xenon Arc Light Apparatus for Exposure of NonMetallic Materials*, https://www.wewontech.com/190116010.pdf
[133] R. Paolini, T. Poli, M. Fiori, A. G. Mainini, *Valutazione delle prestazioni di cool materials esposti all'ambiente urbano: sporcamento e invecchiamento accerelato*, ENEA, Politecnico di Milano, 2012, https://iris.enea.it/retrieve/handle/20.500.12079/6274/197/Rds%202012-114.pdf
[134] Direct Industry, *Camera per test climatica Q-SUN Xe-3*, https://www.directindustry.it/prod/q-lab/product-24582-1420327.html
[135] Ensinger, *Materiali plastici resistenti agli agenti chimici*, https://www.ensingerplastics.com/it-it/semilavorati/soluzioni-in-materiale-plastico/resistenza-chimica
[136] Sigma-Aldrich, Product Specification of Nitric Acid – ACS reagent, 70%, https://www.sigmaaldrich.com/specification-sheets/182/275/438073-6X2.5L-PW__SIGALD_____.pdf
[137] Sigma-Aldrich, Glacial Acetic Acid, https://www.sigmaaldrich.com/IT/it/substance/glacialaceticacid600564197?context=product
[138] SimaPro, https://simapro.com/
[139] SimaPro, https://network.simapro.com/2b/#usp

[140] STRUMENTI, organizzare la complessità, misurare le prestazioni, SimaPro, https://www.to-be.it/strumenti/simapro/
[141] CSQA, NORME LCA ISO 14040|14044, https://www.csqa.it/CSQA/Norme/Sostenibilita-Ambientale/ISO-14040-LCA
[142] 3D Archeolab, La cintura di Isadora del Museo Archeologico di Peccioli (PI), https://www.3d-archeolab.it/portfolio-items/peccioli-pisa-cintura-isadora/
[143] E. Corvo, J. Reyes, C. Valdes, F. Villasenor, O. Cuesta, D. Aguilar, P. Quintana, *Influence of air pollution and humidity on limestone materials degradation in historical buildings located in cities under tropical coastal climates*, Water Air Soil Pollut, 2010, pp. 359-375
[144] Ecoinvent. (2007), *Overview and Methodology*, Data v2.0 (2007), https://www.ecoinvent.org/files/200712_frischknecht_jungbluth_overview_methodology_ecoinvent2.pdf
[145] ENERGIT, *Qual è il consumo medio di un PC?*, https://energit.it/quale-e-il-consumo-medio-di-un-pc/
[146] Consulente energia, http://www.consulente-energia.com/af-quanto-consuma-di-corrente-un-modem-wireless-adsl-watt-consumati-da-modem-adsl-o-router-wifi.html
[147] A. Ashok, J. Keselik, D. Mantzoros, *Comparative Life Cycle Assessment (LCA) of Conventionally manufactured part vs 3D printed part*, 2016
[148] M. Ruschi Mendes Saade, A. Yahia, B. Amor, *How has LCA been applied to 3D printing? A systematic literature review and recommendations for future studies*, Journal of Cleaner Production, 2019, pp. 1-23, https://doi.org/10.1016/j.jclepro.2019.118803
[149] Atlas Copco, https://www.atlascopco.com/it-it/compressors/dicono-di-noi/consumi-energetici-ridotti#:~:text=Tra%20le%20principali%20fonti%20di,anno%2C%20consuma%20circa%20500.000%20kWh.
[150] Antichità Belsito, Gesso alabastrino, https://www.antichitabelsito.it/gesso_alabastrino.htm
[151] F. Carrasco, P. Pages, J. Gamez-Perez, O.O Santana, M.L. Maspoch, *Processing of poly(lactic acid): Characterization of chemical structure, thermal stability and mechanical properties*, Polymer Degradation and Stability, vol. 95, 2010, pp. 116-125, https://doi.org/10.1016/j.polymdegradstab.2009.11.045
[152] J.K. Lee, K.H. Lee, B.S. Jin, *Structure development and biodegradability of uniaxially stretched poly(L-lactide)*, European Polymer Journal, vol. 37, 2001, pp. 907-914
[153] J.Zhang, Y. Duan, H. Sato, H. Tsuji, I. Noda, S. Yan, Y. Ozaki, *Crystal Modifications and Thermal Behavior of Poly(L-lactic acid) Revealed by Infrared Spectroscopy*, Macromolecules , vol. 38, 2005, pp. 8012-8021
[154] D. Bermudez, P.A. Quinonez, E.J. Vasquez, I.A. Carrete, T.J. Word, D.A. Roberson, *A comparison of the physical properties of two commercial 3D printing PLA grades,* Virtual and Physical Prototyping, vol.16, 2021, pp. 178-195
[155] E. Ferreira, C.B.B. Luna, D.D. Siqueira, E. M. Araujo, D. C. de Franca, R.M.R. Wellen, *Annealing effect on Pla/Eva performance,* Journal of Polymers and the Environment, 2021, pp. 1-14

[156] N. De Geyter, R. Morent, T. Desmet, M. Trentesaux, L. Gengembre, P. Dubruel, C. Leys, E. Payen, *Plasma modification of polylactic acid in a medium pressure DBD*, Surface and Coatings Technology, vol. 204, 2010, pp. 3272-3279
[157] M. L. Maminski, I. Novak, M. Micusik, A. Malolepszy, R. T. Maminska, *Discharge Plasma Treatment as an Efficient Tool for Improved Poly(lactide) Adhesive-Wood Interactions*, Materials, vol. 14, 2021, pp. 1-12, https://doi.org/10.3390/ma14133672
[158] P. Sauerbier, R. Kohler, G. Renner, H. Militz, *Surface activation of polylactic acid-based wood-plastic composite by atmospheric pressure plasma treatment*, Advances in Natural Fibers and Polymers, 2020, vol. 13, pp. 1-13, https://doi.org/10.3390/ma13204673
[159] J.C. Lee, D. H. Choi, J. Y. Choi, C. S. Ha, *Poly(lactic acid)/Functionalized silica hybrids by reactive extrusion: thermal, rheological and degradation behavior*, Macromolecolar Research, 2019, pp. 327-335, DOI 10.1007/s13233-020-8045-9
[160] I. G. Marino, P. P. Lottici, D. Bersani, R. Raschellà, A. Lorenzi, A. Montenero, *Micro-Raman monitoring of solvent-free TEOS hydrolysis*, Journal of Non-Crystalline Solids, vol. 351, 2005, pp. 495-498, https://doi.org/10.1016/j.jnoncrysol.2004.11.023
[161] C. A. M. Mulder, A. A. J. M. Damen, *Raman analysis of the initial stages of the hydrolysis and polymerization of tetraethylorthosilicate*, Journal of Non-Crystalline Solids, vol. 93, 1987, pp. 169-178
[162] M. C. Matos, L. M. Ilharco, R. M. Almeida, *The evolution of TEOS to silica gel and glass by vibrational spectroscopy*, Journal of Non-Crystalline Solids, 1992, pp. 232-237
[163] Ph. Colomban, *Raman studies of inorganic gels and of their sol-to-gel, gel-to-glass and glass-to-ceramics transformation*, Journal of Raman Spectroscopy, vol. 27, 1996, pp. 747-758
[164] G. Kister, G. Cassanas, M. Vert, *Effects of Morphology, Conformation and Configuration on the IR and Raman Spectra of Various Poly(lactic acid)s,* Polymers, vol. 39, 1998, pp. 267-273, https://doi.org/10.1016/S0032-3861(97)00229-2
[165] DW Hutmacher, *Scaffolding in Tissue Engineering Bone and Cartilage*, Biomaterial, vol. 21, 2000, pp. 2529-2543, 10.1016/s0142-9612(00)00121-6
[166] Tesi di dottorato in Ingegneria Chimica, Gestionale, Informatica, Meccanica, di E. Morici, *Nanocompositi a base polimerica ad elevate prestazioni: nanoparticelle con stabilizzanti immobilizzati in organo-modificatori*, Università degli Studi di Palermo, 2015
[167] G. Rohman, *Biodegradable Polymers: Recent Developments and New Perspectives*, IAPC Publishing, Zagreb, Croatia, 2017
[168] D. Rasselet, A. Ruellan, A. Guinault, G. Miquelard-Garnier, C. Sollogoub, B. Fayolle, *Oxidative degradation of polylactide (PLA) and its effects on physical and mechanical properties*, European Polymer Journal, vol.50, 2014, pp. 109-116, https://doi.org/10.1016/j.eurpolymj.2013.10.011
[169] S. Baratian, ES Hall, J.S. Lin, R. Xu, J. Runt, *Crystallization and solid-state structure of random polylactide copolymers: poly (L-lactide-co-D-lactide)s*, Macromolecules, vol.34, 2001, pp. 4857-4864
[170] N. T. Dintcheva, S. Al-Malaika, E. Morici, R. Arrigo, *Thermo-oxidative stabilization of poly(lactic acid)-based nanocomposites through the incorporation of clay with in-built antioxidant activity*, Journal of Applied Polymer Science, vol.134, 2017, https://doi.org/10.1002/app.44974

[171] T. Tabi, A.F. Wacha, S. Hajba, *Effect of D-lactide content of annealed poly(lactic acid) on its thermal, mechanical, heat deflection temperature, and creep properties*, Journal of Applied Polymer Science, 2018, pp. 1-10
[172] P. B. Linares, L. A. Castillo, S. E. Barbosa, Pro-Degradant Effect of Talc Nanoparticles on Polypropylene Films, 2019, Journal of Polymers and the Environment, pp. 1666-1676
[173] H. Abourayana, P. Dobbyn, D. Dowling, *Enhancing the mechanical performance of additive manufactured polymer components using atmospheric plasma pre-treatments*, 2017, Plasma Processes and Polymers, pp.1-18
[174] Prova di trazione statica (UNI 551 – UNI 552 – UNI 556 – UNISIDER 4 – UNI EN 10002/1), appunti da lezioni del prof. Di Cara Nicola, Conegliano, http://www.unife.it/interfacolta/design/insegnamenti/materiali-per-prodotto-industriale/PROVA%20DI%20TRAZIONE%20STATICA_sito.pdf
[175] A. Porfyris, S. Vasilakos, C. Zotiadis, C. Papaspyrides, K. Moser, L. Van der Schueren, G. Buyle, S. Pavlidou, S. Vouyiouka, *Accelerated ageing and hydrolytic stabilization of poly(lactic acid) (PLA) under humidity and temperature conditioning*, Polymer Testing, vol. 68, 2018, pp. 315-332
[176] L. Cai, J. Wang, J. Peng, Z. Wu, X. Tan, *Observation of the degradation of three types of plastic pellets exposed to UV irradiation in three different environments*, Science of the Total Environment, 2018, pp. 740-747
[177] A. Copinet, C. Bertrand, S. Govindin, V. Coma, Y. Counturier, *Effects of ultraviolet light (315 nm), temperature and relative humidity on the degradation of polylactic acid plastic films*, Chemosphere, vol. 55, 2004, pp. 763-773, https://doi.org/10.1016/j.chemosphere.2003.11.038
[178] S. K. Saha, H. Tsuji, *Effects of molecular weight and small amounts of D-lactide units on hydrolytic degradation of poly(L-lactic acid)s*, Polymer Degradation and Stability, vol.91, 2006, pp. 1665-1673, https://doi.org/10.1016/j.polymdegradstab.2005.12.009
[179] H. Tsuji, T. Tsuruno, *Accelerated hydrolytic degradation of Poly(L-lactide)/Poly(D-lactide) stereocomplex up to late stage,* Polymer Degradation and Stability, vol.95, 2010, pp. 477-484, https://doi.org/10.1016/j.polymdegradstab.2010.01.008
[180] S. Solarski, M. Ferreira, E. Devaux, *Ageing of polylactide and polylactide nanocomposite filaments*, Polymer Degradation and Stability, vol.93, 2008, pp. 707-713, doi:10.1016/j.polymdegradstab.2007.12.006
[181] G. Gorrasi, A. Sorrentino, *Photo-oxidative stabilization of carbon nanotubes on polylactic acid*, Polymer Degradation and Stability, vol.98, 2013, pp. 963-971, https://doi.org/10.1016/j.polymdegradstab.2013.02.012
[182] E. Stromberg, S. Karlsson, *Photo- and Thermo- oxidation of Polypropylene, Recycled Polypropylene and Polylactide Biocomposites in a Microenvironment Chamber*, Polymers from Renewable Resources, vol.1, 2010, pp. 1-15
[183] VP Sajna, S.K. Nayak, S. Mohanty, *Weathering and Biodegradation study on graft copolymer compatibilized hybrid bionanocomposites of Poly(Lactic Acid)*, Journal of Materials Engineering and Performance, vol. 25, 2016, pp. 2895-2906, DOI: 10.1007/s11665-016-2151-z

[184] F. Carrasco, P. Pages, S. Pascual, X. Colom, *Artificial aging of high-density polyethylene by ultraviolet irradiation*, European Polymer Journal, vol. 37, 2001, pp. 1457-1464
[185] J.W. Wee, M.S. Choi, H.C. Hyun, J.H. Hwang, B.H. Choi, *Effect of weathering-induced degradation on the fracture and fatigue characteristics of injection-molded polypropylene/talc composites*, Internation Journal of Fatigue, vol.117, 2018, pp. 111-120, https://doi.org/10.1016/j.ijfatigue.2018.07.022
[186] Y.W. Leong, M.B. Bakar, Z.A.Mohd Ishak, A. Ariffin, *Characterization of talc/calcium carbonate filled polypropylene hybrid composites weathered in a natural environment*, Polymer Degradation and Stability, vol.83, 2004, pp. 411-422, https://doi.org/10.1016/j.polymdegradstab.2003.08.004
[187] S. J. de Jong, E. R. Arias, D.T.S. Rijkers, C.F van Nostrum, J.J. Kettenes-van den Bosch, W.E. Hennink, *New insights into the hydrolytic degradation of poly(lactic acid): participation of the alcohol terminus*, Polymer, vol. 42, 2001, pp. 2795-2802
[188] A. Belbella, C. Vauthier, H. Fessi, J.P. Devissaguet, F. Puisieux, *In vitro degradation of nanospheres from poly(D,L-lactides) of different molecular weights and polydispersities*, International Journal of Pharmaceutics, vol. 129, 2005, pp. 95-102
[189] Tesi di laurea di E. Rotante, *Formulazioni di blend a base di acido polilattico e biochar per la termoformatura di imballaggi alimentari*, Università di Bologna, 2014-2015